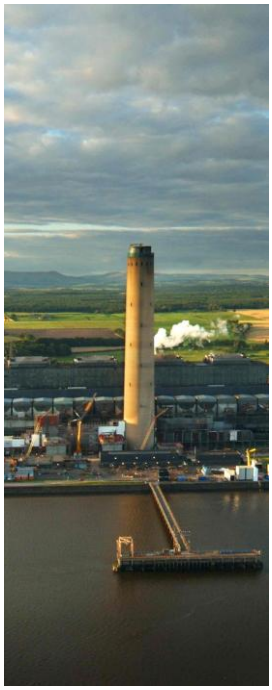

UK Carbon Capture and Storage Demonstration Competition

UKCCS - KT - S7.19 - Shell - 004
Geomechanics Summary Report

April 2011
ScottishPower CCS Consortium

SCOTTISHPOWER nationalgrid
Carbon Capture & Storage Consortium

UK Carbon Capture and Storage Demonstration Competition

UKCCS - KT - S7.19 - Shell - 004
Geomechanics Summary Report

April 2011

ScottishPower CCS Consortium

ScottishPower CCS Consortium FEED study.

Doc No. UKCCS – KT – S7.19 – Shell – 004 - Geomechanics Summary Report

KEYWORDS

Goldeneye, CCS, CO_2, Geomechanics, tensile failure, shear failure, fault reactivation, caprock integrity, temperature, wellbore

Produced by Shell U.K. Limited

ECCN: EAR 99 Deminimus

IMPORTANT NOTICE

Information provided further to UK Government's Carbon Capture and Storage ("CCS") competition to develop a full-scale CCS facility (the "Competition")

The information set out herein (the "**Information**") has been prepared by ScottishPower Generation Limited and its sub-contractors (the "**Consortium**") solely for the Department for Energy and Climate Change in connection with the Competition. The Information does not amount to advice on CCS technology or any CCS engineering, commercial, financial, regulatory, legal or other solutions on which any reliance should be placed. Accordingly, no member of the Consortium makes (and the UK Government does not make) any representation, warranty or undertaking, express or implied as to the accuracy, adequacy or completeness of any of the Information and no reliance may be placed on the Information. In so far as permitted by law, no member of the Consortium or any company in the same group as any member of the Consortium or their respective officers, employees or agents accepts (and the UK Government does not accept) any responsibility or liability of any kind, whether for negligence or any other reason, for any damage or loss arising from any use of or any reliance placed on the Information or any subsequent communication of the Information. Each person to whom the Information is made available must make their own independent assessment of the Information after making such investigation and taking professional technical, engineering, commercial, regulatory, financial, legal or other advice, as they deem necessary.

Table of Contents

1. EXECUTIVE SUMMARY 10
2. INTRODUCTION 12
3. GOLDENEYE CCS: RELEVANT GEOMECHANICAL THREATS IDENTIFIED IN OTHER CCS STUDIES 13
3.1. Loss of containment: migration and leakage scenarios 14
3.1.1. Cap rock seepage 15
3.1.2. Cap rock leakage 15
3.1.3. Fault leakage 18
3.1.4. Spill leakage 19
3.1.5. Well leakage 19
3.2. The effect of re-mineralization induced by the CO_2 on the mechanical effects 19
3.3. Geomechanical threats and monitoring 20
3.4. Conclusions 20
4. GEOMECHANICAL MODEL CONSTRUCTION 21
4.1. Geology, structural model 22
5. STRESS STATE AND PRESSURES 25
5.1. Vertical stress 25
5.2. Horizontal stresses 26
5.3. Pore pressure in overburden and underburden 27
5.4. Pore pressure changes in the reservoir 27
6. ROCK MECHANICAL PROPERTIES IN CAPROCK, OVER- AND UNDERBURDEN 29
6.1. Failure parameters in caprock: 31
7. ROCK MECHANICAL PROPERTIES IN RESERVOIR 32
7.1. Elastic rock properties for the reservoir during depletion and injection 32
7.2. Failure parameters in reservoir: 36
8. INITIALIZATION OF THE SIMULATION 37
9. MODELLING RESULTS, OBSERVATIONS AND INTERPRETATIONS 39
9.1. Compaction and sea-floor subsidence 39
9.1.1. Production phase 39
9.1.2. Injection phase 39
9.2. Stress changes in the reservoir and definition of failure criteria 41
9.2.1. Production phase 43
9.2.2. Injection phase 47
9.3. Stress changes in the Caprock (production and injection) 51
9.4. Tensile failure 53
10. UNCERTAINTY ANALYSIS 55
10.1. Uncertainty analysis, Case B: Poisson's Ratio + 0.05 56
10.2. Uncertainty analysis, Case B: Poisson's Ratio - 0.05 57
10.3. Uncertainty analysis, Case D: Young's modulus in half for over- and underburden formations 58
10.4. Uncertainty analysis, Case E: Worst case rock failure parameters of reservoir and caprock 59
10.4.1. Reservoir formation (Captain E&D) 60
10.4.2. Caprock 62

10.5. Uncertainty analysis, Case F: Poisson's Ratio 0.45 and worst case rock failure parameters of reservoir and caprock 66
10.6. Uncertainty analysis, Case G: Pressure support from aquifer and worst case rock failure parameters of reservoir and caprock 68
10.7. Uncertainty analysis, Case H: Injection pressure is larger than the hydrostatic pressure and worst case rock failure parameters of reservoir and caprock 73
10.8. Uncertainty case I: Pressure after depletion is lowered to 13.8 MPa [2000 psi] and worst case rock failure parameters of reservoir and caprock 76
11. FAULT REACTIVATION 79
11.1. Introduction 79
11.2. Fault interpretation 80
11.3. Workflow 84
11.4. Fault reactivation modelling results and uncertainty 84
11.4.1. Case I 85
11.4.2. Case II 86
11.4.3. Case III 87
11.5. Conclusions 88
12. TEMPERATURE EFFECTS CLOSE TO THE WELLBORE 89
12.1. Temperature and pore pressure profile above the casing shoe 89
12.2. Near wellbore stress state in cemented region 92
12.3. Near wellbore stress state for the caprock exposed to reservoir pressure variations 94
12.4. Possible changes in permeability if shear failure occurs 98
12.5. Conclusions 99
13. CONCLUSIONS AND RECOMMENDATIONS 100
13.1. Recommendations 101
14. GLOSSARY OF TERMS 102

Tables

Table 1-1 Assessment of geomechanical threats assessed for the Goldeneye CCS project. 10
Table 4-1 Data inventory for geomechanical model construction. 21
Table 6-1 Dynamic elastic rock properties for five overburden and two underburden formations. 29
Table 6-2 Key findings from literature for failure parameters of the caprock. 31
Table 7-1 Results from triaxial and acoustic tests on Goldeneye reservoir core samples. 33
Table 7-2 Bi-linear model (which has different elastic rock properties) used to describe the material behaviour during production and injection for all the reservoir formations 35
Table 7-3 Results from literature and experiments of failure parameters of reservoir rock 36
Table 10-1 Cases that were modelled to investigate the effect of different rock properties and pressures in the integrity of the reservoir and caprock. 55
Table 10-2 Base case results 56
Table 10-3 Key results for Case B (as obtained in the area of interest) 56
Table 10-4 Key results for Case C (as obtained in the area of interest) 57
Table 10-5 Key results for Case D (as obtained in the area of interest) 58
Table 10-6 Key results for Case E (as obtained in the area of interest) 59

Table 10-7 Key results for Case F (as obtained in the area of interest). 66
Table 10-8 Key results for Case G (as obtained in the area of interest). 70
Table 10-9 Key results for Case H (as obtained in the area of interest). 74
Table 10-10 Key results for Case I (as obtained in the area of interest). 76
Table 11-1 Parameter sensitivity study. 84
Table 12-1 Undrained material parameters for the Rødby Formation used in the near wellbore stress analysis. 92
Table 12-2 Drained material parameters for the Rødby Shale used in the near wellbore stress analysis. 93
Table 12-3 Base and low case parameters used in the PBore model. 95
Table 14-1 Well name abbreviations 104

Figures

Figure 3.1 Outward pointing DP vector in case of aquifer storage (a), and inward pointing DP vector in case of gas storage (b) (source for background picture: Statoil, Sleipner). 13
Figure 3.2 Bow-tie diagram for CO_2 containment demonstration. 14
Figure 3.3 In-situ stress response to changes in pore pressure during production and injection phase. 16
Figure 3.4 Stress-strain results from a uniaxial test of a core taken from the "Pernis KNNSL" reservoir formation. 17
Figure 3.5 Detection accuracy of a geophone string in an analogue reservoir. The string hangs in the blue monitoring well containing geophones above, below and at the reservoir level (source: ESG). 20
Figure 4.1 Stratigraphy column in the Goldeneye area on left hand picture and the Formations modelled in "Geomechanical Simulation Software" on the right hand picture. 22
Figure 4.2 Bird's-eye view from the south-west towards the north-east direction of the geomechanical model. Colours represent different geological formations. 23
Figure 4.3 Cross-sectional view showing key formations. Slice was made in the middle of the model, North is to the left and South is to the right. 23
Figure 4.4 Plan view of model showing nested mesh resolution. 24
Figure 4.5 Thickness map of Captain E&D reservoir as in "Geomechanical Simulation Software". Colour scale runs from 20 to 70m. 24
Figure 4.6 Thickness of Rødby formation (caprock) as in "Geomechanical Simulation Software". Colour scale runs from 20 to 120m. 24
Figure 5.1 Vertical Stress profile of all the eight wells in the Goldeneye area. 25
Figure 5.2 Total minimum principal stress gradient trend is represented as the lower bound of Leak-off Test (LOT) data. 26
Figure 5.3 Pore pressure as a function of time for a typical location in the reservoir, (a) schematic ranging from 10–28MPa, and (b) more precise (ranging from 13.8–27.6MPa [2000 – 4000psi]) with arrows indicating possible pressure changes due to uncertainty. 27

Figure 5.4 Top view maps of upscaled pore pressures for Captain E&D reservoir formations at initial (a), end of production (b), and end of injection (c) phase. White numbers on the plot indicate typical numbers. Colour scale is in MPa. 28
Figure 6.1 Log of well 14_29a-3 with DTP, DTS, RHOB, and derived E_d and ν_d. 30
Figure 7.1 Uniaxial compressibility as a function of porosity for Captain reservoir rock. 33
Figure 7.2 Elastic rock properties combined in Captain E&D reservoir package during production phase, (a) Young's modulus that ranges from 12-25 MPa, (b) Poisson's ratio ranging from 0.14-0.26 [-], (c) Net to Gross ranging from 0-1 [-], and (d) porosity ranging from 0.2-0.25 [-]. 34
Figure 8.1 Initial in-situ stresses and pore pressure profile compared to "Geomechanical Simulation Software" computed initial total maximum principal stress and initial total minimum principal stress. 37
Figure 9.1 Bird's eye view of the sea-floor with subsidence (max 4.6 cm) after production. Colour scale ranges between 0 and 0.05m. 39
Figure 9.2 Cross section of overburden, reservoirs (indicated by white arrows), and underburden with vertical displacement (8.9cm at the top of the Captain E&D reservoir) after production. Colour scale ranges from -0.025 to 0.09m. 40
Figure 9.3 Bird's eye view of seafloor subsidence (max 3.6cm) after injection. Colour scale ranges from 0 to 0.05m. 40
Figure 9.4 Cross section of overburden, reservoirs (indicated by white arrows), and underburden with vertical displacement (5.6 cm at the top of the Captain E&D reservoir) after injection. Colour scale ranges from -0.025 to 0.09m. 41
Figure 9.5 Tensile failure (top) and shear failure (bottom). 41
Figure 9.6 Mohr-circle diagram relating the principal stress state and the Mohr-Coulomb failure condition. The Shear Capacity is represented by the dashed line through the centre of the circle, whereas the actual shear stress is equal to the radius of the Mohr circle. 42
Figure 9.7 Map view of the pore pressure change from initial to production phase of Captain E&D formation. An area of interest is defined where the absolute pore pressure changes are largest. Colour scale is in MPa. 43
Figure 9.8 3D bird's eye view of two cross sections through all the formations (reservoir indicated by white arrows) showing (a) reduction in pore pressure from initial to production phase, (b) reduction in total minimum principal stress, and (c) reduction in total maximum principal stress. Colour scale is in MPa. 44
Figure 9.9 Map view of Captain E&D reservoir showing (a) reduction in pore pressure of 10.1 MPa from initial to production phase, and (b) reduction in total minimum principal stress of 8.5 MPa. Colour scale is in MPa. 45
Figure 9.10 Mohr circles for Captain E&D reservoir formation at a point in the area of interest (cf. Figure 9.7) before (a) and after (b) production. 46
Figure 9.11 Map of shear capacity results for the Captain E&D reservoir at (a) initial state, and (b) after production. Colour scale is dimensionless. 47
Figure 9.12 3D bird's eye view of two cross sections through all the formations showing (a) reduction in pore pressure from production to injection phase, (b) reduction in total minimum principal stress, and (c) reduction in total maximum principal stress. Colour scale ranges from 0 – 8.6MPa. 48

Figure 9.13 Map view of Captain E&D reservoir showing (a) increase in pore pressure of 8.6MPa from production to injection phase, and (b) increase in total minimum principal stress of 6 MPa. Colour scale ranges from 0 – 8.6MPa. 49
Figure 9.14 Mohr circle for Captain E&D reservoir formation at a point in the area of interest (cf. Figure 9.7) after injection. 50
Figure 9.15 Map of shear capacity results for the Captain E&D reservoir after injection. Colour scale is dimensionless 50
Figure 9.16 3D zoomed-in bird's eye view of two cross-sections (W-E and N-S, intersecting at black line) through parts of the reservoir, caprock, under- and over-burden. Colours display stress changes of the minimum total principal stress due to gas depletion (after production). Scale is in MPa, values are restricted to be within -1 and +1 MPa. 51
Figure 9.17 Mohr circles for the caprock (Rødby shale formation) before production (a) and after production (b). 52
Figure 9.18 Map of shear capacity results for the caprock (Rødby shale formation) at (a) initial state, (b) after production, and (c) after injection. Colour scale is dimensionless and ranges from 0 - 1. 53
Figure 9.19 Minimum effective principal stress after gas depletion (a) and after injection (b). Colour scale ranges from 10 – 40MPa. 54
Figure 10.1 Map of shear capacity results for Captain E&D formation (a) during production and (b) during injection. Colour scale is dimensionless. 57
Figure 10.2 Map of shear capacity results for Captain E&D formation (a) during production and (b) during injection. Colour scale is dimensionless and ranges between 0 and 1. 58
Figure 10.3 Map of shear capacity results for Captain E&D formation (a) during production and (b) during injection. Colour scale is dimensionless and ranges between 0 and 1. 59
Figure 10.4 Map of shear capacity results for caprock formation (Rødby) (a) during production and (b) during injection. Colour scale is dimensionless and ranges between 0 and 1. 59
Figure 10.5 Mohr circle for the Captain E&D formation with worst case failure parameters at (a) initial state of stress, (b) state of stress after production, and (c) state of stress after injection. 61
Figure 10.6 Map of shear capacity results for Captain E&D with worst case failure parameters at (a) initial state, (b) after production, and (c) after injection. Colour scale is dimensionless and ranges between 0 and 1. 62
Figure 10.7 Mohr circle and failure line for caprock with worst case failure parameters at (a) initial state of stress, (b) state of stress after production, and (c) state of stress after injection. 64
Figure 10.8 Map of shear capacity results within and around the area of interest for caprock with worst case failure parameters at (a) initial state, (b) after production, and (c) after injection. Range of dimensionless colour scale is here, contrary to other SCU plots, 0.6 – 1.0. 65
Figure 10.9 Mohr's circle for Captain E&D reservoir with worst case of failure rock properties at Poisson's ratio of 0.45 during injection phase. 67

Figure 10.10 Map of shear capacity results for Captain E&D formation during the injection phase where a Poisson's Ratio of 0.45 and worst case failure parameters were used. Colour scale is dimensionless and ranges between 0 and 1. 67

Figure 10.11 Top view map of pressure changes in the Captain E&D reservoir (inside the box) and aquifer due to gas production. Scale is between -10.9 and 0 MPa. 68

Figure 10.12 Top view map of pressure changes in the Captain E&D reservoir (inside the box) and aquifer due to CO_2 injection (b). Scale is between 0 and 9.6MPa. For reference figure (a) is shown that displays the pressure change without having pressure data from the aquifer in the model (Case A). There the maximum injection pressure is 8.7MPa. 69

Figure 10.13 Map of shear capacity results for Captain E&D formation (a) during the initial phase, (b) after the production, and (c) after injection. Pictures show the domain around the "Area of interest". Support from aquifer pressure and worst case failure parameters were used. Colour scale is dimensionless and ranges between 0 and 1. 71

Figure 10.14 Map of shear capacity results for the caprock formation (a) during the initial phase, (b) after the production, and (c) after injection. Pictures show the domain around the "Area of interest". Support from aquifer pressure and worst case failure parameters were used. Colour scale is dimensionless and ranges here between 0.6 and 1. 72

Figure 10.15 Map of injected pressure in the Captain E&D reservoir in 2025. To the Base case scenario 2.2MPa is added thereby reaching a level above the hydrostatic pressure (25.5MPa at 2549m). Colour scale is in MPa between 15 and 30MPa . 73

Figure 10.16 Map of difference between injected pressure in the Captain E&D reservoir in 2025 and the hydrostatic pressure. Colour scale is in MPa between 0 and 1.6MPa [232psi]. 74

Figure 10.17 Map of shear capacity results for Captain E&D with worst case failure parameters after injection was increased by 2.2MPa. Colour scale is dimensionless and ranges between 0 and 1. 75

Figure 10.18 Map of shear capacity results for the caprock formation after having injected the reservoir with a pressure that is everywhere 1.5MPa (218psi) above the hydrostatic pressure. Also worst case failure parameters were used. Colour scale is dimensionless and ranges between 0.6 and 1. 75

Figure 10.19 Map of shear capacity results for Captain E&D with worst case failure parameters after depletion where minimum pressure was 15.8MPa (a), and 13.8MPa (b). Colour scale is dimensionless and ranges between 0.5 and 1. 77

Figure 10.20 Map of shear capacity results for caprock with worst case failure parameters after depletion where minimum pressure was 15.8MPa (a), and 13.8MPa (b). Colour scale is dimensionless and ranges between 0.6 and 1. 78

Figure 11.1 Stresses acting on a fault 79

Figure 11.2 3D top view of the Captain D with faults, gas water contact (blue line), wells, and seismic sections. 81

Figure 11.3 Top view of many faults (indicated by green lines) crossing the Captain D reservoir. Axes show northing (vertical) and easting (horizontal) coordinates. The blue curve is the gas water contact. Green arrow points to a fault for reference. 82

Figure 11.4 3D bird's-eye view (SW-NE direction) of many faults through the reservoir formations. The green arrow points to a fault that is indicated in Figure 11.3 also by a green arrow. 82

Figure 11.5 3D bird's-eye view (SE-NW direction) of many faults through the reservoir formations. Most faults are crossing the Top Rødby (light brown surface) and a few cross the Top Ekofisk (dark blue surface). 83

Figure 11.6 3D bird's-eye view (SW-NE direction) of many faults. Colours indicate depth in m and range from 1600 – 3900m. The green arrow points to a fault that is also pointed to in Figure 11.3. 83

Figure 11.7 Risk on fault reactivation workflow. 84

Figure 11.8 3D bird's-eye view (SW-NE direction; location and viewing direction are equal to Figure 11.6) showing, for the "Simplified Visualization Software" Case I scenario, the effective normal stress (a), and the maximum shear stress (b) on all the faults after injection. Colours indicate stress in MPa. 85

Figure 11.9 3D bird-eye view (SW-NE direction; location and viewing direction are equal to Figure 11.6) showing, for the "Simplified Visualization Software" Case I scenario shear capacity results of all the faults after injection. Colours indicate shear capacity (fault slip tendency) in dimensionless units. 86

Figure 11.10 3D bird's-eye view (SW-NE direction; location and viewing direction are equal to Figure 11.6) showing, for the "Simplified Visualization Software" Case II scenario shear capacity results of all the faults after injection. Colours indicate shear capacity (fault slip tendency) in dimensionless units. 87

Figure 11.11 3D bird's-eye view (SW-NE direction; location and viewing direction are equal to Figure 11.6) showing, for the "Simplified Visualization Software" Case III scenario shear capacity results of all the faults after injection. Colours indicate shear capacity (fault slip tendency) in dimensionless units. 87

Figure 12.1 Near wellbore temperature profiles as a function of time. Dotted lines represent numerical solutions to the diffusion equation. Solid line is an approximate analytical solution to the diffusion problem for comparison. 90

Figure 12.2 Pore pressure profiles as a function of radial distance from the wellbore and time for permeability in the range of 1 (left) to 10 (right) nanoDarcy. 91

Figure 12.3 Effective stress state of the near wellbore environment after cooling under undrained conditions. The stress state is displayed in Mohr's space relative to the base case (solid), intermediate (dotted), and worst case (dashed), Mohr-Coloumb failure line for the Rødby shale before (red circle) and after cooling (green circles) for three different scenarios (see Table 12-1). 93

Figure 12.4 Effective stress state of the near wellbore environment after cooling under drained conditions. The stress state is displayed in Mohr's space relative to the base case (solid) and worst case (dashed) Mohr-Columb failure line for the Rødby shale before (red circle) and after cooling (blue circles) for three different scenarios (see Table 12-2). 94

Figure 12.5 Temperature (a) and pore pressure (b) distributions as a function of time for the base case PBore model assuming a 100 nD permeability. Pore pressure or temperature after 1 day is shown in black, 60 days in blue, 2 years in green and 4 years in red. 96

Figure 12.6 Comparison of the failed zone (red area) around well from the base case PBore simulation with cooling of the formation for 4 years (a), and no temperature change in the formation (b). 97

Figure 12.7 Evolution of wellbore failure (red areas) from the low case PBore simulation as a function of time under cooling conditions. The amount of failure is shown after 60 days (a), 1 year (b), and 2 years (c). 98

1. Executive summary

For safe storage of carbon dioxide (CO_2) in underground depleted gas reservoirs it is of fundamental importance to understand and control the injection and containment in the subsurface. During CO_2 injection fluid pressure will increase, temperature (close to the wellhead) will change, and chemical reactions between the fluids and rocks will affect the rock strength and the stress state both inside and outside the reservoir. Therefore, the integrity of the reservoir itself and the overlying seal must be investigated with an emphasis on likelihood of leakage. Also the likelihood of fault slip needs to be investigated.

The geomechanical analysis starts with the construction of a model of the Goldeneye reservoir and the formations around it. Therefore, seismic, drilling, logging, and core data are used. A reservoir model provides pressure data as well as porosity and net-to-gross (NtG) distributions from which some mechanical properties can be derived. After initial equilibrium is achieved, the model simulates the deformation and stress changes due to pressure depletion of the original gas reservoir and subsequent re-pressurization due to injection of CO_2. The simulation process allows for stress path predictions and assessment of the mechanical stability of both caprock and faults. Special care was taken to define the different behaviour of the stresses between depletion and injection (hysteresis).

The geomechanical model is used to investigate the limits of CO_2 injection operations such that containment is ensured during (and after) injection.

Relevant geomechanical threats as identified in other CCS studies are summarised in Table 1-1.

Table 1-1 Assessment of geomechanical threats assessed for the Goldeneye CCS project.

Threat	Risk	Evidence	Uncertainty
Tensile failure of the reservoir (Captain E&D sandstones)	No	Plan is not to raise the pressure of the CO_2 above the initial virgin pressure	Negligible as stress state is far away from failure envelope determined by worst case rock properties
Shear failure of the reservoir (Captain E&D sandstones)	No		
Tensile failure of the entire cap-rock	No		
Shear failure of the entire cap-rock	No	For an injection pressure of 25 MPa [3625 psi] the shear capacity utilization is 0.94. A slightly higher injection pressure leads to slightly higher stresses in the cap-rock where the pressure is not changing. So, the Mohr circle moves to the right and away from the failure line.	Worst case might be too pessimistic as cohesion of the Rødby is probably higher than zero. Also the total cap-rock package is thicker than in the current modelling which assessed only the Rødby and did not consider Hedra and Plenus Marl as part of the cap-rock.
Fault slip	No	Stresses in the field were mapped onto 43 faults. Failure parameters are equal to worst case properties of Rødby	Negligible as results are not close to failure
Leaking close to the wellbore due to thermal fracturing	No	Very detailed study on the coupled effects of temperature and pore pressure in the shale close to the wellbore	Results only hold for vertical wells. Effect of deviated wells needs to be investigated.

Note that, after many, many years the aquifer re-pressurises the field. This effect has not been rigorously addressed but preliminary calculations indicate there is not a significant increase in the risk of failure.

2. Introduction

The objective of the work presented in this report is to identify and assess any geomechanical risk that might follow from the injection and storage of CO_2 in the Goldeneye reservoir matrix.

For safe storage of carbon dioxide (CO_2) in underground depleted gas reservoirs, it is of fundamental importance to understand and control the injection and containment in the subsurface. During CO_2 injection fluid pressure will increase, temperature (close to the wellhead) will change, and chemical reactions between the fluids and rocks will affect the rock strength and the stress state both inside and outside the reservoir. Therefore, the integrity of the reservoir itself and the overlying seal must be investigated with an emphasis on likelihood of leakage. Also the likelihood of fault slip needs to be investigated.

The geomechanical analysis starts with the construction of a model of the Goldeneye reservoir and the formations around it. Therefore, seismic, drilling, logging, and core data are used. A reservoir model provides pressure data as well as porosity and net-to-gross (NtG) distributions from which mechanical properties can be derived. After initial equilibrium is achieved, the model simulates the deformation and stress changes due to pressure depletion of the original gas reservoir and subsequent re-pressurization due to injection of CO_2. The simulation process allows for stress path predictions and assessment of mechanical stability of both caprock and faults. Special care was taken to define the different behaviour of the stresses between depletion and injection (hysteresis).

The geomechanical model is used to investigate the limits of CO_2 injection operations such that containment is ensured during (and after) injection. Also, the model is used in helping to decide which monitoring schemes are needed.

An extensive description of the Goldeneye field can be found in the static model (field) report[1].

The chapter hereafter provides an overview of relevant geomechanical issues as identified in other CCS studies. The approach and model construction is described in the next chapter followed by chapters on initial stresses and pressures, rock properties, and model initialization. Then simulation results are discussed for several scenarios. Subsequent chapters give a treatment on fault reactivation and temperature effects close to the wellbore. A chapter on conclusions and recommendations finalises this report.

[1] Shell, 2010. Static model (field)

3. Goldeneye CCS: relevant geomechanical threats identified in other CCS studies

Shell has been involved in CCS and CO_2 enhanced oil recovery (EOR) for several decades and has gained significant knowledge in the area. Some of the projects executed by the company are in the public domain (*e.g.*, the suspended Barendrecht onshore CCS project in the Netherlands) whilst others remain confidential. The following chapter has been compiled from this knowledge bank, coupled with extensive surveying of the available industry literature on CCS.

Containment is a very important topic of discussion in the assessment of any storage project. Thresholds on acceptable leakage rates have been defined by the International Panel on Climate Change (IPCC) report[2]. IPCC stated that a safe CO_2 storage site should demonstrate that it is likely that 99% or more of the injected CO_2 will be retained for 1,000 years. It is difficult for any storage project to unequivocally prove and guarantee this likelihood. However, some first physical principles directly show that there is a fundamental difference in demonstrating containment for aquifer storage and depleted field storage. The largest differentiator between these two storage options is the difference in pressure between reservoir and burden. Most current CCS projects (like Sleipner, Snøhvit, Gorgon and In-Salah) inject CO_2 into an aquifer. Aquifer storage implies that the reservoir pressure will become higher than the pore pressure in the burden, leading to an outward pointing differential pressure (DP) visualised in Figure 3.1a. In a depleted hydrocarbon reservoir the opposite is often the case. The depleted reservoir will be filled to the point that the reservoir pressure is just below the pore pressure in the burden. This implies an inward pointing gradient vector. The leakage of water or natural gas into the reservoir is more likely than the leakage of CO_2 into the burden. The only remaining physical mechanism that can cause an outward and upward pointing DP vector is buoyancy but this mechanism requires the build-up of a continuous column of CO_2, which is an unlikely scenario in the subsurface.

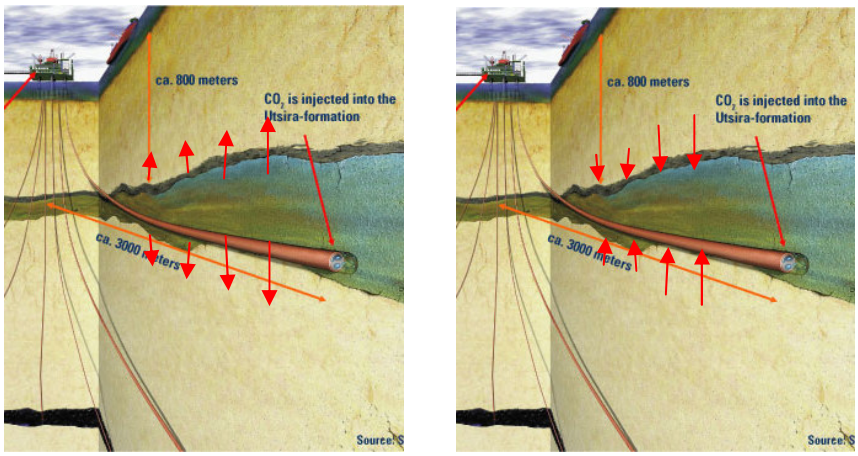

a) b)

Figure 3.1 Outward pointing DP vector in case of aquifer storage (a), and inward pointing DP vector in case of gas storage (b) (source for background picture: Statoil, Sleipner).

This first principle demonstrates that, in general, containment of stored CO_2 in a depleted field is more assured when compared with CO_2 storage in an aquifer.

[2] IPCC (Metz, B., Davidson, O., de Coninck, H., Loos, M. and Meyer, L. eds.) 2005. *Carbon Dioxide capture and storage,* Cambridge, UK: Cambridge University Press

3.1. Loss of containment: migration and leakage scenarios

Before geomechanical threats are able to be described it is necessary to map them in possible risk scenarios. This can be visualized in a bow-tie diagram as it is used in the containment risk assessment (see Storage Development Plan[3]). The bow-tie consists of several elements that are described in the glossary and visualized in Figure 3.2. The scenarios combine threats making cause–consequence relations that run from left to right through the bow-tie (consequence means here: the potential hazardous outcomes arising from the top event). Note that the hazard, in the depleted reservoir case, is defined by buoyant gas and not overpressured gas.

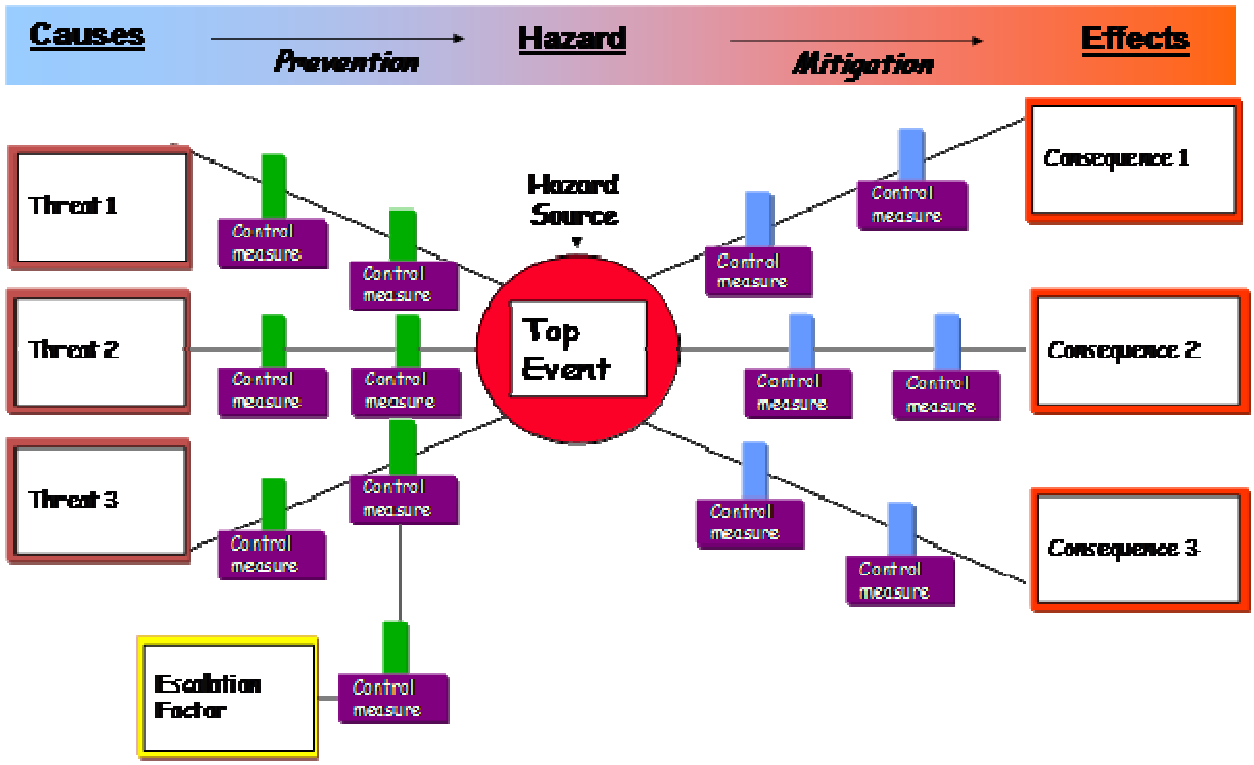

Figure 3.2 Bow-tie diagram for CO_2 containment demonstration.

A leakage scenario connects possible subsurface threats via the top event (in our case leakage of CO_2 out of the containment) to the possible consequences. In the case of CO_2 containment, five leakage scenarios were defined:

- Cap rock seepage which includes acid fluids increasing permeability and also diffusion
- Cap rock leakage, which includes stress of injection
- Fault leakage, which includes faults fractures and features
- Spill leakage, which includes lateral migration
- Well leakage, which includes abandoned wells and injection wells

[3] Shell, 2011. Storage development plan

The difference between leakage and seepage is explained in the glossary. Geomechanical threats are involved in any of these scenarios and will be described per scenario below.

More details on threats can be found in the Storage Development Plan[3].

3.1.1. Cap rock seepage

Cap rock seepage considers a low flux and low concentration flow out of the reservoir. However, significant integrity of the cap rock is proven by the existence of low density hydrocarbons, although seepage on a geological time scale (millions of years) can never be totally ruled out. Gas chimneys can reveal old or existing migration routes and production of hydrocarbons can impact the integrity. In general, production of a reservoir leads to a perturbation of rock stress having the highest impact in the reservoir itself. A change in stress can lead to a change in volumetric strain impacting the porosity and permeability of the cap rock. It is concluded from previous studies that the risk for permeability increase as a result of a change in volumetric strain is negligible.

3.1.2. Cap rock leakage

The concern in this context is that the "very high pressure" will lead to rupturing of the subsurface and subsequent high flux leakage at the surface. The coupling between injection and fracturing is well known from water disposal and cutting injection and this knowledge is, therefore, often used during technical discussions on containment.

Caprock leakage is migration and leakage of CO_2 out of the reservoir at a relatively high flux. In general, this scenario requires the existence of natural or induced fractures. The word "induced" is important in the case of depleted field storage as the gas occurrence has proven gas containment. Therefore, it can be concluded that the existence of natural conductive fractures in the cap rock is extremely unlikely, although it is possible that stress changes during the production phase created or reactivated shear fractures. During the injection phase both tensile and shear fractures can result as well as being produced from stress changes. It is therefore necessary to investigate the threat of fracturing in and outside the reservoir.

3.1.2.1. Joule-Thomson effect

The Joule-Thomson effect describes the change in temperature when a gas or liquid expands. For most gasses and fluids the temperature will decrease, and this is also the case for CO_2 expansion. Expansion of CO_2 is most relevant in the first stage of injection when the reservoir pressure is very low. A subsequent effect of a decreasing temperature is the impact on rock stress. Total minimum principal stress decreases with decreasing temperature where analytical expressions are provided for limit cases, *e.g.*, Fjaer *et al.* 2008[4]. Considering the case (first stage of cooling) of a very small diameter (d) versus height (h) ratio ($d/h \rightarrow 0$), the change of stress can be described as follows:

$$\Delta S_h = \frac{E}{2(1-\nu)}\alpha_t(\Delta T), \qquad (1)$$

where,

E is the Young's modulus,

ν is the Poisson's Ratio, and

α_t is the coefficient of linear thermal expansion.

A typical cemented sandstone has an α_t of $1*10^{-5}$/°C.

[4] Fjaer, E., Holt, R.M., Horsrud, P., Raaen, A. M. and Risnes, R. 2008. *Petroleum related rock mechanics*, Hungary: Elsevier Science Ltd.

To give an example: if a reservoir sandstone has an average (second cycle uni-axial compaction tests, calibration by computer model) Young's modulus of 21 GPa and a Poisson's ratio of 0.18, the reduction in stress is 1.28 bar per degree Celsius cooling.

When the cooling region has grown also the opposite limit case can be computed where d/h → ∞. In this case the change in stress is expressed by:

$$\Delta S_h = \frac{E}{(1-\nu)} \alpha_t (\Delta T). \qquad (2)$$

The reduction in stress will then double (2.56 bar per degree Celsius).

3.1.2.2. Barriers to prevent negative thermal effects

In a literature survey from other fields two barriers were found/defined that mitigate negative effects of temperature on the stress. The first barrier is the implementation of a heater at the injector. The second barrier relates to the stress and fluid pressure in the caprock. The stress in the caprock is always higher than the CO_2 pressure making the induced tensile fracturing in the cap rock an unlikely scenario including temperature effects. In the unlikely case of tensile fracturing CO_2 cannot escape as it is likely that the fracture will be filled with water due to the relative high pressure of the water in the cap rock.

3.1.2.3. Reversible stress path

Another significant geomechanical issue is related to the question of whether production induced stress changes are reversible during the injection phase. Depletion leads to compaction and an effective stress increase in all directions. If the material behaves as an ideal elastic material, the grains will "store the energy" and release it during pore pressure increase. This leads to the situation of perfect reversible compaction. In general, rocks never behave ideally and compaction is the result of both elastic and plastic behaviour. These types of behaviour can be time dependent as well. Plastic behaviour caused by gliding, sliding and cracking of grains or small rock interfaces leads to a loss of energy and irreversible behaviour during the phase of pore pressure increase. Possible behaviour is sketched in Figure 3.3.

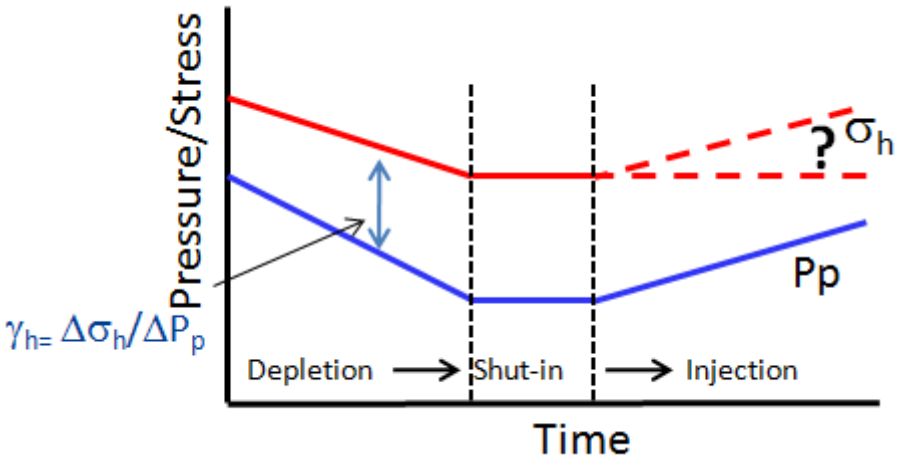

Figure 3.3 In-situ stress response to changes in pore pressure during production and injection phase.

De-pressuring and re-pressuring of core plugs can reveal plastic behaviour. The basic idea behind this test is to mimic the process of production at reservoir conditions. Generally it is believed that plasticity can occur when the effective stress will be higher due to de-pressuring than the maximum natural effective stress ever "seen" in the past. Core plug measurements from a similar field (uni-axial strain, pore pressure controlled) show different stress-strain behaviour between the first and second cycle (Figure 3.4, notice the different slopes). At first sight it can be interpreted as a partly irreversible behaviour of the sample. The phenomenon is however common for many rock types and is often ascribed to core damage. Core damage leads to an additional component of inelastic deformation during the first-time loading of reservoir core in the laboratory experiment. In other words, this core-damage-induced inelastic strain may not occur in the in-situ reservoir (that has not undergone the unloading and possible damage by coring, tripping, transport, *etc.*). It is nearly impossible to distinguish the contribution of core damage from "real" plastic behaviour.

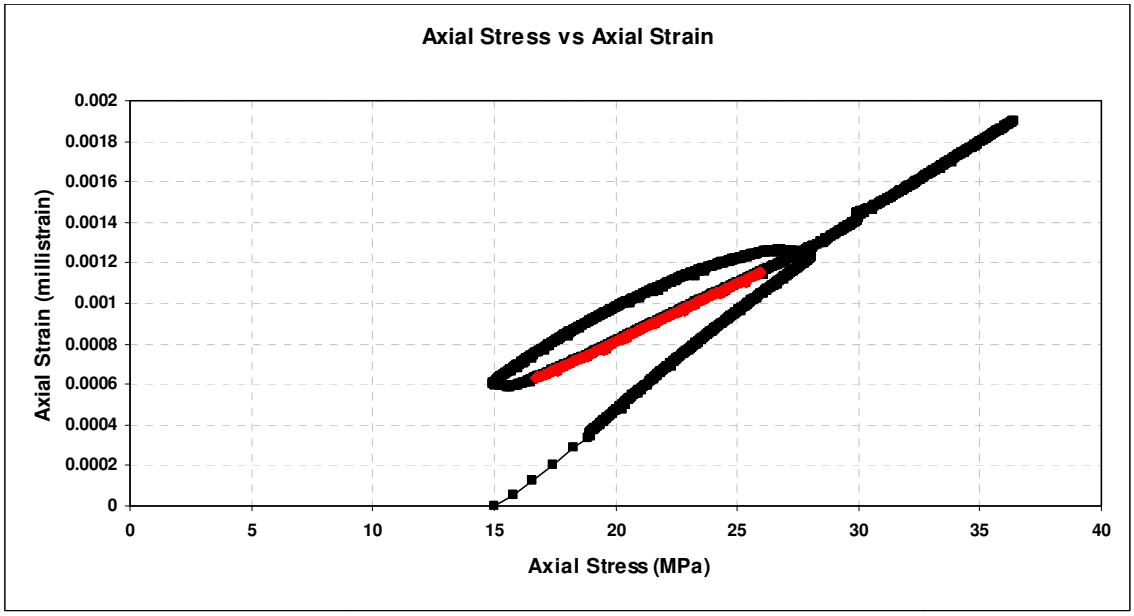

Figure 3.4 **Stress-strain results from a uniaxial test of a core taken from the "Pernis KNNSL" reservoir formation.**

Indirect observations of compaction in some other fields leads to the conclusion that most of the compressibility difference between first and second cycle can be explained by core damage:

- It is observed in many fields that the second cycle compressibility better matches the subsidence measurements.

- Also, interferometric synthetic aperture radar (InSAR) measurements above the Norg UGS support the theory that consolidated sandstone behaves in its majority as an elastic material. It was observed that at least 80% of the subsidence resulting from a depletion phase was restored during injection applying the same DP for both phases.

To quantify the effect of stress changes in relation to pressure changes a so called "reservoir depletion coefficient" or "gamma" is defined as the ratio of change in horizontal total stress (denoted by $\Delta\sigma_h$) and the change in pore pressure (denoted by ΔPp).

$$\gamma_h = \frac{\Delta\sigma_h}{\Delta P_p} \tag{3}$$

A similar definition holds for the vertical gamma,

$$\gamma_v = \frac{\Delta\sigma_v}{\Delta P_p} \tag{4}$$

If the assumption is made that the rock in the reservoir is an elastic material and deforms in an oedometric manner (strains in the horizontal plane are zero), the reservoir stress path can be related to the Poisson's ratio of the rock. But, these depletion coefficients that are calculated from measured values of Poisson's ratio or derived from sonic logs are not always in good agreement with field measurements. This might be due to the following hypotheses

- rocks may not behave elastically upon loading (under normal in-situ stress conditions),
- above the compacting reservoirs localised deformation could lead to stress arching resulting into an increase (at the "pillars") or decrease (under the arch) of the vertical stresses,
- the structure of faults and overburden formations play a role.

Geomechanical models should be able to predict depletion coefficients as observed in the field. Obviously, this requires rock properties that are representative for the field behaviour.

3.1.3. Fault leakage

The fault leakage scenario is basically part of the cap rock leakage scenario. The occurrence of a gas reservoir in Goldeneye proves that the faults in the cap rock are sealing at the virgin gas pore pressure. The virgin pressure even had a slightly higher value then the proposed end pressure of the CO_2. Also, no impedance contrasts were observed above the structure on seismic data (*i.e.*, a gas chimney) that could indicate a leaking gas trap.

In this report, fault reactivation for Goldeneye is discussed in §11.

3.1.3.1. Fault reactivation and induced seismicity during injection

In a normal faulting tectonic regime (vertical stress is larger than the horizontal stresses) geomechanical models have shown that fault shear tractions in general decrease during injection. This depends heavily on the assumed ranges of the model parameters and the pore pressure increase in the faults themselves. If the injection takes place in a fault plane, the probability of reactivation increases as the increased pore pressure lubricates the fault plane.

3.1.3.2. Fault movement and impact on fault transmissivity

Faults are often described in geomechanical and dynamic reservoir models by simple planar surfaces having no thickness. In reality faults can express themselves in many forms and geometries and therefore it is logical that faults can behave differently than forecasted by models. According to what is concluded in the literature it is accepted that brittle crustal fault slip causes dilatant behaviour that results in an increase of the fault transmissivity parallel to the fault plane. In Zoback, 2007[5], a firm statement is made on the conductivity of faults:

[5] Zoback, M. 2007. *Reservoir Geomechanics*, Cambridge, UK: Cambridge University Press

"faults that are mechanically alive are hydraulically alive and faults that are mechanically dead are hydraulically dead".

3.1.4. Spill leakage

The risk of spill leakage normally results from injection into high permeable streaks within the reservoir. In case of very high injection pressures it would be possible that the pore pressure in the streak at spill point exceeds the pore pressure in the side aquifer leading to the flow of CO_2 in the aquifer. Fracturing could be an escalation factor that provides a fast route to the spill point[6]. This scenario though was considered to be unlikely as the creation of a huge fracture is considered to be unlikely for very low viscosity supercritical fluids like CO_2. The surface area that arises from such a huge fracture would allow for a pressure reduction in a permeable reservoir. For Goldeneye, 'fracturing' of the reservoir and caprock formations is discussed in the Injection Fraccing report[7].

3.1.5. Well leakage

In all studied CO_2 storage opportunities, it is identified that the well leakage scenario is one of the concerns. The impact, however, is still considered to be low. The status of the cement can be examined with cement bond logs that were run after the cement job but it is possible that stress and strain changes during the production impacted the bound of cement. Stress and strain values were deduced from the finite element model and compared with threshold values that can be found in the literature. Mulders *et al.* 2007[8], concluded that compaction strain could lead to mechanical degradation but only in the reservoir. Mechanical degradation as a result of depletion or injection is unlikely in the overburden cement section. Leakage via the well is only a concern during the injection phase.

3.2. The effect of re-mineralization induced by the CO_2 on the mechanical effects

Although this document is limited to geomechanical threats only, rock mechanical behaviour could be impacted by chemical alteration of the rock itself. Rock compressibility is normally a function of porosity and therefore a change in the porosity by re-mineralisation could lead to a change in the compressibility. CO_2 coupled (flow-mechanical-chemical) dynamic modelling is still under research and would be the preferred method in future studies. A progressive and aggressive reaction of acidised water with carbonate or siderite minerals, nodules and streaks is considered to be unlikely as no free water is available and short term mineral reactions will quickly buffer the pH. Large scale weakening of reservoir rock is therefore not expected. The geochemical reactivity study carried out for Goldeneye[9] came to a similar conclusion.

Preliminary results from experiments on Goldeneye core indicate that mineralisation is not having an effect on the geomechanical properties of the core. In that experiment the core was constantly flushed with CO_2 such that possible minerals were removed. From a geomechanical strength and failure point of view, this case was considered worse than a setup where minerals would form and stay in between the sand grains.

---

[6] MER ondergrondse opslag van CO_2 in Barendrecht. 2008. Den Haag: Shell CO_2 Storage B.V.

[7] Shell, 2011. SP-PT050D3 Injection fraccing conditions

[8] Mulders, F.M.M., Gouwen, R., Orlic, B. and Benedictus, T. 2007. Well Integrity for CO_2 storage in the fields Barendrecht and Barendrecht-Ziedewij, Utrecht: TNO report 2007-U-R0377/C

[9] Shell, 2010. SP-PG010D3 Geochemical Reactivity Study

3.3. Geomechanical threats and monitoring

For all studied reservoirs it is identified that the risk on migration of CO_2 in all scenarios is low to negligible. Leakage to the surface is considered to be unlikely. Still some of the scenarios possess a higher risk (migration along the well) than others.

Shell executed a feasibility study (carried out by ESG) into the effectiveness of 4D seismic monitoring of geomechanical events. The conclusions of the study pointed out that the range of detection by one string was sufficient to cover most of the reservoir dimension. An example of a result is given in Figure 3.5.

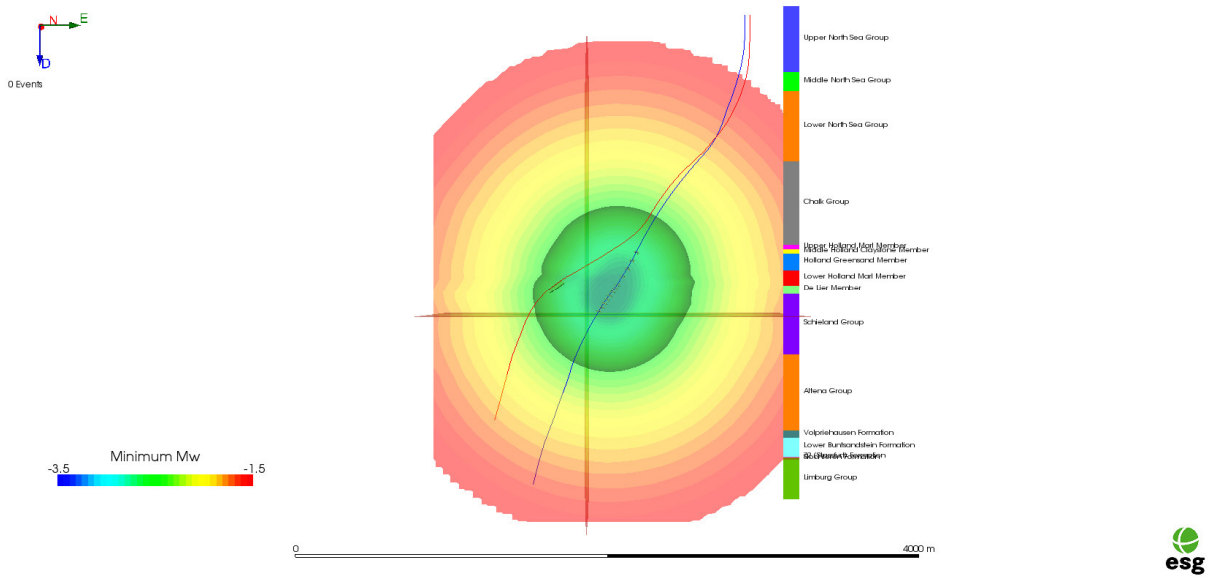

Figure 3.5 **Detection accuracy of a geophone string in an analogue reservoir. The string hangs in the blue monitoring well containing geophones above, below and at the reservoir level (source: ESG).**

This type of monitoring, and more, is extensively discussed in the Monitoring Feasibility report[10].

3.4. Conclusions

None of the geomechanical threats identified in these studies have a significant impact on leakage risk. It is pointed out that aquifer storage should not be compared with storage in a depleted field like Goldeneye. Storage in a depleted field reduces the impact and probability of all threats and leakage scenarios that have a relationship with pressure and therefore also geomechanical behaviour.

[10] Shell, 2010. Monitoring feasibility study

4. Geomechanical model construction

The geomechanics workflow makes use of the Shell proprietary pre- and post-processor that uses the commercially available finite element package to carry out the simulations. For the study described in this report, the choice was made to use a hexagonal mesh without explicit faults as this could be built relatively quickly. Fault slip was then investigated via an alternative route (see Chapter 11 - Fault reactivation).

The geomechanical model is composed of

- the structural geometry of the reservoir, overburden and underburden formations,
- in-situ stress and pore pressure profile,
- mechanical rock properties of all the formations, and
- pressure changes in the reservoir due to depletion and injection at different times.

Table 4-1 shows the data inventory and integrated approach to arrive at the geomechanical model for the Goldeneye field.

Table 4-1 Data inventory for geomechanical model construction.

GEOMECHANICAL MODEL CONSTRUCTION	DATA SOURCE
Structural geometry of reservoir, overburden and underburden	Static models SRM 3.1 (key reservoir formations)[11] and "Overburden model" (over- and under-burden formations)[12]
In-situ stress and pore pressure profile	Mainly from previous wellbore stability studies on the drilling of Goldeneye wells[13]
Mechanical rock properties in overburden and underburden	Dynamic rock properties derived from six well logs using compressional and shear wave velocities, and densities
Reservoir pressure change during production (of gas) and injection (of CO_2) cycles	Reservoir pressures from Shell proprietary fluid flow simulation software (model is also the basis for the aforementioned static models). Upscaling method is based on 1D scale independent compaction[14]
Mechanical rock properties in the reservoir section	Young's modulus and Poisson's ratio can be derived from the upscaled porosity and NtG distributions from "Simulation Software". So, variations in the geology have been taken into account. Also validated with nearby triaxial tests (of the FRAM field) and other empirical correlations.

[11] Shell, 2011. Dynamic Modelling Report

[12] Shell, 2010. Static model (Overburden)

[13] Shell, 2011. Pore Pressure Prediction.

[14] Schutjens, P., and Snippe, J. 2009. Upscaling mechanical rock properties and pore fluid pressure: An application to geomechanical modelling. Oral presentation given at DEVEX 2009 (presentation 2B1335), Aberdeen, UK, 12-13 May

4.1. Geology, structural model

Static reservoir model SRM3.1[1] contains the key reservoir formations. A model of the overburden is also available and contains overburden and underburden formations[12]. A "Geomechanical Simulation Software" model was constructed by combining the horizons from the two models. Several formations were grouped together for construction and run time efficiency resulting into five overburden, three reservoir and two underburden formations (see Figure 4.1).

- The overburden formations are: Nordland group, Coals, Dornoch, Chalk group (Ekofisk, Tor, Hod) and Rødby (Caprock).
- The three reservoir units are: Captain E and Captain D combined together, Captain C, and Captain A combined with Valhall and Scapa.
- The underburden formations are: Humber and Heron groups.

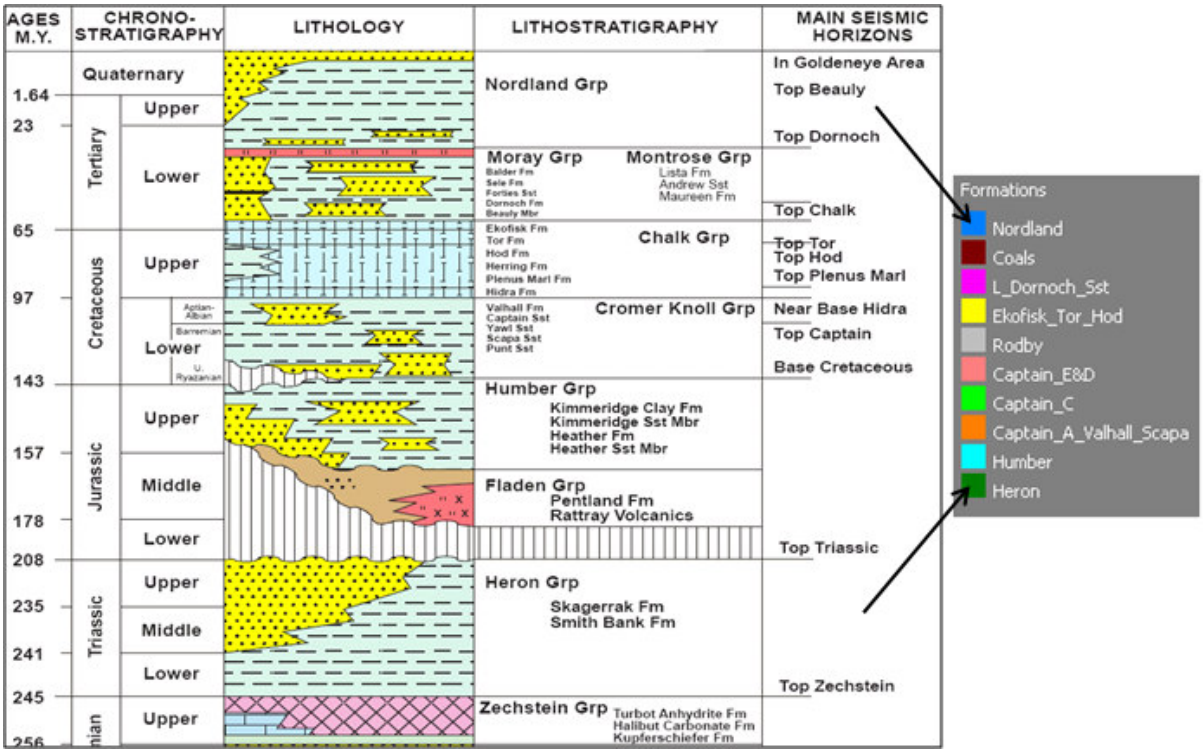

Figure 4.1 **Stratigraphy column in the Goldeneye area on left hand picture and the Formations modelled in "Geomechanical Simulation Software" on the right hand picture.**

The "Geomechanical Simulation Software" model with hexahedral elements has overall dimensions of 50km east-west by 20km north-south (see Figure 4.2). The mesh resolution is of 250m in the area where production has taken place and injection is planned surrounded by mesh elements that are 500m in length (see Figure 4.2 - Figure 4.4). The model has 364736 elements. Unless otherwise stated all map views in the remainder of this report show an area of 20 x 50km while the bird's eye view shows a volume of 20 x 50 x 8km. Cross sections are, therefore, 20 x 8km (N-S) and/or 50 x 8km (W-E). The reservoir area is smaller. Thickness maps of the Captain E&D units and the Rødby Formation (caprock) are displayed in Figure 4.5 and Figure 4.6 respectively. This is discretised to hexahedral elements that go into the geomechanical model where a minimum thickness of 20m is enforced to prevent numerical problems.

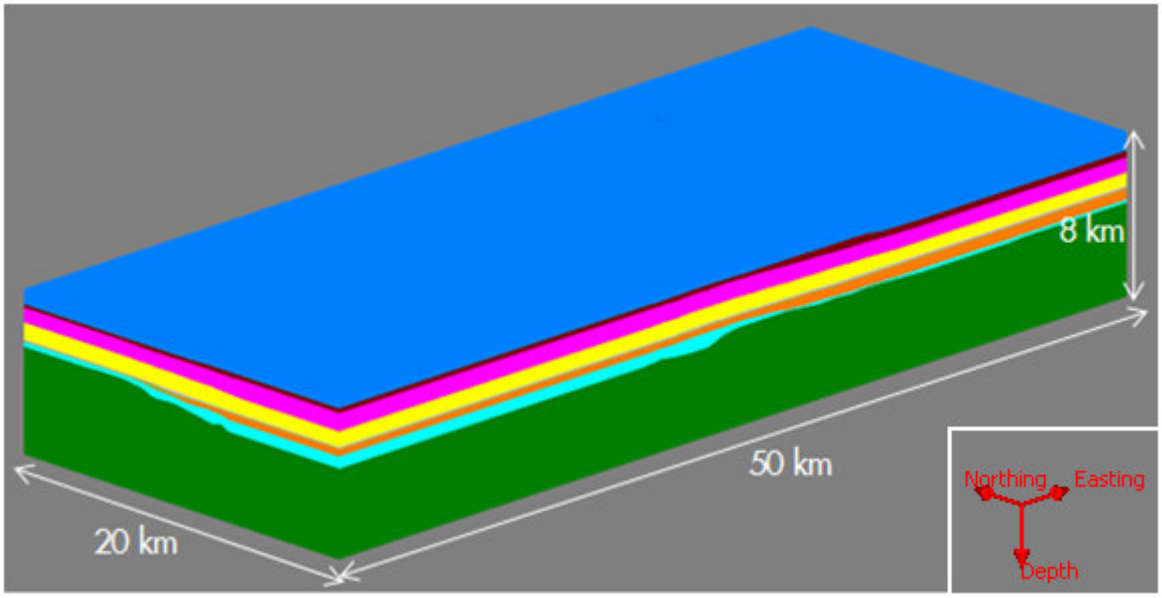

Figure 4.2 **Bird's-eye view from the south-west towards the north-east direction of the geomechanical model. Colours represent different geological formations.**

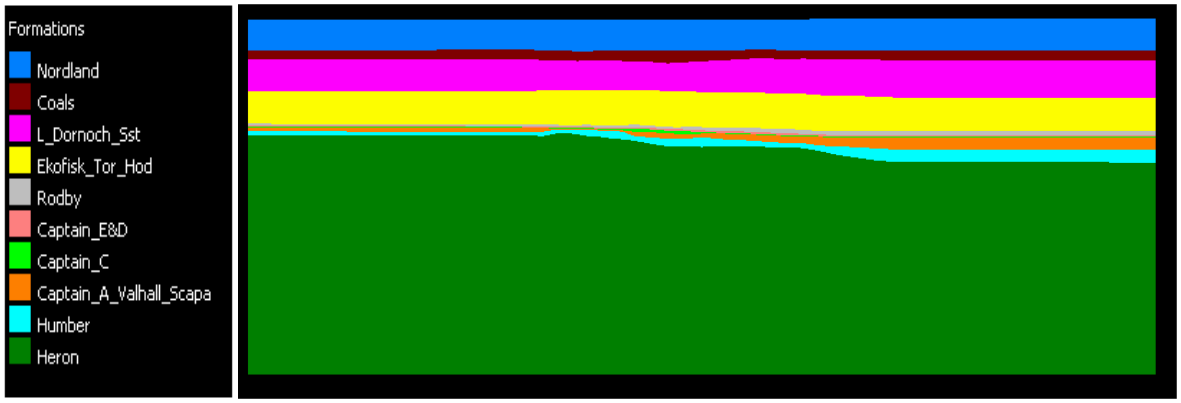

Figure 4.3 **Cross-sectional view showing key formations. Slice was made in the middle of the model, North is to the left and South is to the right.**

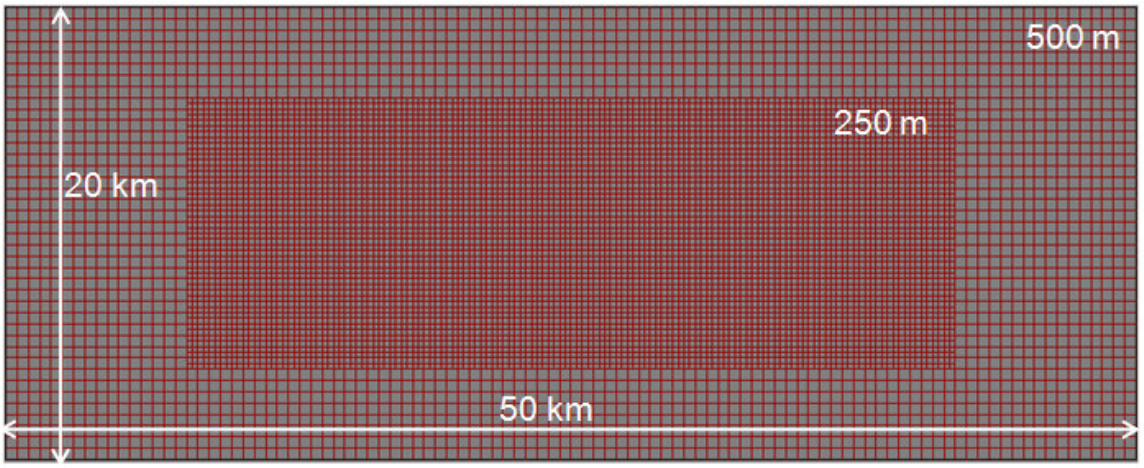

Figure 4.4 Plan view of model showing nested mesh resolution.

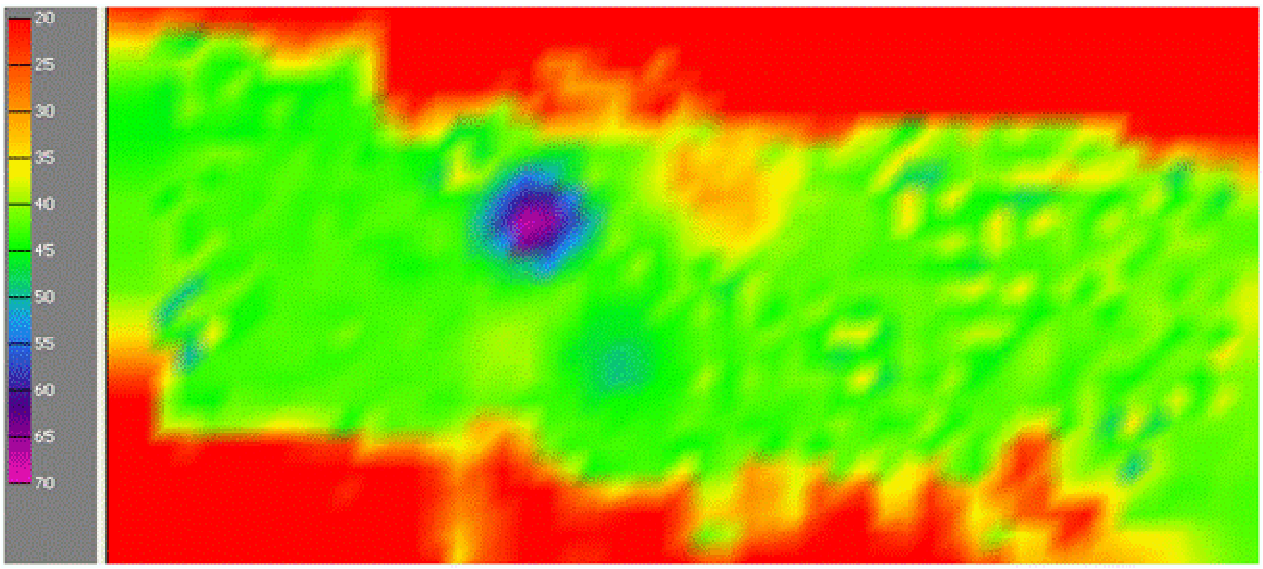

Figure 4.5 Thickness map of Captain E&D reservoir as in "Geomechanical Simulation Software". Colour scale runs from 20 to 70m.

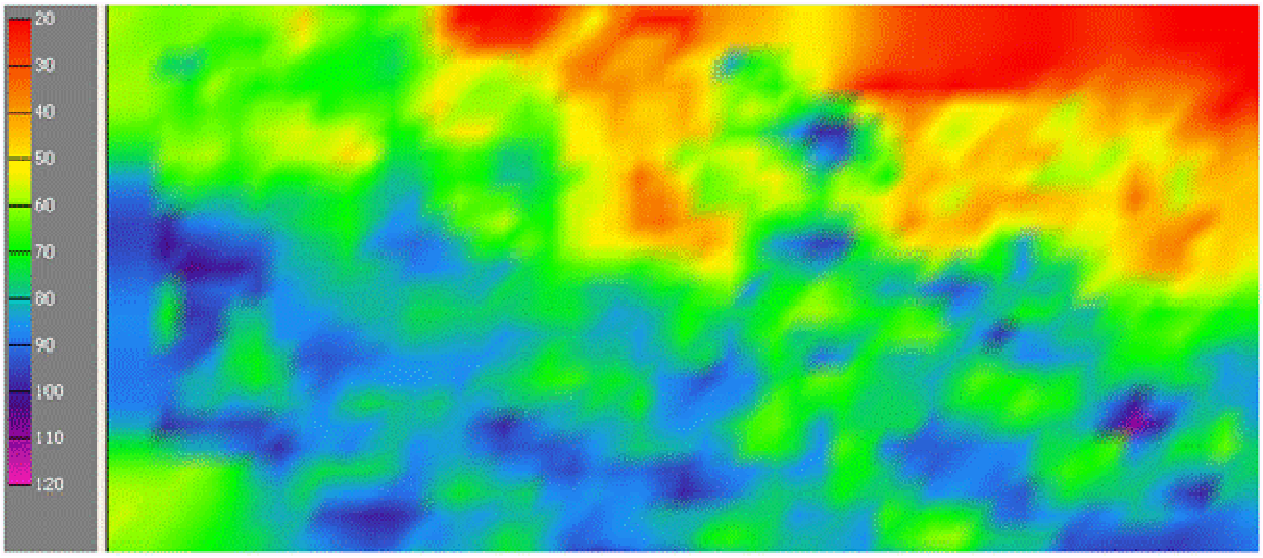

Figure 4.6 Thickness of Rødby formation (caprock) as in "Geomechanical Simulation Software". Colour scale runs from 20 to 120m.

5. Stress state and pressures

The in-situ stress and pore pressure profile for the Goldeneye area is constructed using pore pressure information, log data, leak-off test (LOT) and Limit test (LT) data. The formation pore pressure is hydrostatic in the overburden. Vertical stress is calculated by the integration of the density log. Total minimum principal stress is estimated from the LOT/LT data available from the offset wells. There is a normal stress regime (vertical stress is larger than the horizontal stresses) in the Goldeneye area. The direction of maximum horizontal stress is NNW-SSE as inferred from image log, caliper data and World Stress map[15]. The next sections describe in detail the data and methodology that was used to derive the stresses and pore pressures.

5.1. Vertical stress

Eight wells are available with density logs in the Goldeneye area. An estimate of the vertical stress is calculated by integrating the density logs of these wells. Vertical stress profiles generated from the well data are shown in Figure 5.1. As the curves overlie each other there is sufficient consistency in the data to be conclusive in the vertical stress.

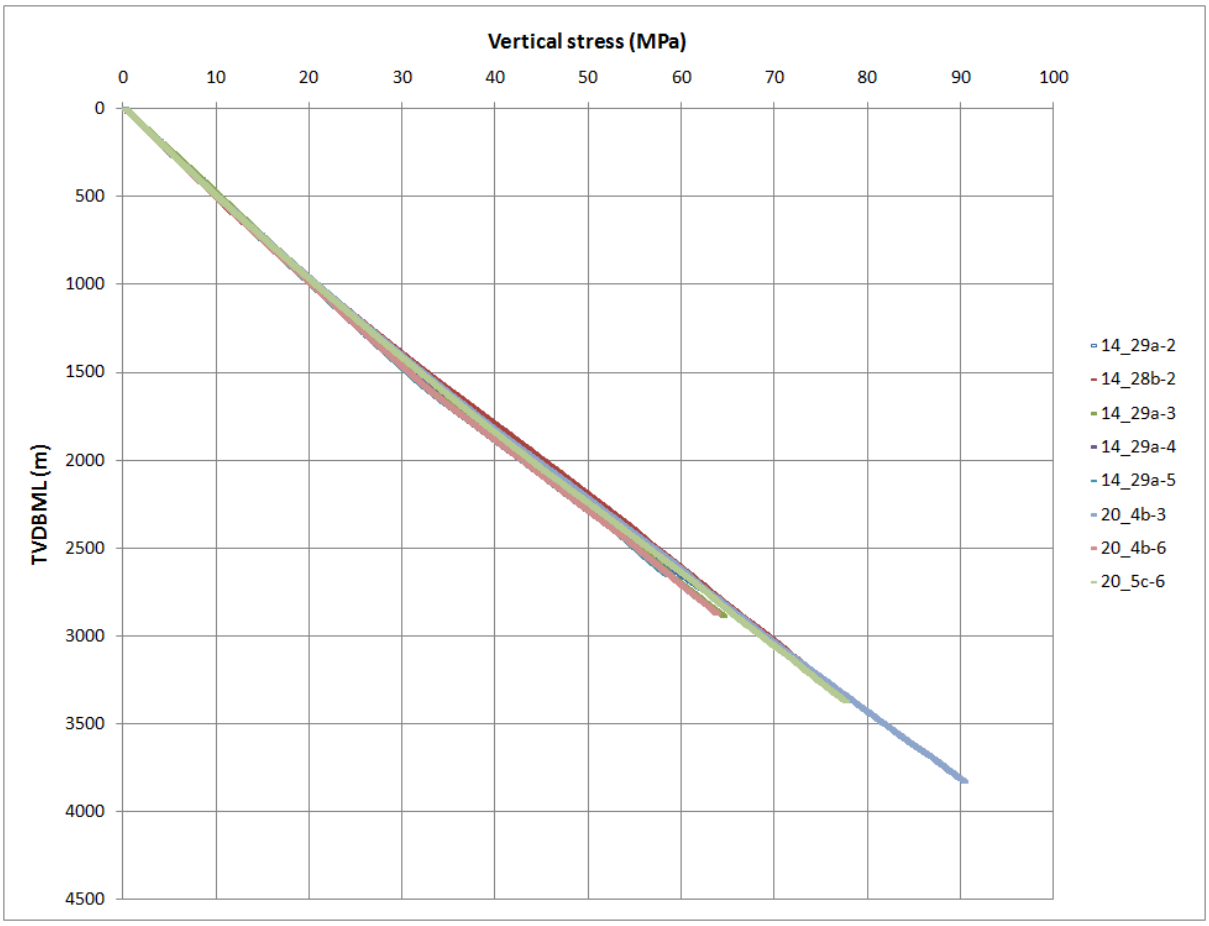

Figure 5.1 Vertical Stress profile of all the eight wells in the Goldeneye area.

[15] Sperner B., Müller, B., Heidbach, O., Delvaux, D., Reinecker, J. and Fuchs, K. 2003. Tectonic stress in the Earth's crust: advances in the World stress map project, *Geol. Soc. Lond. Spec. Publ*, **212**: 101-116

5.2. Horizontal stresses

Leak-off tests (LOT) and Limit tests (LT) data are available from 18 wells (Goldeneye field and offset wells less than 10km away). This data is plotted in Figure 5.2 that was copied from the recent pore pressure prediction study of Goldeneye[13]. It can be seen that there is a clear change in the trend of the total minimum principal stress gradient that starts at the top of the Chalk group at about 2000m. Sand prone sediments above Chalk group also give some variability to the LOT and have 7% lower LOT values, similar to other North Sea fields.

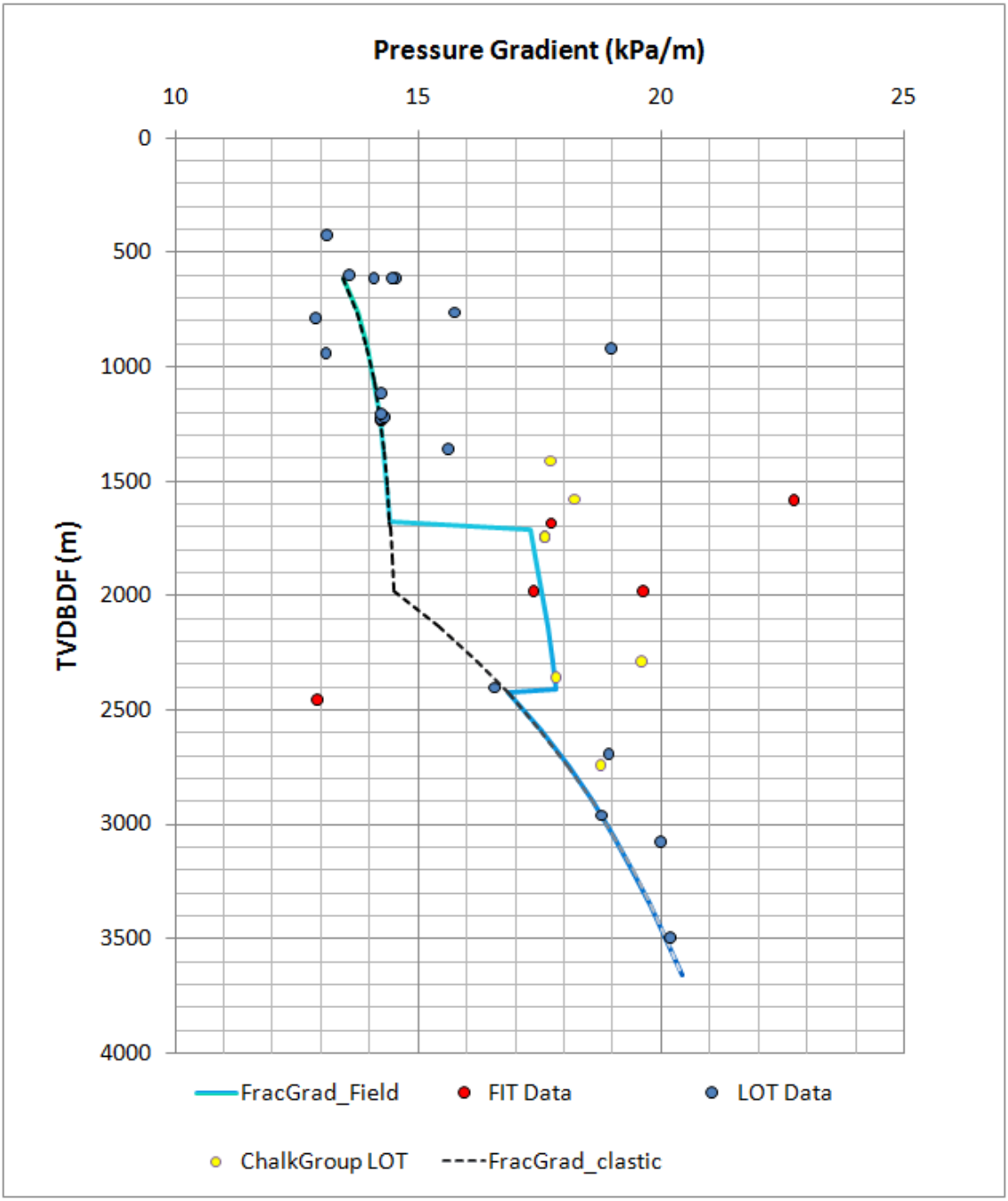

Figure 5.2 **Total minimum principal stress gradient trend is represented as the lower bound of Leak-off Test (LOT) data.**

In the wider Goldeneye area a normal-stress regime is seen so, the vertical stress is larger than the horizontal stresses. Borehole image logs show there is limited extent of borehole breakouts and drilling induced tensile fractures it is reasonable to assume the horizontal stresses are not direction dependent so, maximum and minimum horizontal stresses are assumed to be equal. The small differences in the magnitudes of the horizontal stresses indicate the direction of the maximum horizontal stress is in the NNW-SSE direction. This is based on FMI/CBIL, UBI, and caliper logs, and the World Stress Map[16].

5.3. Pore pressure in overburden and underburden

When overburden formations (and a small part of the underburden) were drilled, pore pressures were found to be hydrostatic[13]. So, a hydrostatic pore pressure gradient of 10kPa/m [0.442psi/ft] – see the Dynamic Modelling Report[11] – is used outside the reservoir and is unaffected by pore pressure changes in the reservoir due to production or injection.

5.4. Pore pressure changes in the reservoir

The Goldeneye field started gas production in 2004 and is assumed to be close to cessation of production at the time of writing this report. CO_2 injection is planned from 2014 till 2024 targeting two million tons of CO_2 per year. History-matched reservoir simulations (modelled by the Shell reservoir simulator software) are available for the production phase. Forward reservoir simulations are done for the CO_2 injection phase.

Key pressure changes, shown in Figure 5.3, are used in "Geomechanical Simulation Software" as a source that leads to stress changes during the production phase for the years 2005-2010 and the injection phase for the years 2014-2025. In between these periods the aquifer is causing the pressures in the reservoirs to rise.

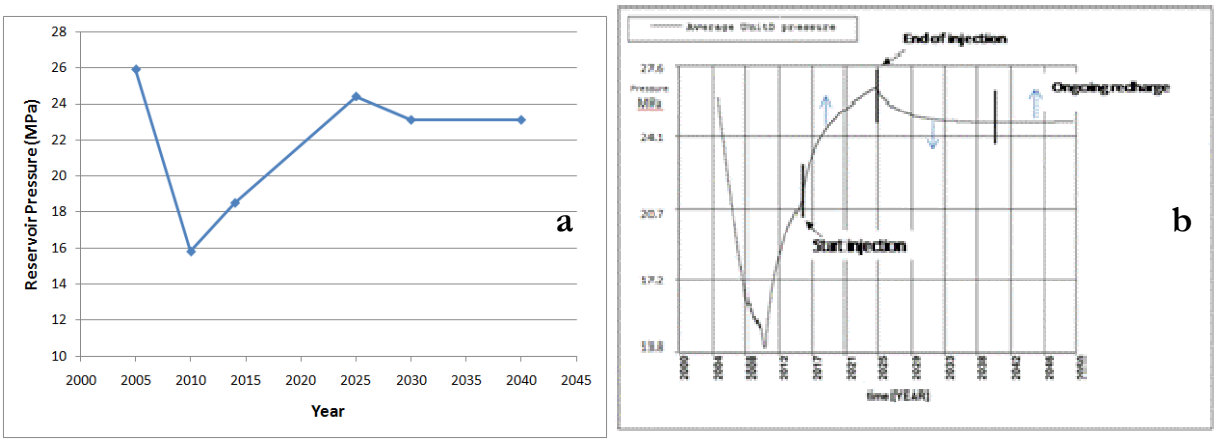

Figure 5.3 **Pore pressure as a function of time for a typical location in the reservoir, (a) schematic ranging from 10–28MPa, and (b) more precise (ranging from 13.8–27.6MPa [2000 – 4000psi]) with arrows indicating possible pressure changes due to uncertainty.**

Reservoir pressures are not uniform in the reservoir but can have different values at different locations (lateral and vertical). The pressures that come from "Simulation Software" (Full Field Model[11]) needed to be rescaled to the mesh used in "Geomechanical Simulation Software" (meter

[16] World Stress Map, http://www.world-stress-map.org

scale to 250m scale). An upscaling method is used whereby vertical compaction is analytically calculated (1D) for both scales and made equal[14]. Maps of upscaled pressures are shown in Figure 5.4.

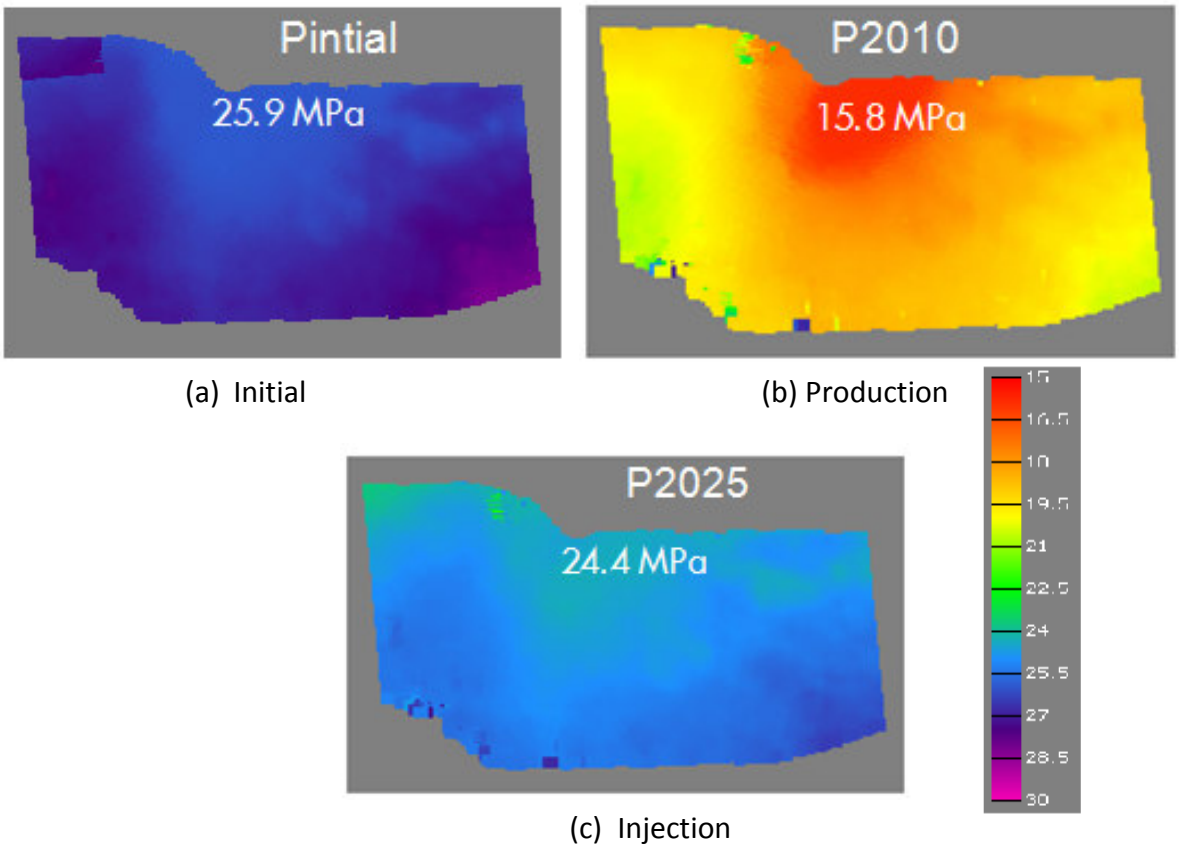

Figure 5.4 **Top view maps of upscaled pore pressures for Captain E&D reservoir formations at initial (a), end of production (b), and end of injection (c) phase. White numbers on the plot indicate typical numbers. Colour scale is in MPa.**

The "Simulation Software" Full Field Model (FFM) also takes pressure effects from the aquifer into account. These pressures were modelled analytically in the FFM.

6. Rock mechanical properties in caprock, over- and underburden

Logs from six wells are available with compressional (DTP) and shear (DTS) wave travel times, and density (RHOB). From this compressional or P-wave speeds, shear or S-wave speeds, dynamic Young's modulus and dynamic Poisson's Ratio can be derived using the standard theory of linear elastic wave propagation in isotropic, homogenous, and lossless solids, *i.e.*,

$$E_{\mathrm{d}} = \rho \mathrm{v_s}^2 \left(\frac{3\mathrm{v_p}^2 - 4\mathrm{v_s}^2}{\mathrm{v_p}^2 - \mathrm{v_s}^2} \right), \tag{5}$$

$$\nu_{\mathrm{d}} = \frac{\mathrm{v_p}^2 - 2\mathrm{v_s}^2}{2(\mathrm{v_p}^2 - \mathrm{v_s}^2)}, \tag{6}$$

where,

E_{d} is the dynamic Young's modulus (Pa),
ν_{d} is the dynamic Poisson's Ratio,
ρ is the density (kg/m^3),
$\mathrm{v_p}$ is the compressional wave velocity (m/s), and
$\mathrm{v_s}$ is the shear wave velocity (m/s).

Figure 6.1 shows the log for well 14_29a-3 with averaged/blocked dynamic elastic rock properties as computed from Equations (5)-(6). For all the over- and underburden formations material behaviour is defined as linear elastic. The average dynamic elastic rock properties for these formations, as listed in Table 6-1, are used in the geomechanical modelling.

Table 6-1 Dynamic elastic rock properties for five overburden and two underburden formations.

Stratigraphic unit	Dynamic Young's modulus [GPa]	Dynamic Poisson's Ration [-]	Density [kg/m^3]
Nordland	2	0.46	2200
Coals	2	0.46	2100
Dornoch sandstone.	4	0.43	2140
Ekofisk, Tor, Hod	32	0.32	2550
Rødby	10	0.38	2440
Humber, Heron	20	0.3	2300

For deformation modelling it is best to use the dynamical properties as they represent best the mechanical properties of the undrained rocks.

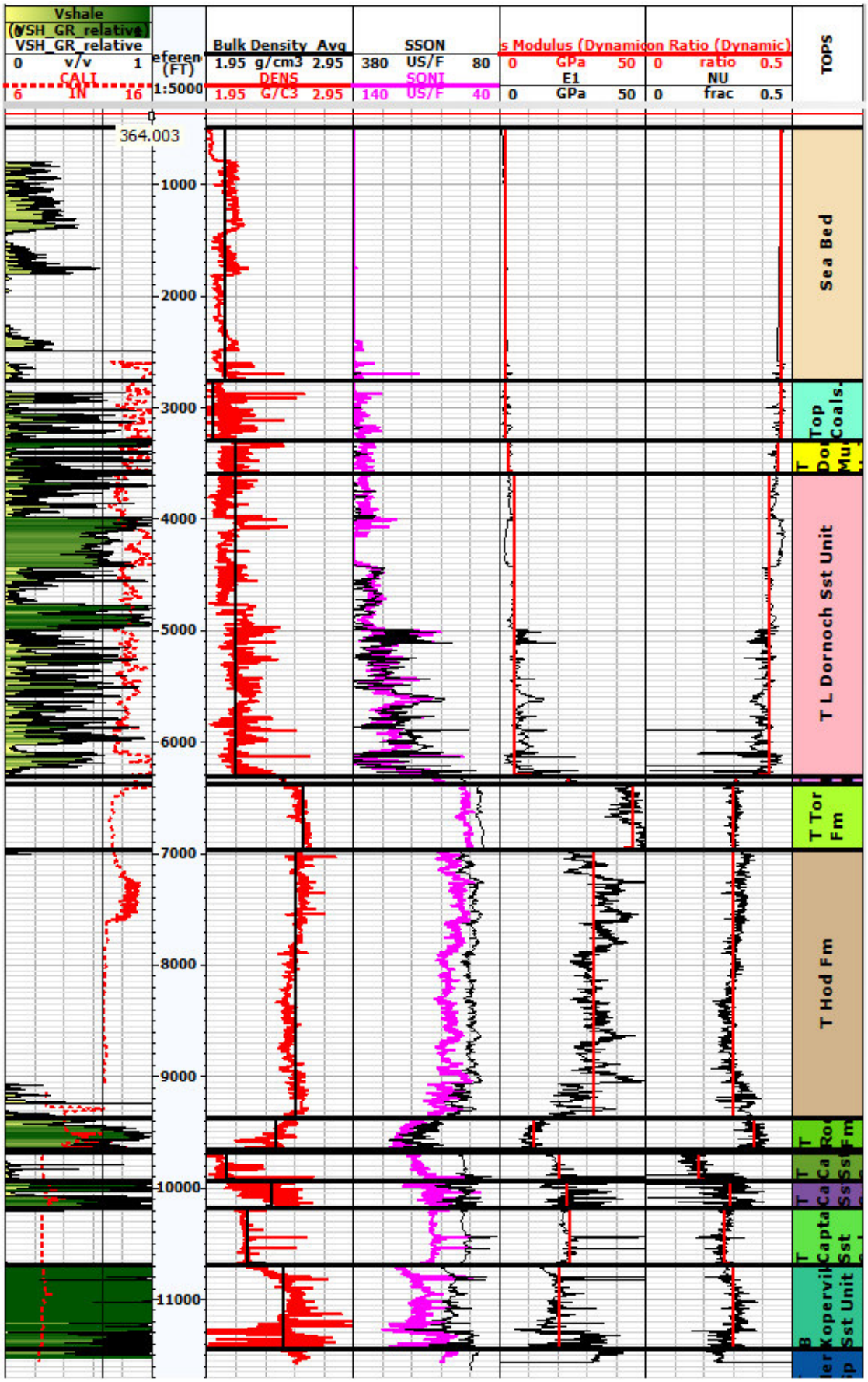

Figure 6.1 Log of well 14_29a-3 with DTP, DTS, RHOB, and derived E_d and ν_d.

6.1. Failure parameters in caprock:

Owing to core degradation, no measurements were taken from core samples of the unpreserved caprock. However, surface area measurements were carried out on shale cuttings taken from the Goldeneye appraisal well 14/29a-3 and can be correlated to the friction angle[17]. The bore hole stability study carried out in 2002 used friction angles between 13° and 22° for the Rødby formation. As sonic log data is also available for the caprock, it is possible to correlate this data to cohesion using Shell proprietary correlations. A few published correlations[18] on shale are used to review the failure parameters from the Shell correlations, see Table 6-2.

Table 6-2 Key findings from literature for failure parameters of the caprock.

Reference	Comment	Cohesion [MPa]	Friction Angle [Deg]
Shell correlations	Based on SA measurements on shale cuttings and sonic log (105 μs/ft)	6.2-8.2	13-22
Lal's correlations[18]	Empirical relation for Friction angle in Shales based on Vp (DTP=105 μs/ft)		29
Mohr-Coulomb failure criterion Eq. (7)	Based on UCS=17.48 MPa from Horsrud's correlation[18] (mostly high porosity tertiary, North Sea shales) and Friction Angle from Lal[18] 29°.	5.1	

Cohesion (C) is calculated from the linear Mohr-Coulomb failure criterion via

$$C = \frac{UCS\,(1-\sin\varphi)}{2\cos\varphi}, \qquad (7)$$

where, UCS is the unconfined compressive strength, and

φ is the friction angle.

Different values for the cohesion and friction angle as displayed in Table 6-2, are due to measured differences in shale lithology within the caprock. For these failure parameters the base case is defined as the lowest numbers that follow from these measurements, *i.e.*, a cohesion of 6MPa and a friction angle of 13°. To investigate the full uncertainty range of the failure parameters worst case values are defined as cohesion = 0 and friction angle = 13°.

[17] Leung, P.K. and Steig, R.P. 1992. Dielectric Constant Measurements: A New, Rapid Method To Characterize Shale at the Wellsite. Paper SPE 23887 presented at the SPE/IADC Drilling Conference, New Orleans, Louisiana, 18-21 February 1992.

[18] Chang, C., Zoback, M. and Khaskar, A. 2006. Empirical relations between rock strength and physical properties in sedimentary rocks, *Journal of Petroleum Science and Engineering* **51** (3-4), 223-237

7. Rock mechanical properties in reservoir

Mechanical rock strength and failure parameters are in general not uniform but have different values at different locations. As the reservoir is the driver (source) to changes in the overall stress distribution accuracy of the geomechanical modelling is increased when non-uniform mechanical parameters will be used in "Geomechanical Simulation Software". Rock properties of the reservoir will be taken from lab measurements, empirical relations, porosity, and NtG. As the latter two come from upscaled values of the reservoir simulator, overall consistency of flow and strength modelling is ensured. Note that the elastic rock properties during production and injection are not necessarily equal. Failure parameters are assumed to be constant in the reservoir and have been measured on some core plugs.

Rock properties are directly measured or derived from another measurement via a physical law or a correlation. Obviously measurements and correlations have uncertainties of which a reasonable range needs to be investigated. This is where balance needs to be found between rigour, time, and available modelling tools (Health, Safety, Security and Environment – HSSE – is never an issue in this balancing act). In this chapter ranges of data will be discussed when possible and likelihood defined (base and worse cases).

7.1. Elastic rock properties for the reservoir during depletion and injection

A uniaxial compressibility test was carried out on plugs taken from the Captain D reservoir rock in the Goldeneye field which yielded a vertical bulk compressibility of 5.4×10^{-7} [/psi] under uniaxial strain conditions for a 25% porosity sample. A uniaxial compressibility-porosity function was established, see Eq. (8) based on this single test result as is shown in Figure 7.1.

$$C_m = 0.3132\ \Phi\ , \tag{8}$$

where,

C_m is the uniaxial bulk compressibility ($\times 10^{-5}$/MPa) at constant pore pressure, and

Φ is the porosity (%).

C_m is allowed to go to zero at zero porosity because it is assumed that the grain compressibility is much, much smaller than the bulk compressibility. This also implies the Biot-Willis coefficient=1.

More lab measurements were carried out recently on Goldeneye Captain reservoir rock. The core sample was loaded and unloaded in a triaxial cell while flushing it with CO_2. Stresses, strains, and elastic wave travel times were measured. Results show a different behaviour between loading the sample (equivalent behaviour from pressure depletion due to gas production) and unloading (equivalent behaviour from pressure increase due to CO_2 injection). This "hysteresis" effect is also discussed in §3.1.2.3 and 10.5. So, the Young's Modulus and Poisson's Ratio have different values during depletion and injection. These material properties are modelled as "bi-linear" in the geomechanical simulator "Geomechanical Simulation Software". Lab results are presented in Table 7-1.

The lab measurements carried out on Goldeneye core before field development showed (via back calculation) values for the Young's modulus in the range of 0.7 - 12 GPa and for the Poisson's Ratio 0.01 - 0.38. The very low values are not representative as these are probably due to measurement errors.

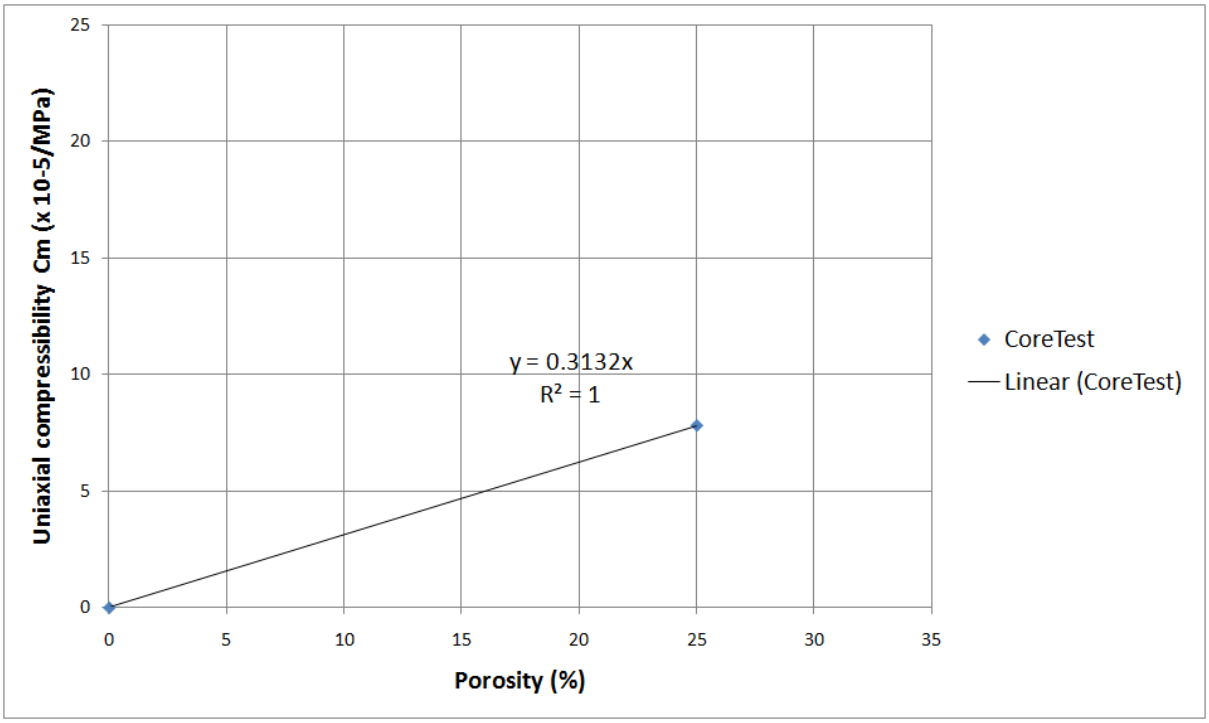

Figure 7.1 **Uniaxial compressibility as a function of porosity for Captain reservoir rock.**

Table 7-1 **Results from triaxial and acoustic tests on Goldeneye reservoir core samples.**

Captain D core tests		Young's modulus [GPa]	Poisson's Ratio [-]
Test 1	Production	12	0.18
	Injection	20	0.26
Test 2	Production	6.9	0.18
	Injection	13.9	0.33
	Grain modulus = 16 GPa		
	Drained thermal expansion coefficient = 11 x 10^{-6} per ^{o}C		

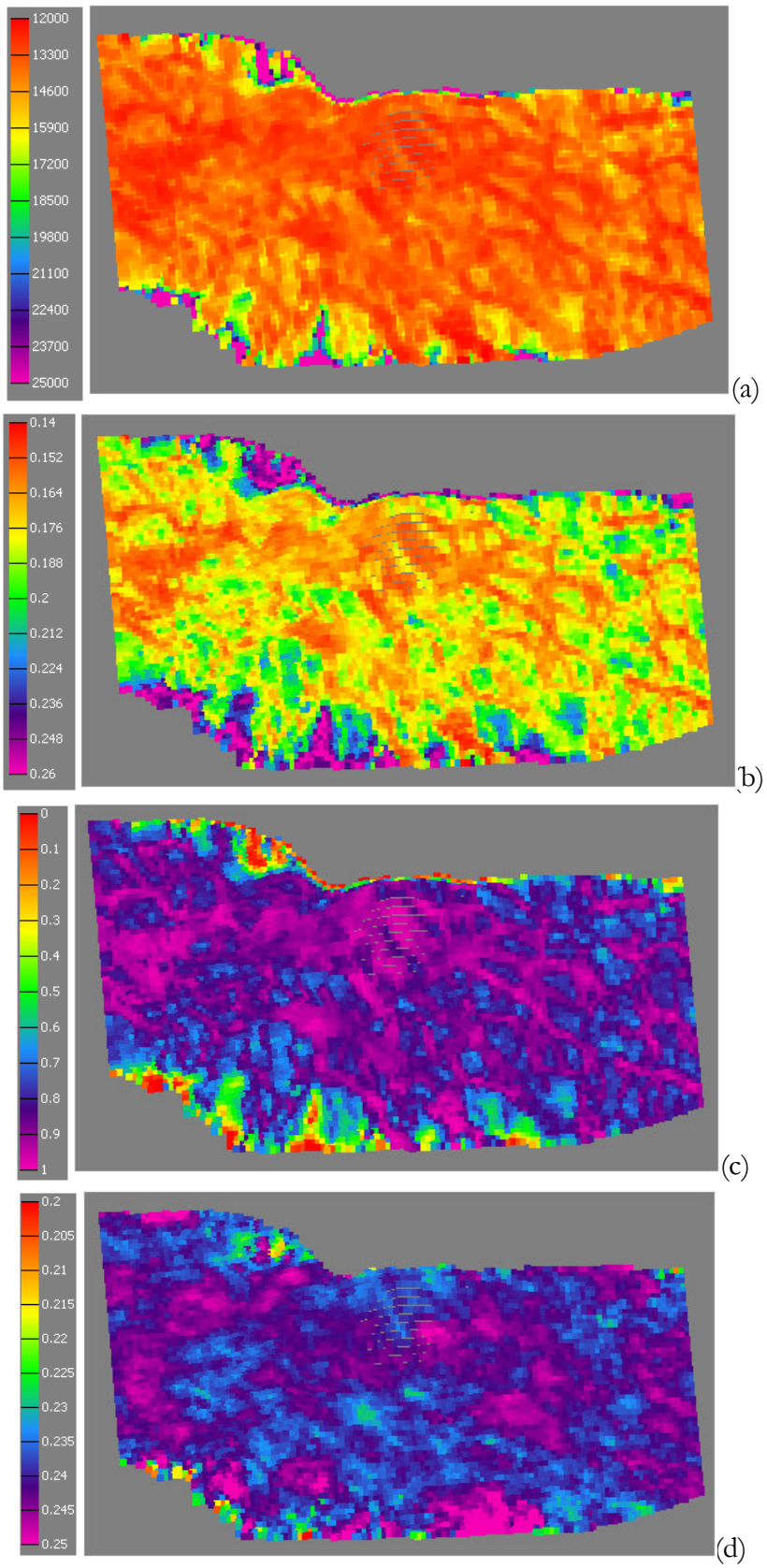

Figure 7.2 **Elastic rock properties combined in Captain E&D reservoir package during production phase, (a) Young's modulus that ranges from 12-25 MPa, (b) Poisson's**

ratio ranging from 0.14-0.26 [-], (c) Net to Gross ranging from 0-1 [-], and (d) porosity ranging from 0.2-0.25 [-].

Given upscaled values for porosity (output from "Simulation Software") it becomes clear the uniaxial compressibility as defined in Eq. (8) will become location dependent. Further, the Poisson's Ratio is also defined as a function that depends on the porosity (a Shell correlation derived from North Sea field data was used). Since the Young's modulus E is related to the compressibility C_m and Poisson's Ratio ν as

$$E = \frac{1}{C_m} * \frac{(1-2\upsilon)(1+\upsilon)}{(1-\upsilon)}, \tag{9}$$

it becomes clear how the Young's modulus and the Poisson's Ratio can be derived within the reservoir. As the upscaling procedure for the pore pressure[14] lies on the basis of the calculation of E and ν, net-to-gross values are also used. Following this procedure leads to distributed values (point sets) for the Young's modulus and Poisson's Ratio for a gross rock as presented in Table 7-2. Note the three reservoir sections have different NtG ratios. It can be observed from Figure 7.2 that Young's modulus and Poisson's ratio distribution follow NtG and porosity distributions for the reservoir – an east-west trend is visible.

The high values of old and new lab measurements (so, NtG=1) during the production phase (see Table 7-1) are well represented in the upscaled elastic rock properties for the Captain E&D sands as shown in Figure 7.2.

Table 7-2 Bi-linear model (which has different elastic rock properties) used to describe the material behaviour during production and injection for all the reservoir formations

Formation	Phase	Young's modulus E [GPa]	Poisson's ratio ν [-]	E and ν derived from	Average Net to Gross
Captain E&D	Production	12-25	0.15-0.26	upscaling methodology[14]	1 (lab test on pure sand)
	Injection	20	0.26	lab test, see Table 7-1	
Captain C	Production	12-30	0.24-0.26	upscaling methodology[14]	0.186 (from reservoir simulator)
	Injection	107 (=20/0.186)	0.26	lab test, see Table 7-1	
Captain A, Valhall, Scapa	Production	12-30	0.18-0.26	upscaling methodology[14]	0.445 (from reservoir simulator)
	Injection	45 (=20/0.445)	0.26	lab test, see Table 7-1	

Note that for simplicity reasons values of E and ν for the injection phase have been taken uniform and equal to the latest lab measurements as presented in Table 7-1.

7.2. Failure parameters in reservoir:

Triaxial tests were done on seven samples from the Goldeneye field looking at failure properties of reservoir rock. Various empirical correlations and rock test results from nearby fields are also analysed in order to arrive at reservoir rock strength parameters namely cohesion and friction angle or angle of internal friction. Table 7-3 shows the key findings.

Table 7-3 Results from literature and experiments of failure parameters of reservoir rock

Reference	Comment	Cohesion [MPa]	Friction Angle [deg]
Goldeneye Triaxial tests	Seven triaxial failure strength measurements were carried out on reservoir core samples	3±1.2	34.4±1.6
Correlation from Weingarten et al.[17]	Empirical relation for Friction angle based on porosity (assumed 25%)		14
Mohr-Coulomb failure criterion Eq. (7) with UCS from Vemik[17]	Based on UCS=26.8 MPa from Vemik et al.[17] (Empirical correlation for very clean, well-consolidated sandstone with porosity<0.30) and Friction Angle from Weingarten[17] 14°.	10.5	

Cohesion (C) is calculated from the linear Mohr Coulomb failure criterion as given by Eq. (7).

Different values for the cohesion and friction angle as displayed in Table 7-3 are due to differences between direct measurements and results obtained via correlations. As these correlations were not derived from Goldeneye data, it is best to use measured failure parameters for the base case, *i.e.*, a cohesion of 3 MPa and a friction angle of 34.4°. To investigate the full uncertainty range of the failure parameters, worst case values are defined as cohesion = 0 and friction angle = 20°.

8. Initialization of the simulation

Shell's "Geomechanical Simulation Software", is used for the computations. "Geomechanical Simulation Software" needs density, horizontal over vertical stress ratios, and azimuth of maximum horizontal stress to be able to compute initial equilibrium. "Geomechanical Simulation Software" applies gravity and initial pore pressure loads, then calculates an equilibrium stress state between the applied loads, applies the boundary conditions and, the assumed initial stress state. As the gravity load is vertical, the lateral stresses are not uniquely constrained by the initial loads and the boundary conditions applied. "Geomechanical Simulation Software" uses an iterative procedure whereby the in situ horizontal stresses at the beginning of each iteration are altered such that they match the specified stress ratios; subsequently an equilibrium state is calculated. This process is repeated until the change in total force balance from one iteration to the next is less than a user specified threshold. In general, mechanical units are not perfectly horizontal and/or there are lateral density changes such that the target stress ratios will never be matched everywhere in the model but, the iteration process assures that they are matched on average. From the six components of the stress tensor three principal stresses are calculated.

Figure 8.1 displays initial total maximum principal stress and initial total minimum principal stress as computed by "Geomechanical Simulation Software". These are in close agreement with vertical stress computed from the density logs in the wells, see §5.1) and total minimum principal stress inferred from the depth trend from LOT data, *c.f.* §5.2. The close agreement can be seen as a calibration of the model in the initial state.

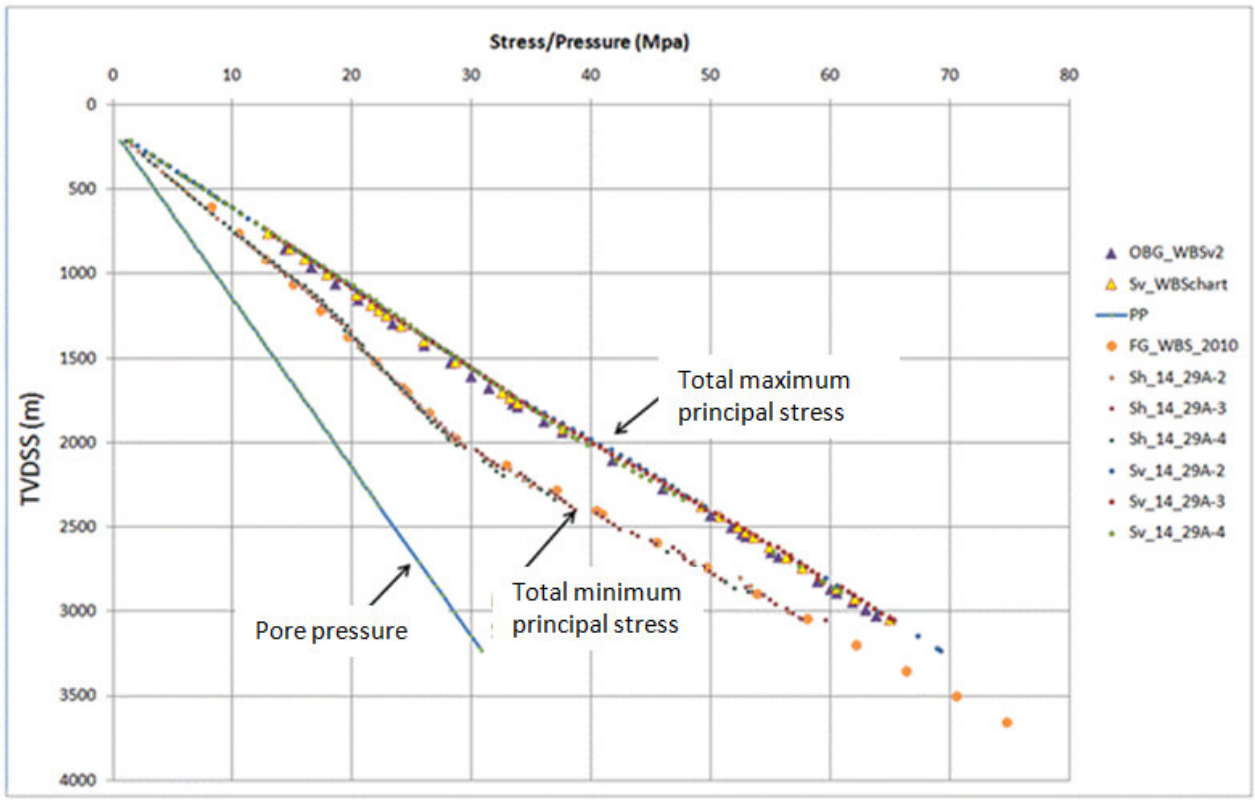

Figure 8.1 **Initial in-situ stresses and pore pressure profile compared to "Geomechanical Simulation Software" computed initial total maximum principal stress and initial total minimum principal stress.**

With this the input of "Geomechanical Simulation Software" is complete and modelling runs can take place. In the next two chapters results will be discussed, first for the base case and in the following chapter different uncertainties will be modelled (the worst cases). Ideally, results should be used to calibrate the model. This is often done by comparing calculated and measured subsidence but, unfortunately, this is not possible as there is no subsidence (or compaction) data available.

9. Modelling results, observations and interpretations

In this chapter results are presented for the geomechanical modelling, before and after gas production, and after CO_2 injection. Material parameters used are from the so-called "Base-case" as discussed in the previous chapters. First vertical deformation will be discussed, then stress changes in the reservoir, and finally there is a section on stress changes in the caprock.

9.1. Compaction and sea-floor subsidence

9.1.1. Production phase

After gas production the pressure in the reservoir has dropped by approximately 10.1MPa (see §5.4). As a consequence the maximum subsidence of the sea-floor and vertical displacement at the top of the Captain E&D reservoir is 4.6 cm and 8.9 cm respectively, see Figure 9.1 and Figure 9.2. The subsidence bowl, as is shown in Figure 9.1, has an extent of about 14 km in the East-West direction and 9 km in the North-South direction. Results indicate no vertical stress arching (non-uniform stresses over a plane due to local out of plane loading) has occurred over the reservoir during depletion. The predicted amount of subsidence is commensurate with observations from other fields producing from similar reservoir rocks in the North Sea[19].

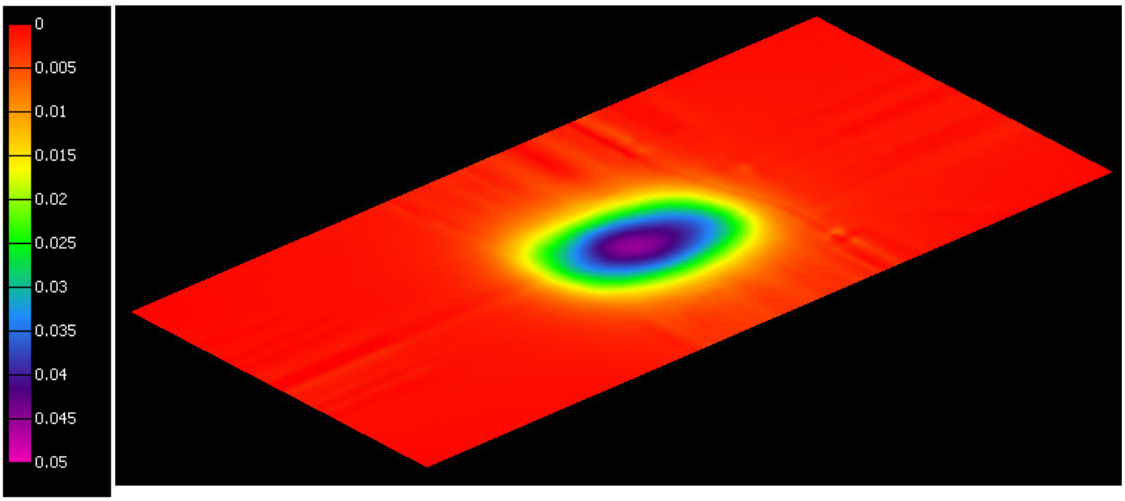

Figure 9.1 **Bird's eye view of the sea-floor with subsidence (max 4.6 cm) after production. Colour scale ranges between 0 and 0.05m.**

9.1.2. Injection phase

After having the gas depleted, CO_2 is injected to a level of 8.6MPa above the maximum depletion value (see §5.4). Then a maximum sea-floor subsidence of 3.6cm is predicted by "Geomechanical Simulation Software", see Figure 9.3. A maximum subsidence of 5.6cm is predicted at the top of the Captain E&D sands, see Figure 9.4. Comparing sea-floor subsidence after the gas production phase (4.6cm) and injection phase (3.6cm) leads to uplift (heave) of only 1cm. due to injection and therefore not leading to subsidence problems that need to be mitigated. The subsidence at the top of the Captain E&D sands after the gas depletion is 8.9cm, the injection will cause an uplift of 3.3cm resulting in a new subsidence of 5.6cm after depletion and injection.

[19] De Gennaro, S., Schutjens, P., Frumau, M., Fuery, M., Ita. J. and Fokker, P. 2010. The Role of Geomechanics in the Development of an HPHT Field. Paper ARMA 10-450 presented at the 44th US Rock Mechanics Symposium, Salt Lake City: Utah, 27-30 June.

Unfortunately these numbers could not be quantified as no subsidence information is available. The amount is of an order that could have been detected via accurate vertical positioning measurements.

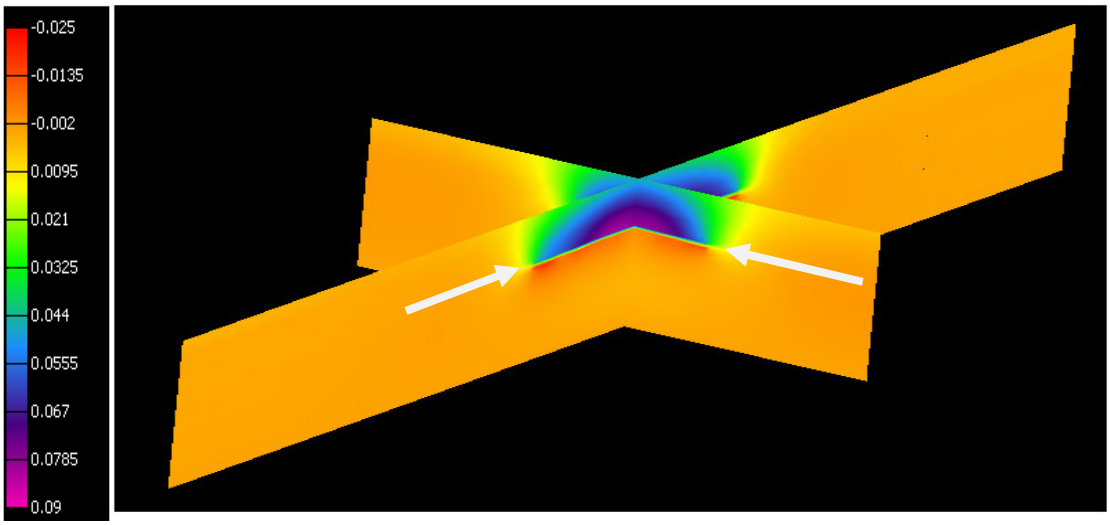

Figure 9.2 **Cross section of overburden, reservoirs (indicated by white arrows), and underburden with vertical displacement (8.9cm at the top of the Captain E&D reservoir) after production. Colour scale ranges from -0.025 to 0.09m.**

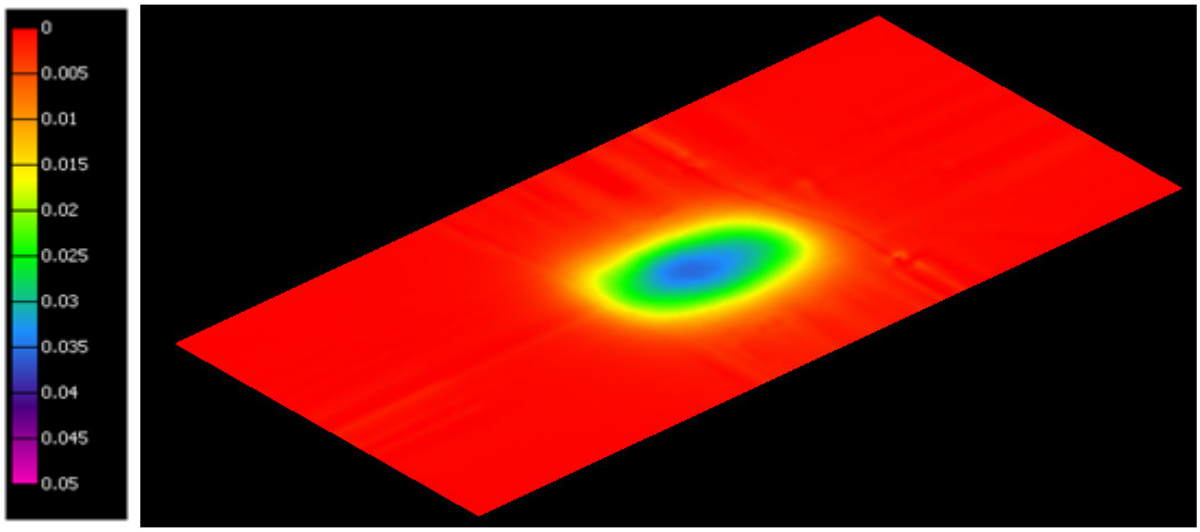

Figure 9.3 **Bird's eye view of seafloor subsidence (max 3.6cm) after injection. Colour scale ranges from 0 to 0.05m.**

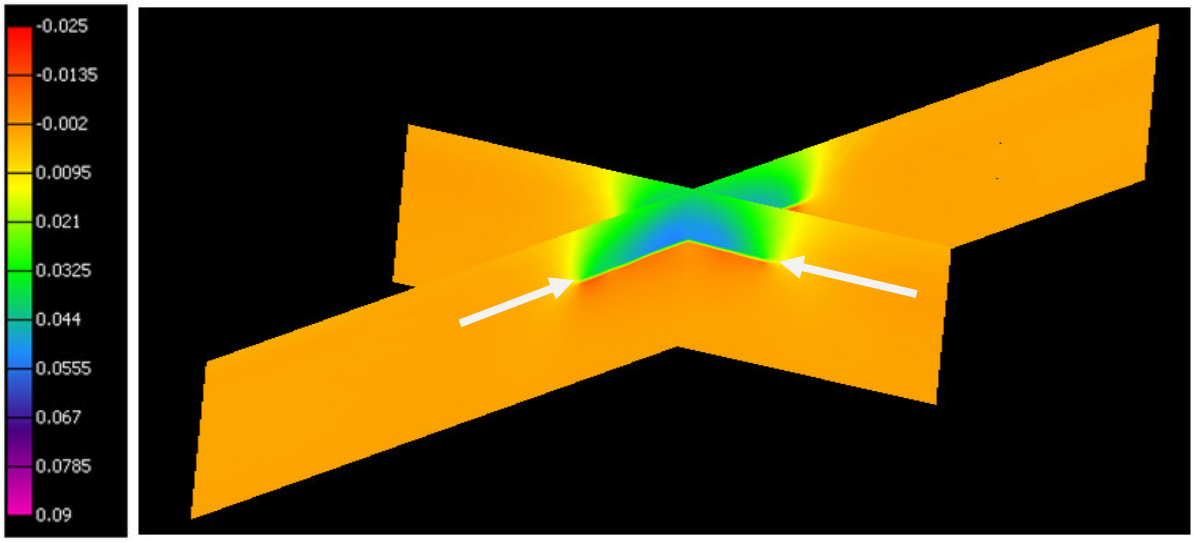

Figure 9.4 **Cross section of overburden, reservoirs (indicated by white arrows), and underburden with vertical displacement (5.6 cm at the top of the Captain E&D reservoir) after injection. Colour scale ranges from -0.025 to 0.09m.**

9.2. Stress changes in the reservoir and definition of failure criteria

Reservoir depletion or injection causes the stress to change inside and outside the reservoir. These changes are greatly affected by the magnitude of pore pressure change, rock properties and structure of the depleting volume. Stress changes can lead to possible tensile or shear failure in the formations (see Figure 9.5), reactivation of existing faults, or slip along very weak overburden layers. Stress changes are often described in terms of stress arching (non-uniform stresses over a plane due to local out of plane loading) by so called gamma factors or depletion constants, see §3.1.2.3 for definitions. Stress changes can lead to possible shear failure in the formations, reactivation of existing faults, or slip along very weak overburden layers.

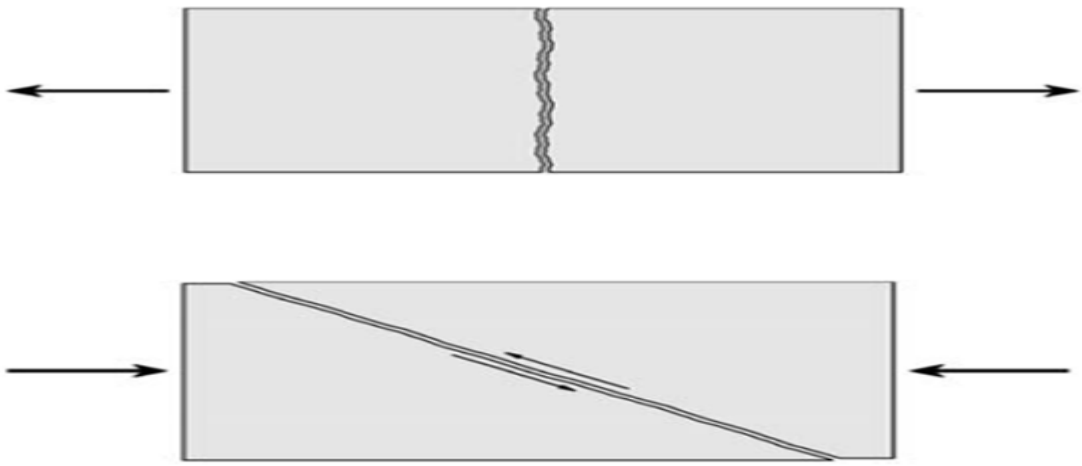

Figure 9.5 **Tensile failure (top) and shear failure (bottom).**

The Mohr-Coulomb shear failure criterion is specified by the cohesion C and the friction angle φ, as outlined by the Mohr-circle diagram in Figure 9.6. The stress condition of a material point is represented by three Mohr circles of which the largest (between the effective principal stresses σ_1 and σ_3) is given in Figure 9.6. A material point under consideration is perceived in an elastic state of deformation if the Mohr circle remains below the failure line, whereas the material is in shear failure if the circle touches the failure line. Stress conditions that cause the Mohr circle to intersect the failure line are not feasible.

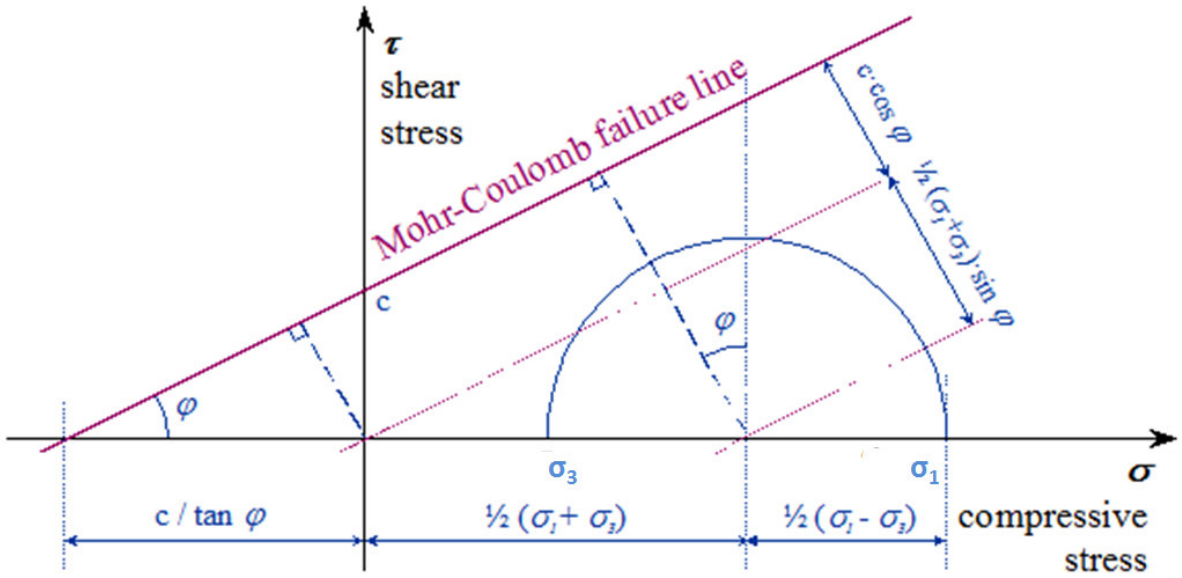

Figure 9.6 **Mohr-circle diagram relating the principal stress state and the Mohr-Coulomb failure condition. The Shear Capacity is represented by the dashed line through the centre of the circle, whereas the actual shear stress is equal to the radius of the Mohr circle.**

The failure condition of a material point can be expressed by the Shear Capacity Utilisation (SCU) that relates the actual level of shear stress with the shear capacity of that point. Alternatively, this is also referred to as the τ/τ_{max} ratio or the Mohr-Coulomb failure ratio. The value for the shear capacity τ_{max} can be calculated from the cohesion C and the friction angle φ as indicate in Figure 9.6 according to:

$$\tau_{max} = C\cos\varphi + \tfrac{1}{2}(\sigma_3 + \sigma_1)\sin\varphi, \qquad (10)$$

where,

σ_1 is the maximum effective principal stress and

σ_3 is the minimum effective principal stress.

The actual shear stress τ that is mobilised is equal to the radius of the Mohr circle:

$$\tau = \tfrac{1}{2}(\sigma_1 - \sigma_3)\,. \qquad (11)$$

Then the Shear Capacity Utilisation becomes

$$SCU = \frac{\tau}{\tau_{max}} = \frac{\frac{1}{2}(\sigma_1 - \sigma_3)}{C\cos\varphi + \frac{1}{2}(\sigma_1 + \sigma_3)\sin\varphi}. \quad (12)$$

By definition, the τ/τ_{max} ratio cannot become larger than 1, because that would require the Mohr circle to intersect the failure line. However, any value beyond 1 can be calculated in the absence of appropriate redistribution of stress due to failure by employing linear elasticity theory only.

SCU plots will be shown in the rest of the report as it is the major tool that easily shows the failure condition of the reservoir or caprock for every pressure state applied to different rock property scenarios. Further, Mohr circles and failure lines are presented for a few selected points where the SCU has relatively high values. At these locations the total maximum and minimum principal stresses along with the absolute pore pressure are taken from "Geomechanical Simulation Software". These locations are within the circle as shown in Figure 9.7. This circle is a schematic outline of the "Area of interest" that is the area in the reservoir where the pressure changes are largest.

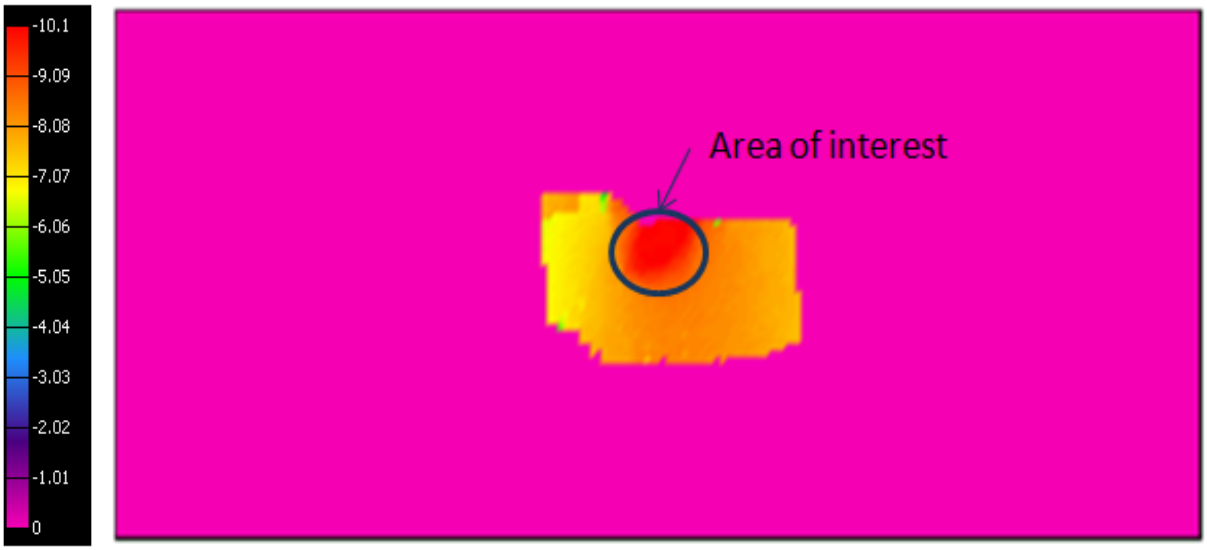

Figure 9.7 **Map view of the pore pressure change from initial to production phase of Captain E&D formation. An area of interest is defined where the absolute pore pressure changes are largest. Colour scale is in MPa.**

Note that the map as displayed in Figure 9.7 shows similarity with results from the "Simulation Software" full field models. This was also observed in relation to Figure 7.2. Obviously the geomechanical modelling uses data (derived) from "Simulation Software", *e.g.*, pore pressures and some rock properties.

In the following sections shear failure will be investigated further. At the end of this chapter there is a section discussing tensile failure.

9.2.1. Production phase

After gas production the pressure in the Captain E&D reservoir has dropped by approximately 10.1MPa (see §5.4). Significant changes in the total minimum principal stress of the Captain reservoirs are predicted and displayed in. Total minimum principal stress changes are negligible outside the reservoir. Very small changes in total maximum principal stress are predicted in the reservoir and outside. The high values at the border and outside the defined "area of interest" (blue

spots or brushes in Figure 9.8) are due to unrealistic jumps in the material properties due to missing data and the "Geomechanical Simulation Software" extrapolation algorithm. These high numbers should therefore be ignored.

As a consequence the maximum subsidence of the sea-floor and the top of the Captain E&D reservoir is 4.6 cm and 8.9 cm respectively, see Figure 9.1 and Figure 9.2.

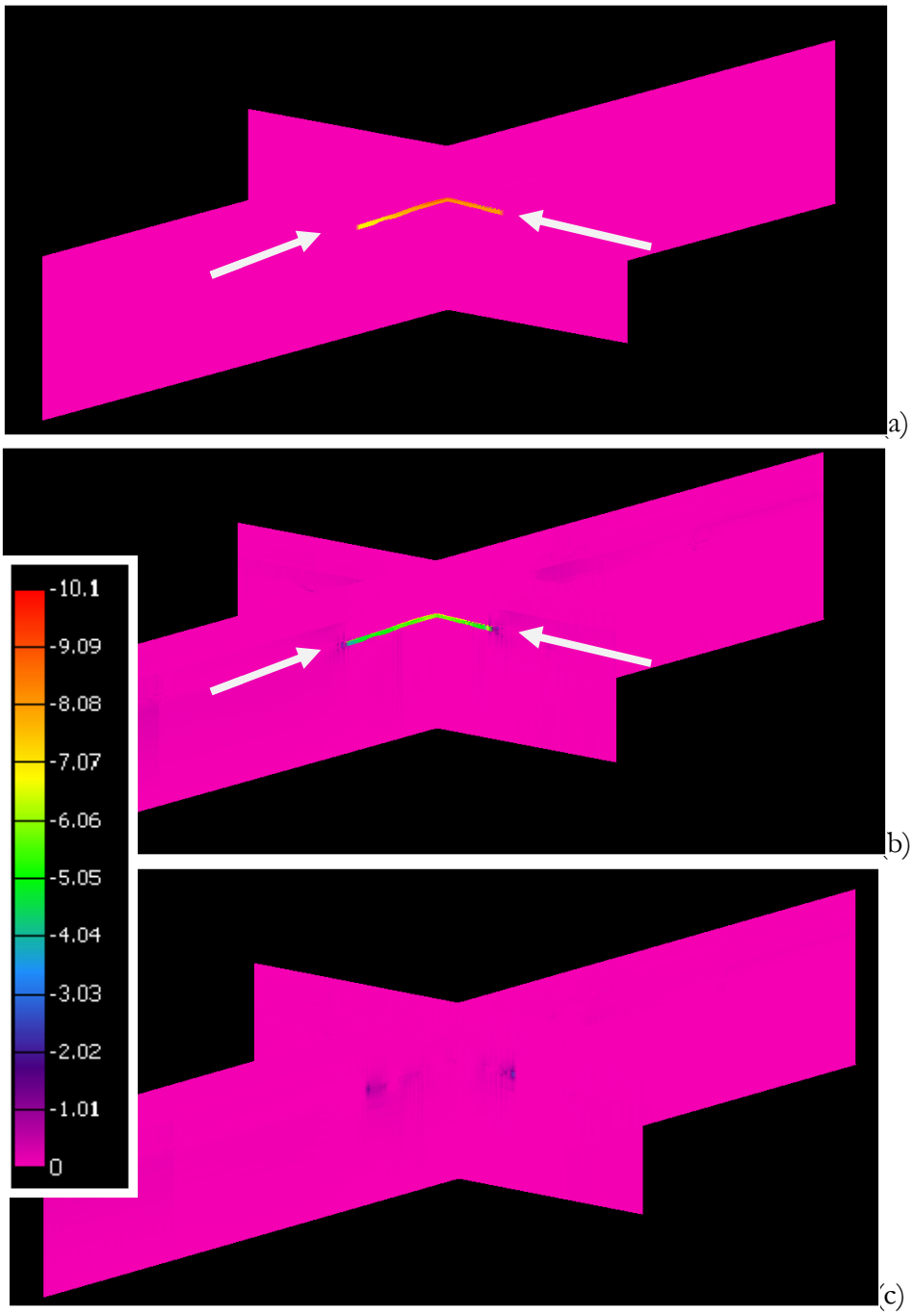

Figure 9.8 **3D bird's eye view of two cross sections through all the formations (reservoir indicated by white arrows) showing (a) reduction in pore pressure from initial to production phase, (b) reduction in total minimum principal stress, and (c) reduction in total maximum principal stress. Colour scale is in MPa.**

For a reduction in pore pressure of 10.1MPa [1465psi] from initial to the end of the production phase for the Captain E&D sands, the reduction in total minimum horizontal stress is predicted to be 8.5MPa as is shown in Figure 9.8 (cross sections) and Figure 9.9 (map view). The gamma horizontal is then 0.84 (8.5/10.1). Reduction in total maximum vertical stress is low and calculated to be 1MPa leading to a gamma vertical of 0.1 (1/10.1). These gamma values will be used for reference when cases will be modelled to explore the effect of uncertainties in relation to hysteresis (see §3.1.2.3).

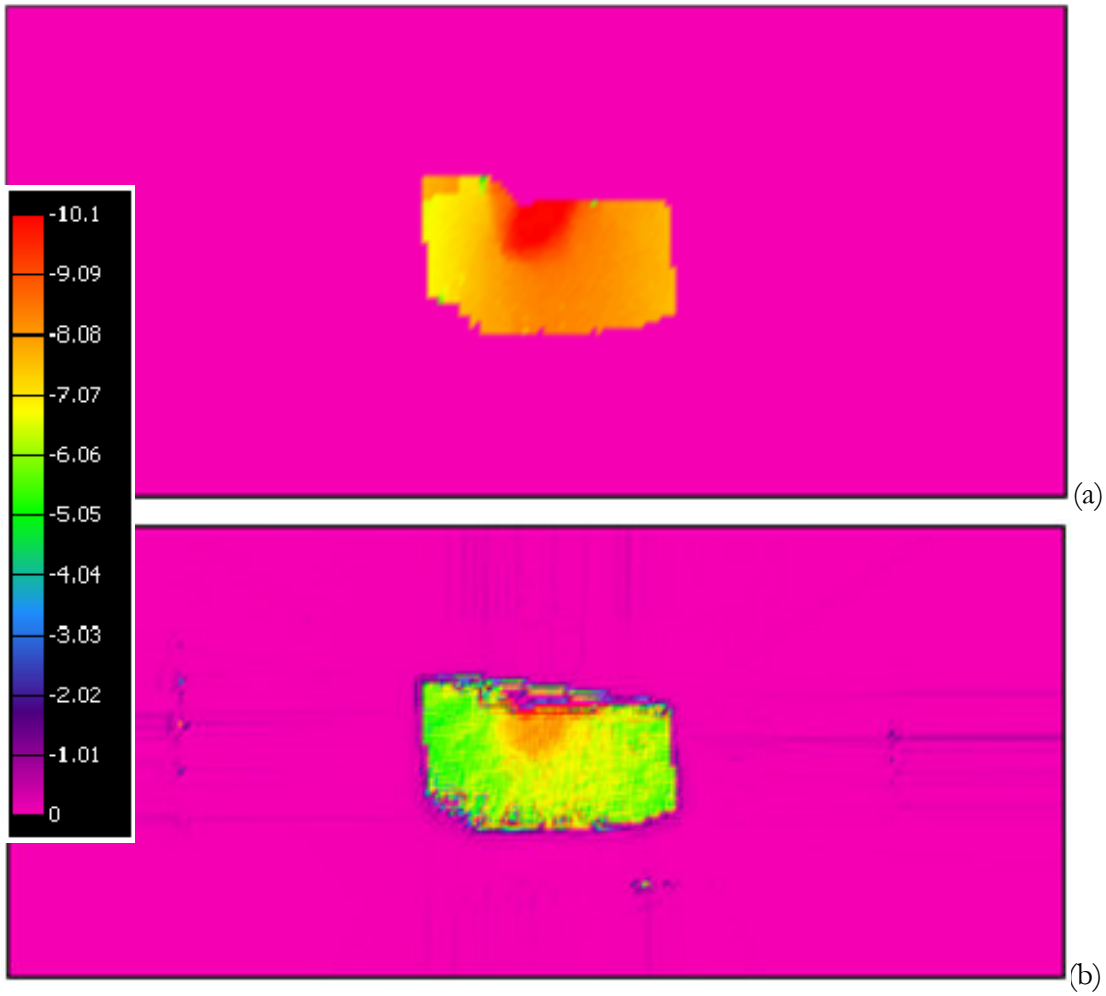

Figure 9.9 **Map view of Captain E&D reservoir showing (a) reduction in pore pressure of 10.1 MPa from initial to production phase, and (b) reduction in total minimum principal stress of 8.5 MPa. Colour scale is in MPa.**

At a point where the SCU was having its largest value in the area of interest as defined in Figure 9.7, a Mohr-Coulomb failure analysis was done before and after production for the Captain E&D reservoir. Results as shown in Figure 9.10 indicate no shear failure as the Mohr circles are well below the failure line. (Note the circles have become ellipsoids due to non equal scales at the axes.) Failure parameters are described in §7.2.

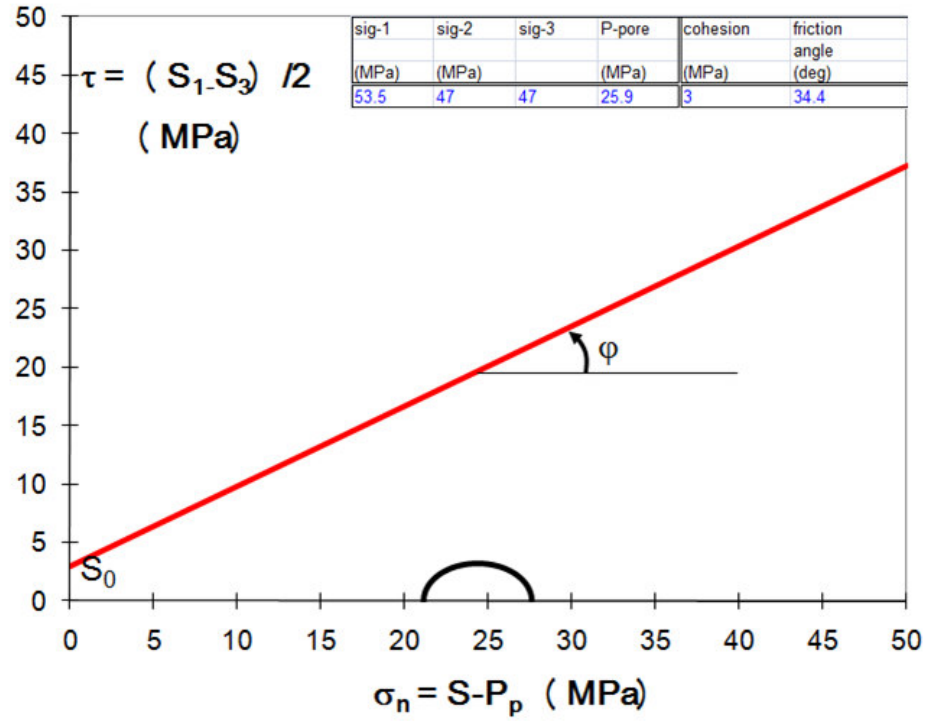

(a)

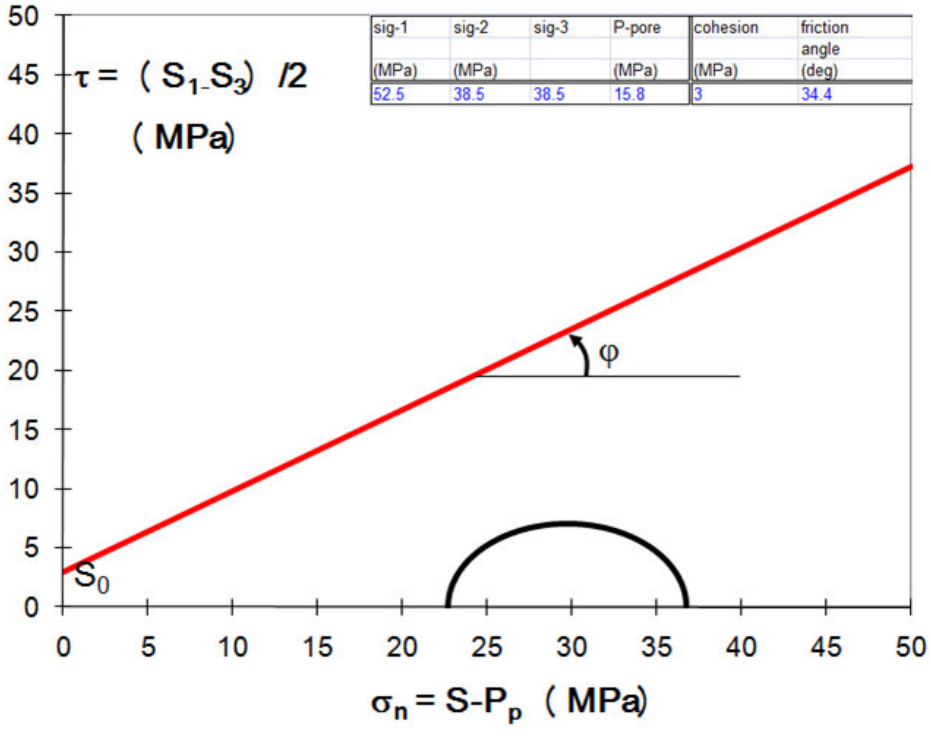

(b)

Figure 9.10 **Mohr circles for Captain E&D reservoir formation at a point in the area of interest (cf. Figure 9.7) before (a) and after (b) production.**

The SCU has been calculated by "Geomechanical Simulation Software" and is plotted in Figure 9.11. The shear capacity increases when going from the initial state of stress to the depleted state but is still well below 1. Therefore no shear failure is predicted for the Captain E&D reservoir after depletion.

This is in line with current field observations, *i.e.*, production data did not indicate shear failure. But, the current production data cannot preclude some shear failure.

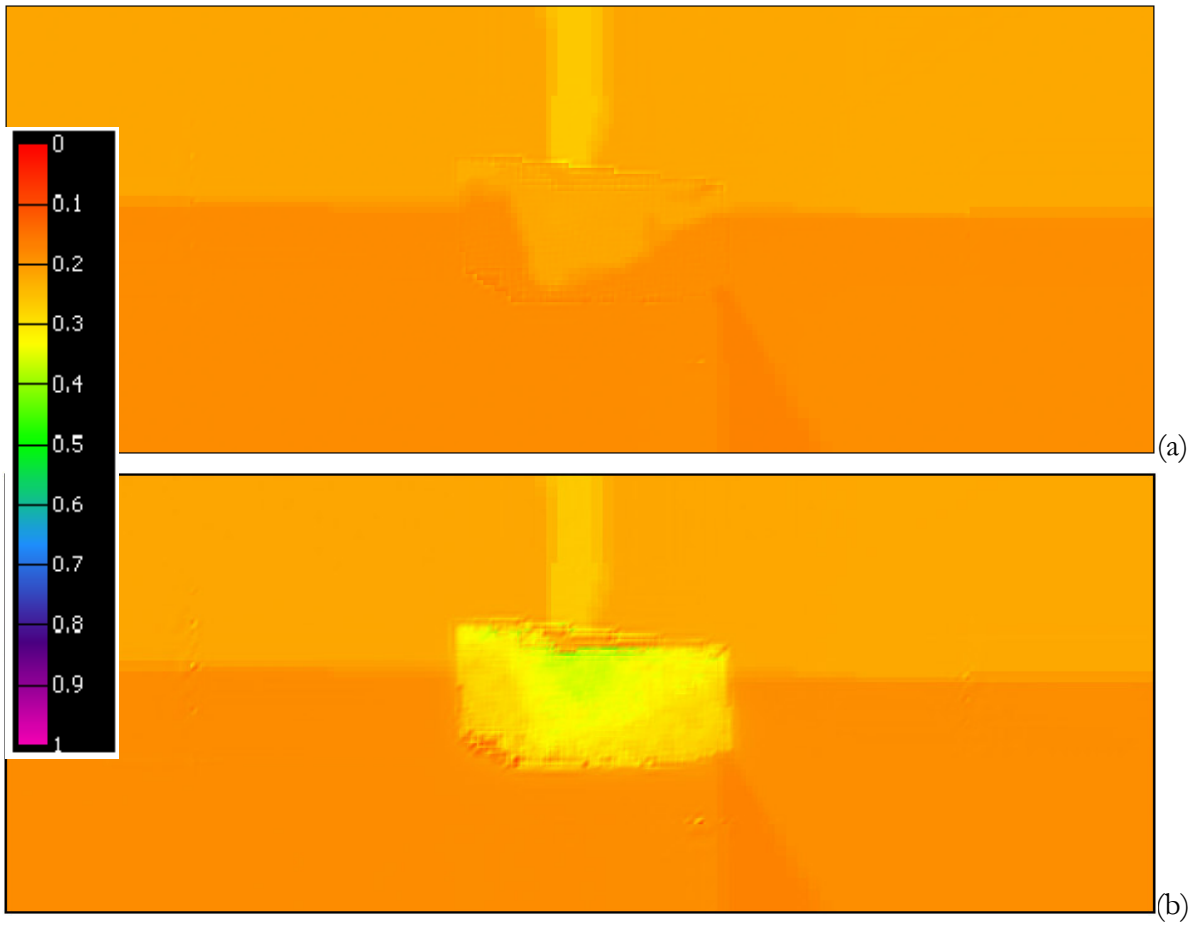

Figure 9.11 Map of shear capacity results for the Captain E&D reservoir at (a) initial state, and (b) after production. Colour scale is dimensionless.

SCU has also been calculated by "Geomechanical Simulation Software" for the Captain A and Captain C reservoir formations. As the shear capacity stays below 1 it might be concluded that this part of the geomechanical modelling is in line with field observations, *i.e.*, production did not report shear failure problems.

9.2.2. Injection phase

After CO_2 injection the pressure in the Captain E&D reservoir has increased by approximately 8.6MPa [1247psi] (see §5.4). Significant changes in the total minimum principal stress of the Captain E&D reservoir due to this increase is predicted and displayed in Figure 9.12. Total minimum principal stress changes are negligible outside the reservoir. Very small changes in total maximum principal stress are predicted inside and outside the reservoir.

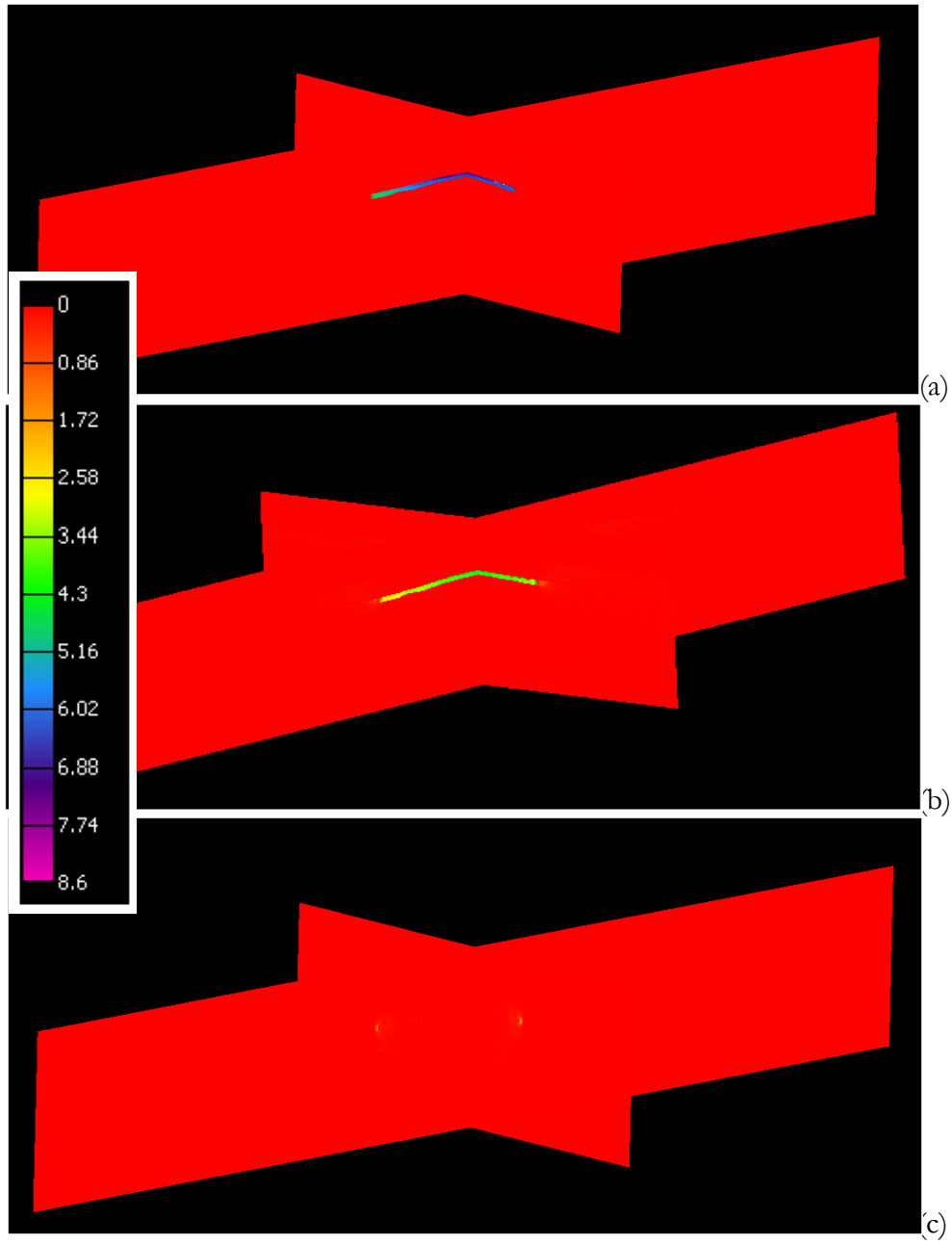

Figure 9.12 **3D bird's eye view of two cross sections through all the formations showing (a) reduction in pore pressure from production to injection phase, (b) reduction in total minimum principal stress, and (c) reduction in total maximum principal stress. Colour scale ranges from 0 – 8.6MPa.**

For a typical increase in pore pressure of 8.6MPa from production to injection phase for the Captain E&D reservoir the increase in total minimum horizontal stress is 6MPa which leads to a gamma horizontal of 0.69 (6/8.6) as is shown in Figure 9.12 (cross sections) and in Figure 9.13 (map view). The total maximum vertical stress is increased by 0.5MPa leading to a gamma vertical of 0.06 (0.5/8.6). These gamma values will be used for reference when cases will be modelled (see §10.5) that explore the effect of uncertainties in relation to hysteresis (see §3.1.2.3).

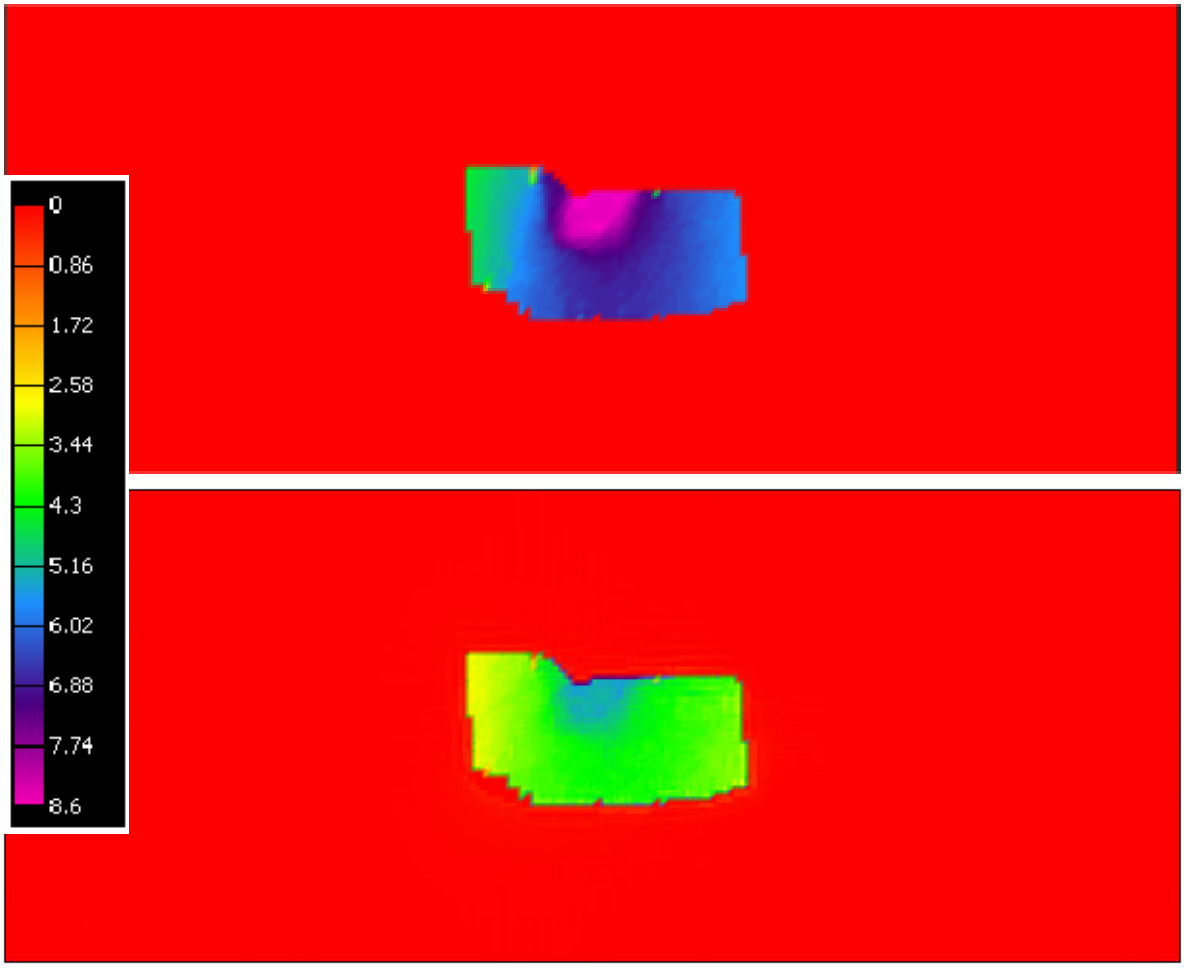

Figure 9.13 **Map view of Captain E&D reservoir showing (a) increase in pore pressure of 8.6MPa from production to injection phase, and (b) increase in total minimum principal stress of 6 MPa. Colour scale ranges from 0 – 8.6MPa.**

At a point where the SCU was having it's largest value in the area of interest as defined in Figure 9.7, a Mohr-Coulomb failure analysis was done after injection for the Captain E&D reservoir. Result as shown in Figure 9.14 indicates no shear failure as the Mohr circle is well below the failure line. (Note the circle is an ellipsoid due to non equal scales at the axes.) Failure parameters are described in §7.2.

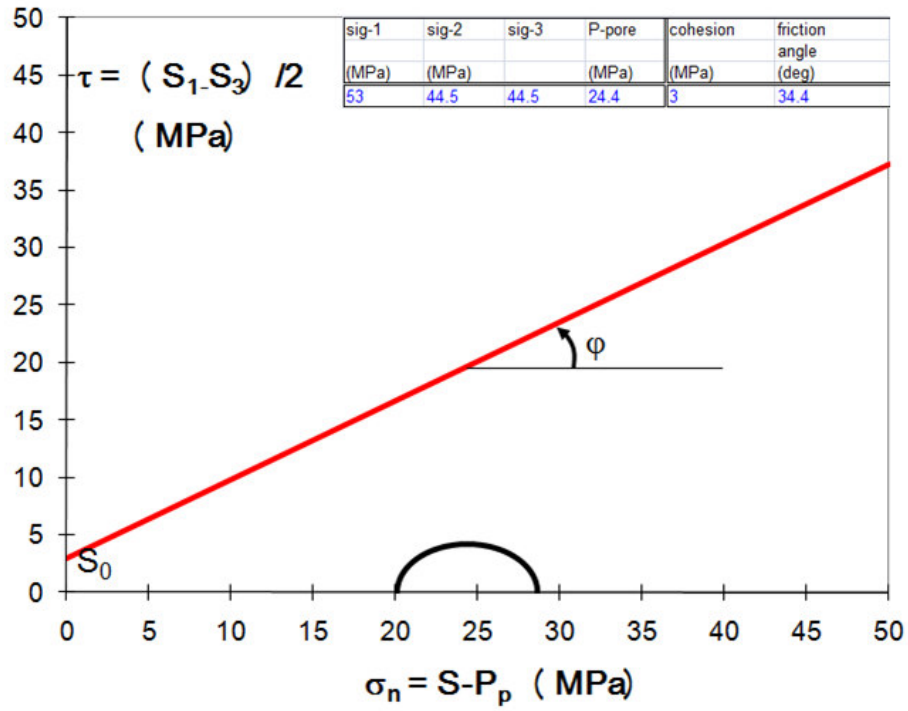

Figure 9.14 **Mohr circle for Captain E&D reservoir formation at a point in the area of interest (cf. Figure 9.7) after injection.**

During injection the minimum principal stress has increased much more than the maximum principal stress leading to a decrease of the radius of the Mohr circle. This explains why the SCU is expected to decrease during injection. The SCU as calculated by "Geomechanical Simulation Software" is plotted in Figure 9.15. The shear capacity decreases during injection but is still well below 1. Therefore no shear failure is predicted for the Captain E&D reservoir after injection.

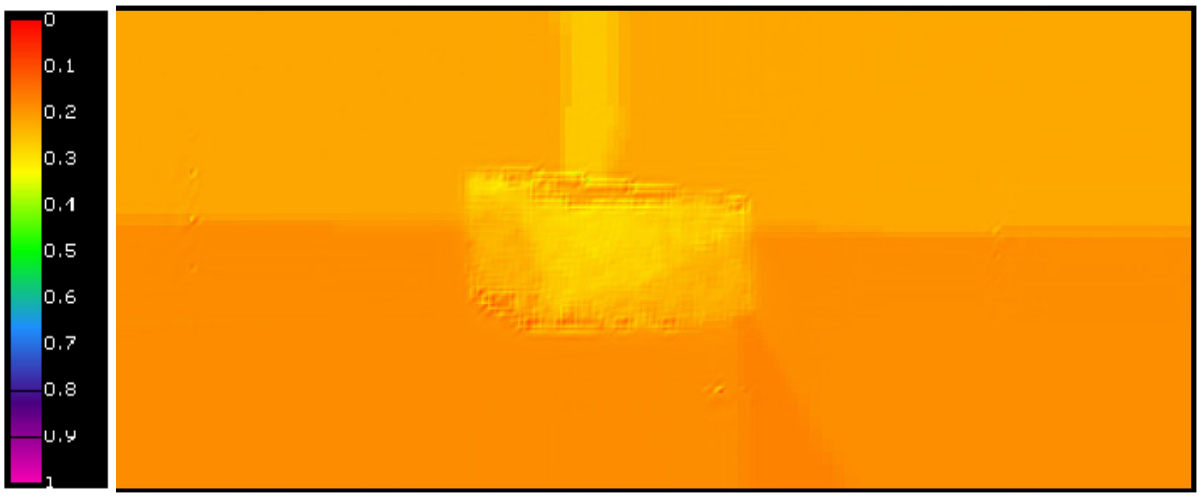

Figure 9.15 **Map of shear capacity results for the Captain E&D reservoir after injection. Colour scale is dimensionless**

SCU has also been calculated for the Captain A and Captain C reservoir formations. As the shear capacity stays below 1 it can be concluded there is no shear failure expected in these reservoirs during injection.

9.3. Stress changes in the Caprock (production and injection)

Stress changes in the reservoir due to production or injection are transferred to the caprock since the top of the Captain reservoir is mechanically connected to the bottom of the Rødby shale. 3D geomechanical modelling is needed to predict stress changes in the caprock.

If the pore pressure in the Captain E&D reservoir is reduced by 10.1MPa (due to gas production) the reduction of the total minimum and maximum principal stresses in the caprock are 0.4MPa and 0.6MPa respectively, see Figure 9.16. Gas production leads to stress changes in the caprock that are small compared to stress changes in the Captain E&D reservoir (*cf.* Figure 9.8).

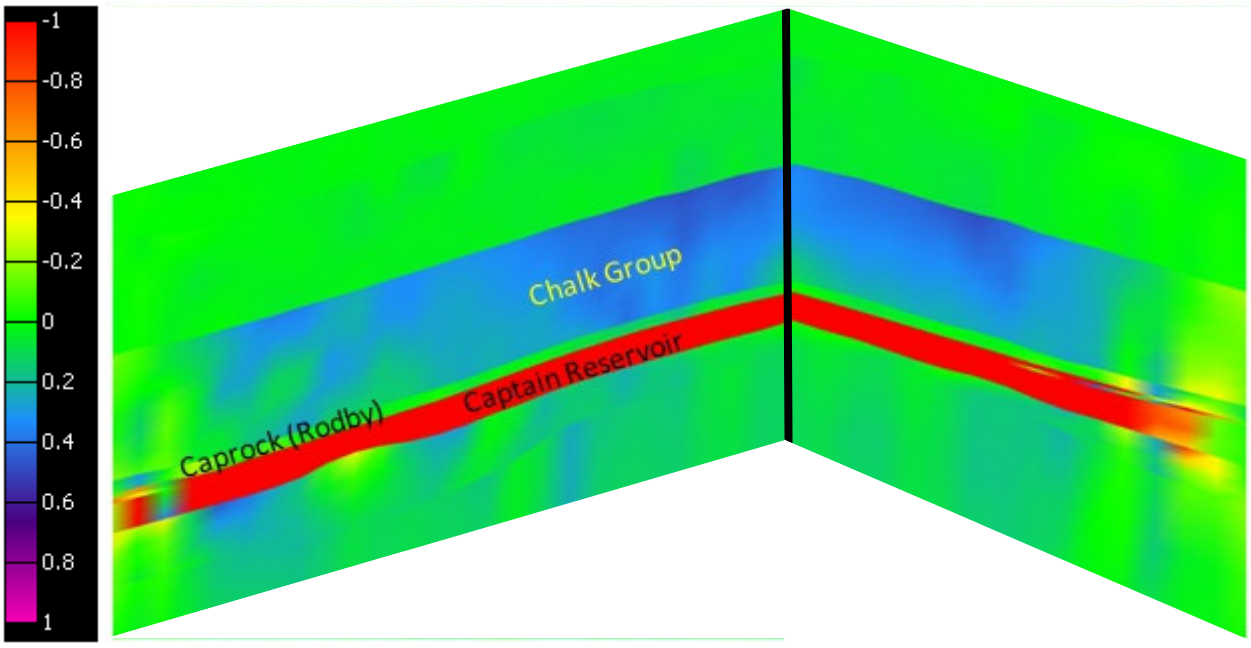

Figure 9.16 **3D zoomed-in bird's eye view of two cross-sections (W-E and N-S, intersecting at black line) through parts of the reservoir, caprock, under- and over-burden. Colours display stress changes of the minimum total principal stress due to gas depletion (after production). Scale is in MPa, values are restricted to be within -1 and +1 MPa.**

These pressure and stress changes are plotted as Mohr circles in Figure 9.17. No shear failure is observed as the Mohr circles are well below the failure line. Failure parameters are described in §6.1.

If the pore pressure in the Captain E&D reservoir is increased by 8.6MPa (due to CO_2 injection after production) the reduction of the total minimum and maximum principal stresses in the caprock are 0.2MPa and 0.35MPa respectively. CO_2 injection leads to stress changes in the caprock that are small compared to stress changes in the Captain E&D reservoir (*cf.* Figure 9.12).

Shear capacity results for the caprock are presented in Figure 9.18. No shear failure is observed in the caprock as shear capacity is less than 1 at initial, after production, and after injection phase.

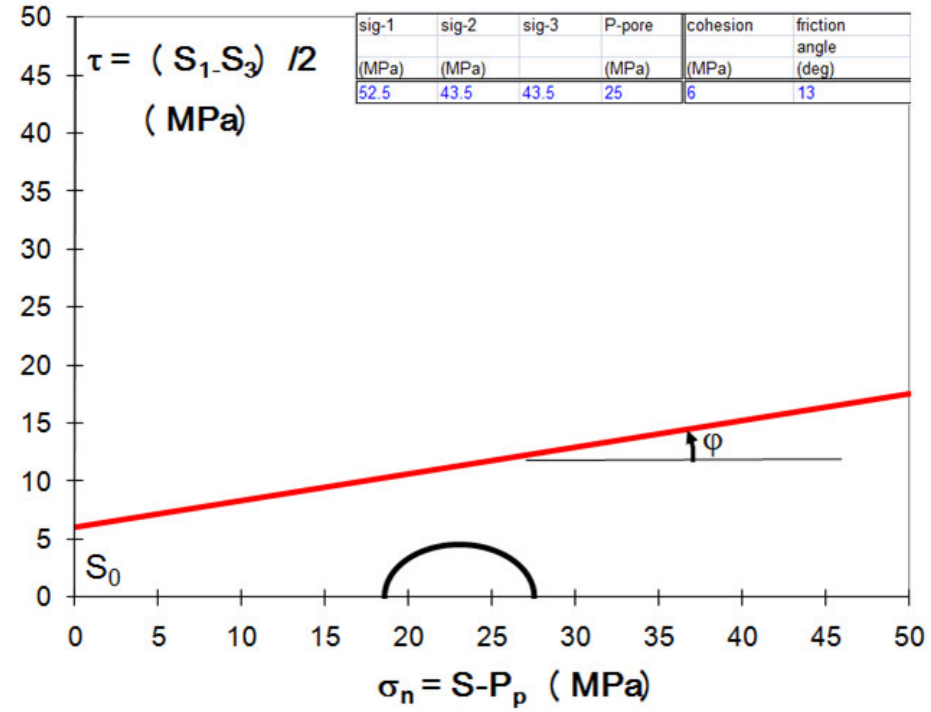

(a)

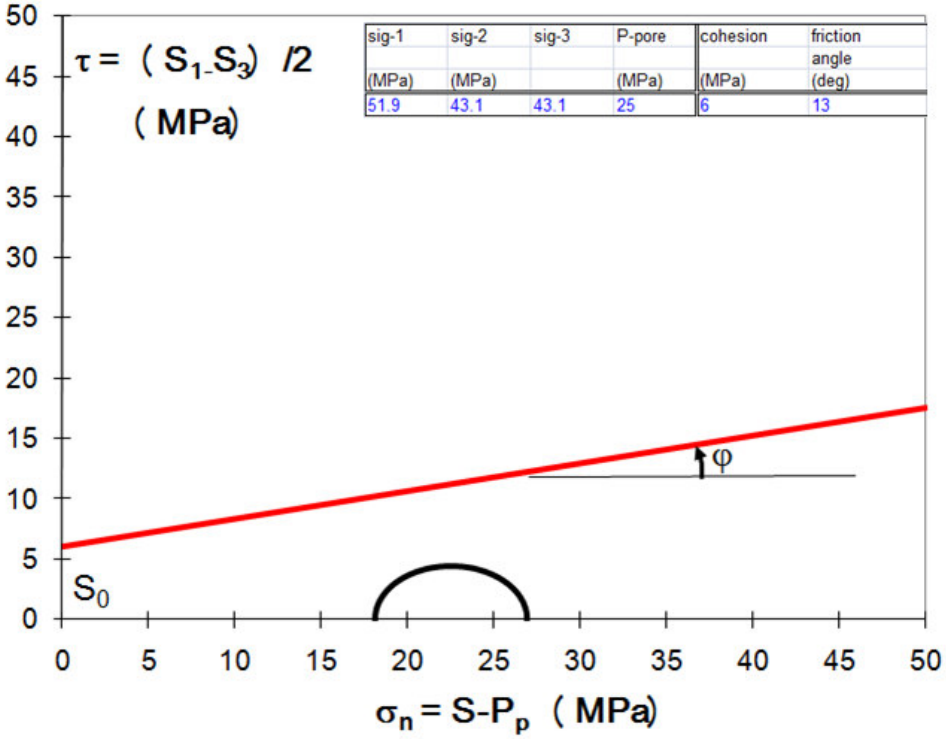

(b)

Figure 9.17 **Mohr circles for the caprock (Rødby shale formation) before production (a) and after production (b).**

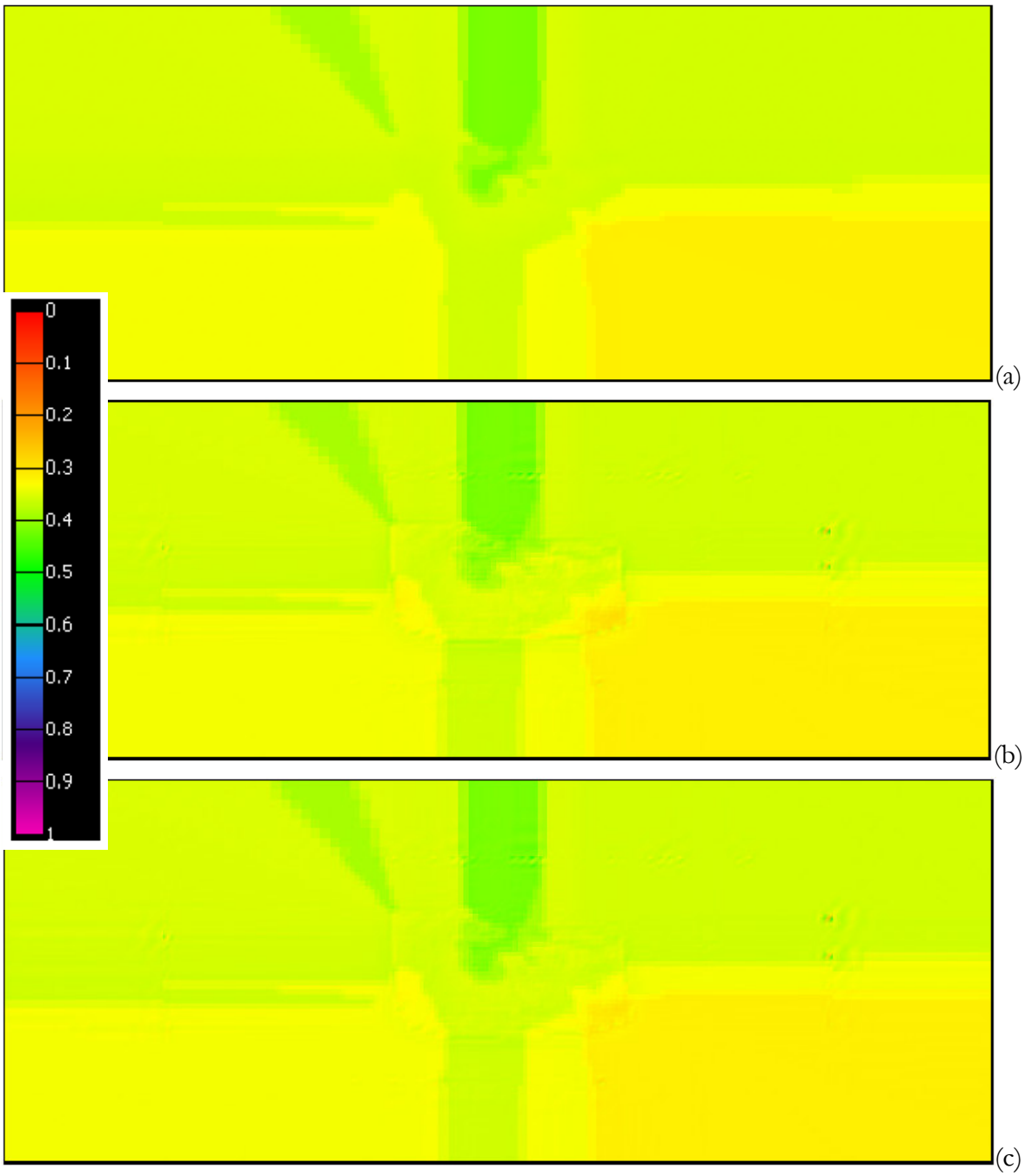

Figure 9.18 **Map of shear capacity results for the caprock (Rødby shale formation) at (a) initial state, (b) after production, and (c) after injection. Colour scale is dimensionless and ranges from 0 - 1.**

9.4. Tensile failure

The Mohr circles as presented in the previous sections show there is no tensile failure at these locations as the minimum effective principal stress is always positive. Figure 9.19 shows a map for the Captain E&D reservoir where the colours display the minimum effective principal stress. The extreme low and high values at the border of the defined "area of interest" are due to unrealistic jumps in the material properties due to missing data and the "Geomechanical Simulation Software" extrapolation algorithm. These numbers should therefore be ignored. As these stresses are positive

everywhere, it can be concluded there is no tensile failure after the gas has been depleted and after the CO_2 has been injected.

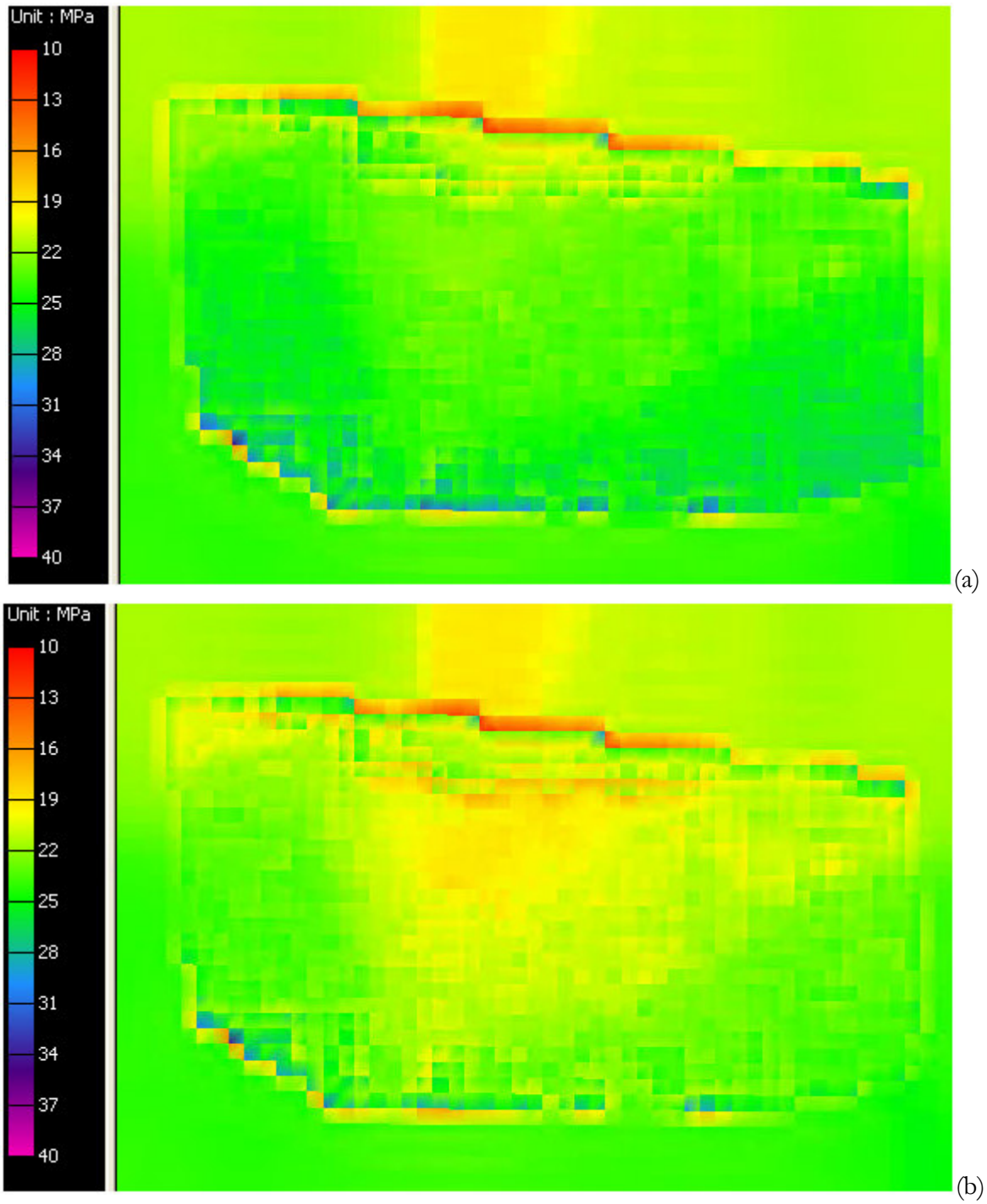

Figure 9.19 **Minimum effective principal stress after gas depletion (a) and after injection (b). Colour scale ranges from 10 – 40MPa.**

10. Uncertainty analysis

As all input parameters of the underlying geomechanical study have uncertainties it is important to extend the modelling by investigating the effect of different parameters, especially those that affect the integrity of the reservoir and caprock most. Table 10-1 gives an overview of the parameters that were varied in the reservoir and caprock, *i.e.*, rock strength parameters (Young's modulus and Poisson's Ratio), rock failure parameters (cohesion and friction angle), and pore pressure.

Table 10-1 Cases that were modelled to investigate the effect of different rock properties and pressures in the integrity of the reservoir and caprock.

Case	Described in Section	Description of modelled cases
A	Chapters 4 - 9	Base case
B	10.1	Same as Base case except Poisson's Ratio is increased by 0.05 for the three Captain reservoir formations for both production and injection phase
C	10.2	Same as Base case except Poisson's Ratio is decreased by 0.05 for the three Captain reservoir formations for both production and injection phase
D	10.3	Same as Base case except Young's modulus in over- and underburden are reduced by half compared to the Base case
E	10.4	Same as Base case except failure parameters are reduced to worst case, i.e., cohesion=0 and friction angle=20° for the reservoir while cohesion=0 and friction angle=13° for the caprock
F	10.5	Same as case E and Poisson's Ratio increased from 0.26 to 0.45 for all three reservoir formations during the injection phase
G	10.6	Same as Base case but now with pressure support from aquifer and worst case rock failure parameters of reservoir and caprock
H	10.7	Maximum injection pressure is increased to a value that is higher than the hydrostatic pressure by adding 2.2MPa to the Base case injection pressure and worst case rock failure parameters of reservoir and caprock
I	10.8	Base case pressures after gas depletion are lowered by 2MPa to a level where the absolute minimum pressure is 13.8MPa [2000psi]. Also worst case rock failure parameters of reservoir and caprock are used

In the following sections results are presented for the Captain E&D reservoir and the Rødby formation (caprock). Results will focus on shear failure. Tensile failure has not been predicted from the geomechanical modelling of the cases as described in Table 10-1.

For reference the most important results for the base case that were presented in §9 are summarised in Table 10-2. Pressure and stress state numbers area also shown on all Mohr circle plots. Note that these numbers were taken at a location in the area of interest (as defined in Figure 9.7) where the SCU was having its largest value. This holds for all tables in the following sections.

Table 10-2 Base case results

Case A		Change of pore pressure ΔP [MPa]	Change of minimum principal stress $\Delta\sigma_3$ [MPa]	Change of maximum principal stress $\Delta\sigma_1$ [MPa]	Maximum SCU (approx)
Reservoir Captain E&D	Initial to production	15.8-25.9= -10.1	38.5 – 47.0 = - 8.5	52.5 – 53.5 = - 1.0	0.5
	Production to injection	24.4 – 15.8 = +8.6	44.5 – 38.5 = + 6.0	53 – 52.5 = + 0.5	0.3
Rødby Caprock	Initial to production	25 – 25 = 0	43.1 – 43.5 = - 0.4	51.9 – 52.5 = - 0.6	0.5
	Production to injection	25 – 25 = 0	43.3 -43.1 = + 0.2	52.25 - 51.9 = 0.35	0.5

10.1. Uncertainty analysis, Case B: Poisson's Ratio + 0.05

Poisson's Ratio of the Base case was increased by 0.05 for the three Captain reservoir formations for both production and injection. This change was chosen to represent the high value in the uncertainty range as seen on the logs, *e.g.*, Figure 6.1. Changes in total minimum and maximum principal stresses are summarized in Table 10-3. Stress changes in the Captain E&D reservoir are small compared to the base case while stress changes in the caprock are equal to the base case.

Table 10-3 Key results for Case B (as obtained in the area of interest)

Case B		Change of pore pressure ΔP [MPa]	Change of minimum principal stress $\Delta\sigma_3$ [MPa]	Change of maximum principal stress $\Delta\sigma_1$ [MPa]	Maximum SCU (approx)
Reservoir Captain E&D	Initial to production	-10.1	-8.0	-1.2	0.5
	Production to injection	+8.6	+5.5	+0.5	0.3
Rødby Caprock	Initial to production	0	-0.4	-0.6	0.5
	Production to injection	0	+0.2	+0.35	0.5

Shear capacity results for Case B of the Captain E&D reservoir at initial state of stress are the same as presented in Figure 9.11(a). Shear capacity results after production and after injection are displayed in Figure 10.1. No shear failure is predicted as shear capacity is less than 1. Shear capacity is marginally decreased compared to the Base case *cf.* Figure 9.11(b) and Figure 9.15.

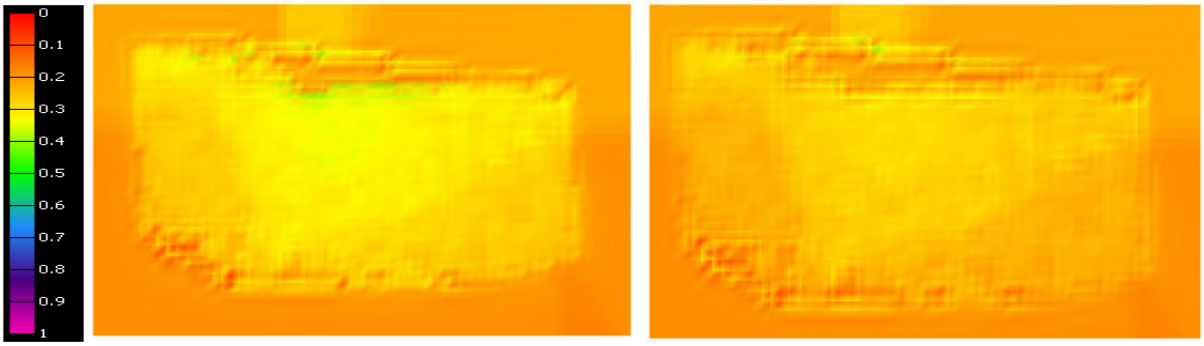

Figure 10.1 **Map of shear capacity results for Captain E&D formation (a) during production and (b) during injection. Colour scale is dimensionless.**

10.2. Uncertainty analysis, Case B: Poisson's Ratio - 0.05

Poisson's Ratio of the base case was decreased by 0.05 for the three Captain reservoir units for both production and injection. This change was chosen to represent the low value in the uncertainty range as seen on the logs, e.g., Figure 6.1. Changes in total minimum and maximum principal stresses are summarized in Table 10-4. Stress changes in the Captain E&D reservoir are small compared to the base case while stress changes in the caprock are equal to the base case.

Table 10-4 **Key results for Case C (as obtained in the area of interest)**

Case C		Change of pore pressure ΔP [MPa]	Change of minimum principal stress $\Delta\sigma_3$ [MPa]	Change of maximum principal stress $\Delta\sigma_1$ [MPa]	Maximum SCU (approx)
Reservoir Captain E&D	Initial to production	-10.1	-9.0	-1.2	0.5
	Production to injection	+8.6	+6.5	+0.6	0.3
Rødby Caprock	Initial to production	0	-0.4	-0.6	0.5
	Production to injection	0	+0.2	+0.35	0.5

Shear capacity results for Case C of the Captain E&D reservoir at initial state of stress are the same as presented in Figure 9.11(a). Shear capacity results after production and after injection are displayed in Figure 10.2. No shear failure is predicted as shear capacity is less than 1. Shear capacity is marginally increased compared to the Base case *cf.* Figure 9.11(b) and Figure 9.15.

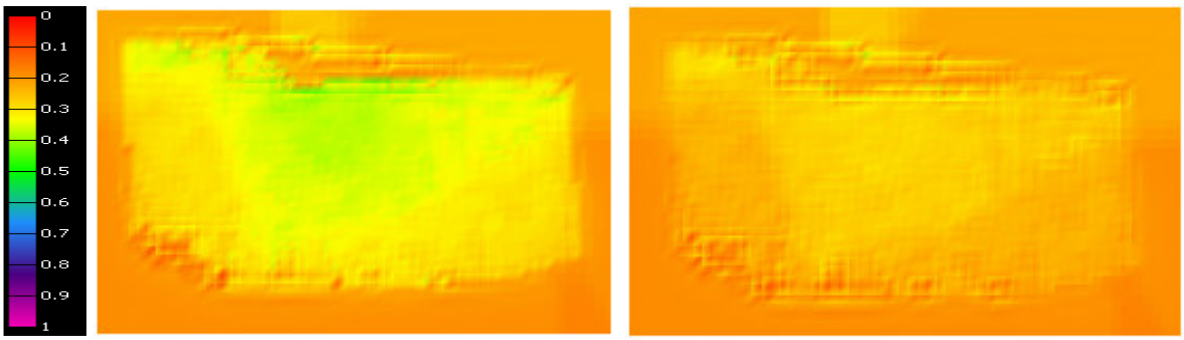

Figure 10.2 **Map of shear capacity results for Captain E&D formation (a) during production and (b) during injection. Colour scale is dimensionless and ranges between 0 and 1.**

10.3. Uncertainty analysis, Case D: Young's modulus in half for over- and underburden formations

Young's modulus of the base case was decreased by 50% for the over- and underburden formations for both production and injection. This change was chosen to represent the low value in the uncertainty range as seen on the logs, e.g., Figure 6.1. Changes in total minimum and maximum principal stresses are summarized in Table 10-5. Stress changes in the Captain E&D reservoir and the caprock are very small compared to the base case.

Table 10-5 **Key results for Case D (as obtained in the area of interest)**

Case D		Change of pore pressure ΔP [MPa]	Change of minimum principal stress $\Delta\sigma_3$ [MPa]	Change of maximum principal stress $\Delta\sigma_1$ [MPa]	Maximum SCU (approx)
Reservoir Captain E&D	Initial to production	-10.1	-8.5	-1.0	0.5
	Production to injection	+8.6	+6.0	+0.3	0.3
Rødby Caprock	Initial to production	0	-0.4	-0.6	0.5
	Production to injection	0	+0.2	+0.35	0.3

Shear capacity results for Case D of the Captain E&D reservoir at initial state of stress are the same as presented in Figure 9.11(a). Shear capacity results after production and after injection are displayed in Figure 10.3. No shear failure is predicted as shear capacity is less than 1. Shear capacity is marginally changed compared to the Base case cf. Figure 9.11(b) and Figure 9.15.

Shear capacity results for Case D of the Rødby caprock at initial state of stress are the same as presented in Figure 9.18(a). Shear capacity results after production and after injection are displayed in Figure 10.4. No shear failure is predicted as shear capacity is less than 1. Shear capacity is marginally decreased compared to the Base case *cf.* Figure 9.18(b) and (c).

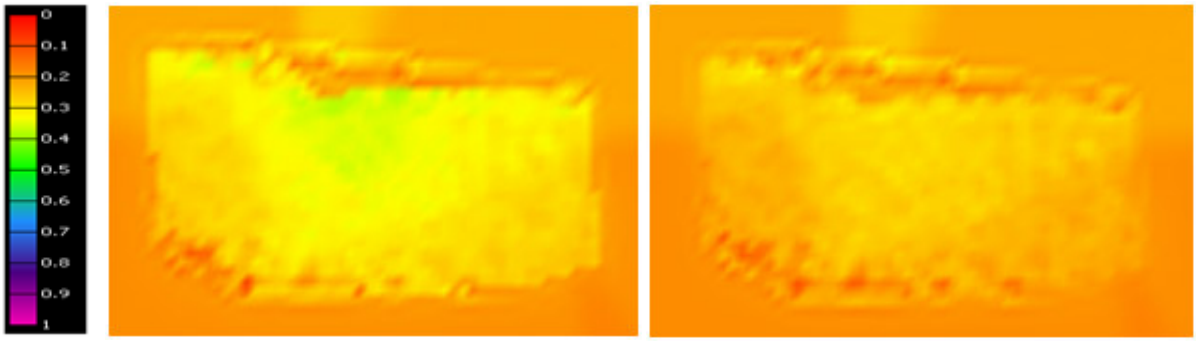

Figure 10.3 Map of shear capacity results for Captain E&D formation (a) during production and (b) during injection. Colour scale is dimensionless and ranges between 0 and 1.

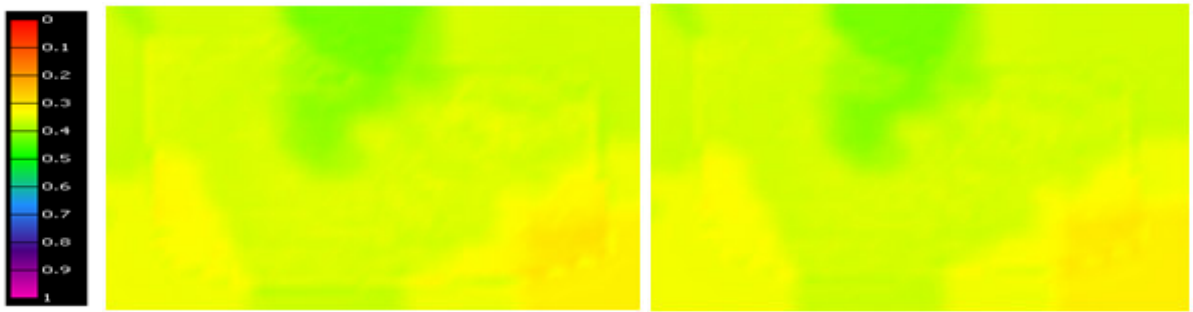

Figure 10.4 Map of shear capacity results for caprock formation (Rødby) (a) during production and (b) during injection. Colour scale is dimensionless and ranges between 0 and 1.

10.4. Uncertainty analysis, Case E: Worst case rock failure parameters of reservoir and caprock

In this section pressure and stress changes are used from the base case but, the rock properties that describe the failure are taken to be different. Cohesion and friction angle are changed to the worst case values for all the Captain reservoirs and the caprock. Results are summarised in Table 10-6 and described in the following two sections. Shear failure is not expected as the SCU < 1 at all locations.

Table 10-6 Key results for Case E (as obtained in the area of interest)

Case E		Change of pore pressure ΔP [MPa]	Change of minimum principal stress $\Delta\sigma_3$ [MPa]	Change of maximum principal stress $\Delta\sigma_1$ [MPa]	Maximum SCU (approx)
Reservoir Captain E&D	Initial to production	-10.1	-8.5	-1.0	0.80
	Production to injection	+8.6	+6.0	+0.5	0.65
Rødby Caprock	Initial to production	0	-0.4	-0.6	0.90
	Production to injection	0	+0.2	+0.35	0.92

10.4.1. Reservoir formation (Captain E&D)

Failure parameters of the reservoir formations are reduced to a cohesion of 0 (representing an unconsolidated porous reservoir sandstone) and a friction angle of 20°. These very low values are considered to be the worst case failure numbers for the rock properties of the Captain reservoir. As a consequence the shear capacity utilization (SCU) τ/τ_{max} or the Mohr-Coulomb failure ratio will get worse as becomes clear from Eqs. (10)-(12). Graphically speaking, the failure line gets closer to the Mohr circle. This is shown in Figure 10.5 (cf. Figure 9.10 and Figure 9.14). (Note the circles have become ellipsoids due to non equal scales at the axes.)

Shear capacity results for all locations of the Captain E&D reservoir are displayed in Figure 10.6. The high values at the border and outside the defined "area of interest" are due to unrealistic jumps in the material properties due to missing data and the "Geomechanical Simulation Software" extrapolation algorithm. These high numbers should therefore be ignored. As expected the SCU increases when going from initial to production and decreases when going to injection. SCU numbers for a typical location in the area of interest are presented in Table 10-6. No shear failure is predicted in any of the phases as shear capacity is below 1.

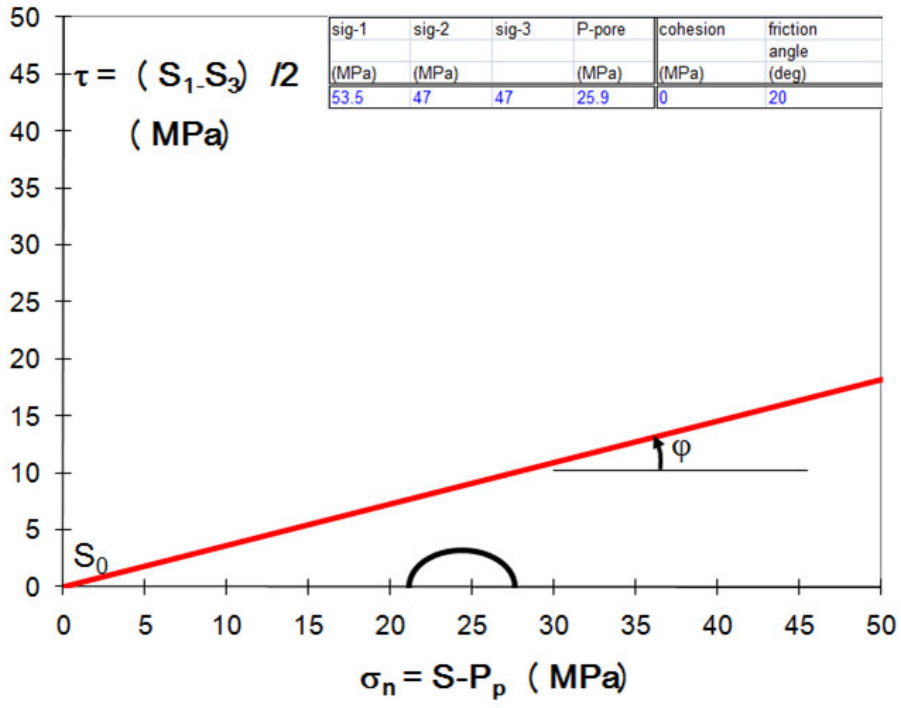

(a)

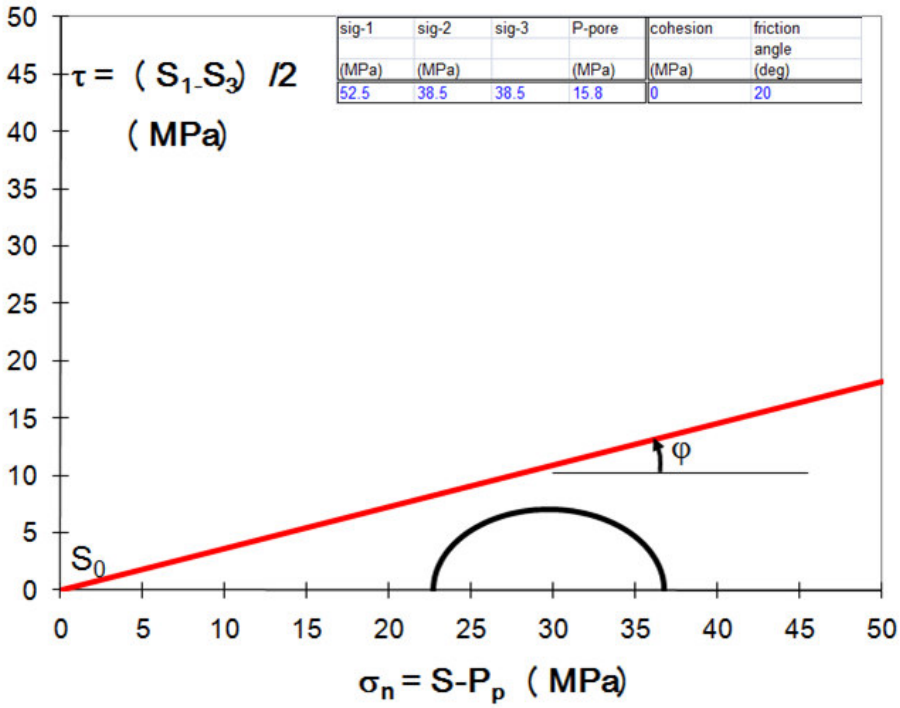

(b)

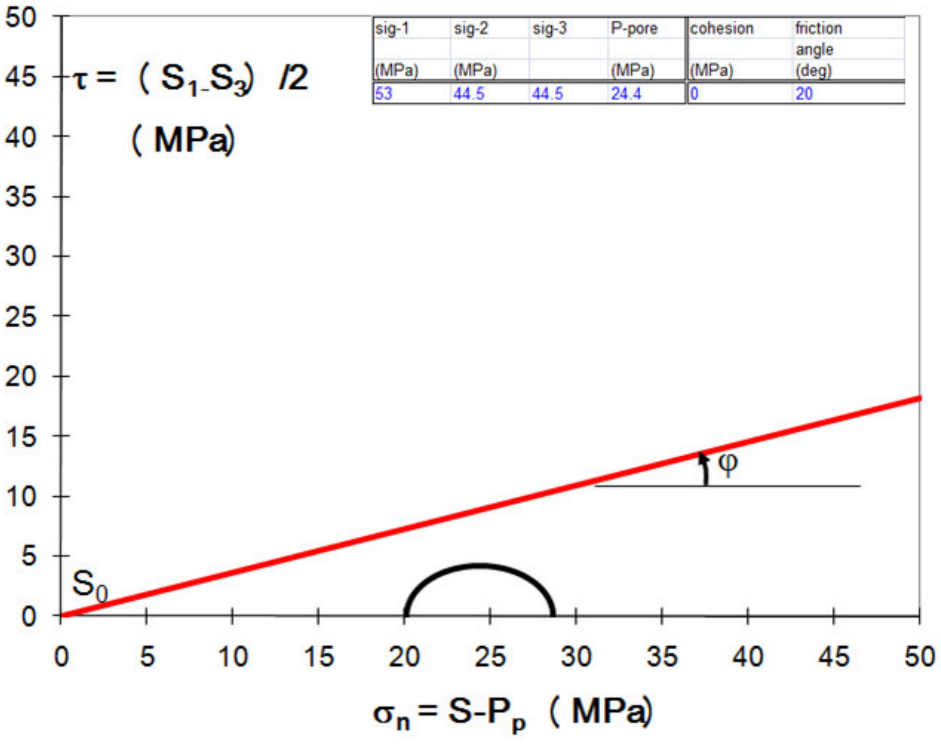

(c)

Figure 10.5 **Mohr circle for the Captain E&D formation with worst case failure parameters at (a) initial state of stress, (b) state of stress after production, and (c) state of stress after injection.**

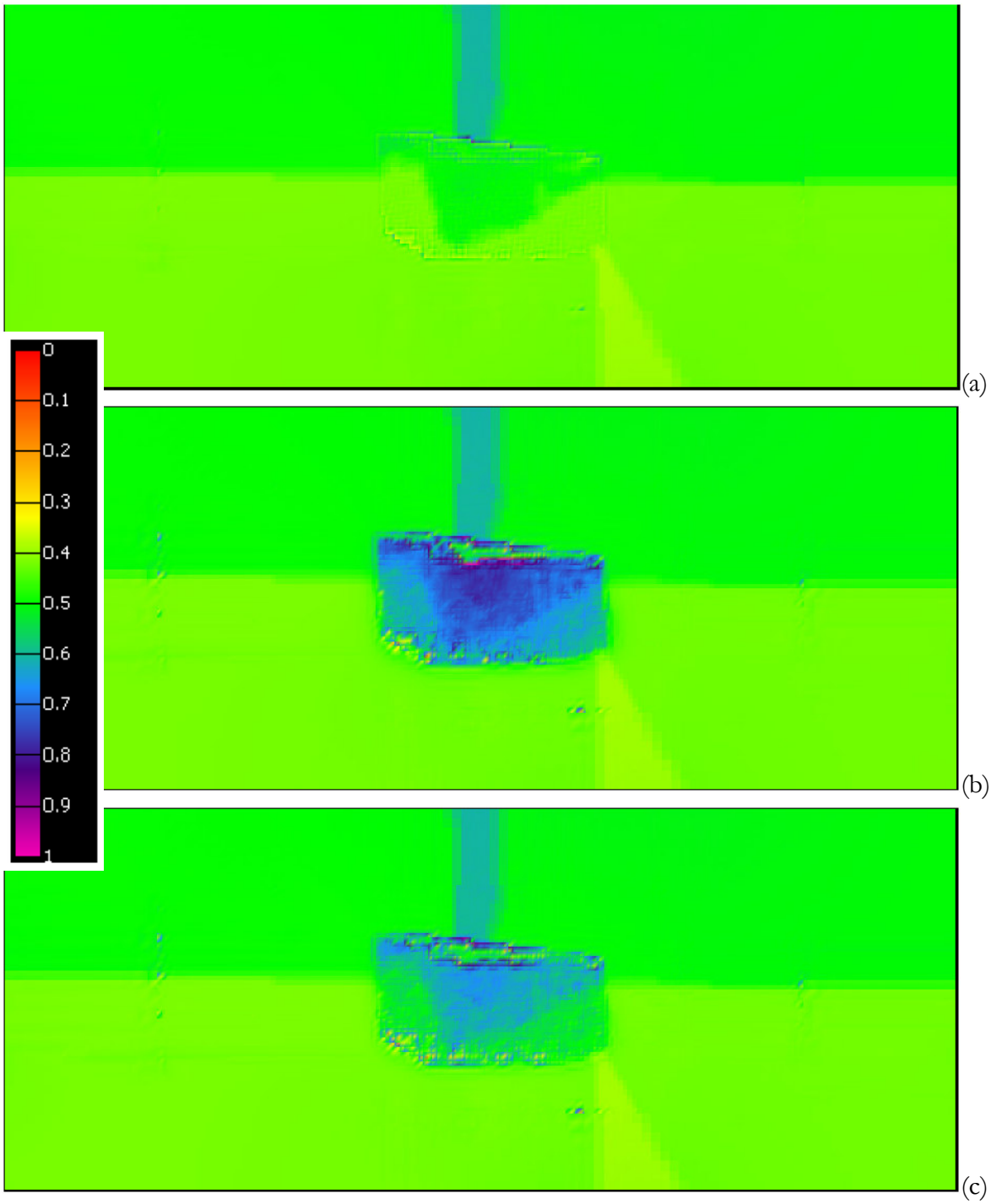

Figure 10.6 **Map of shear capacity results for Captain E&D with worst case failure parameters at (a) initial state, (b) after production, and (c) after injection. Colour scale is dimensionless and ranges between 0 and 1.**

10.4.2. Caprock

Failure parameters of the caprock are reduced to a cohesion of 0 (representing an unconsolidated shale) and a friction angle of 13°. These very low values are considered to be the worst case failure numbers for the rock properties of the Rødby shale. As a consequence the shear capacity utilization (SCU) τ/τ_{max} or the Mohr-Coulomb failure ratio will get worse as becomes clear from Eqs. (10)-(12). Graphically speaking, the failure line gets closer to the Mohr circle. This is shown in Figure 10.7 (*cf.*

Figure 9.17). (Note the circles have become ellipsoids due to non equal scales at the axes.) The Mohr circle lies just below the failure envelope for the stress situation after depletion. Due to injection the circle moves slightly to the right, hence shear failure in caprock becomes less likely.

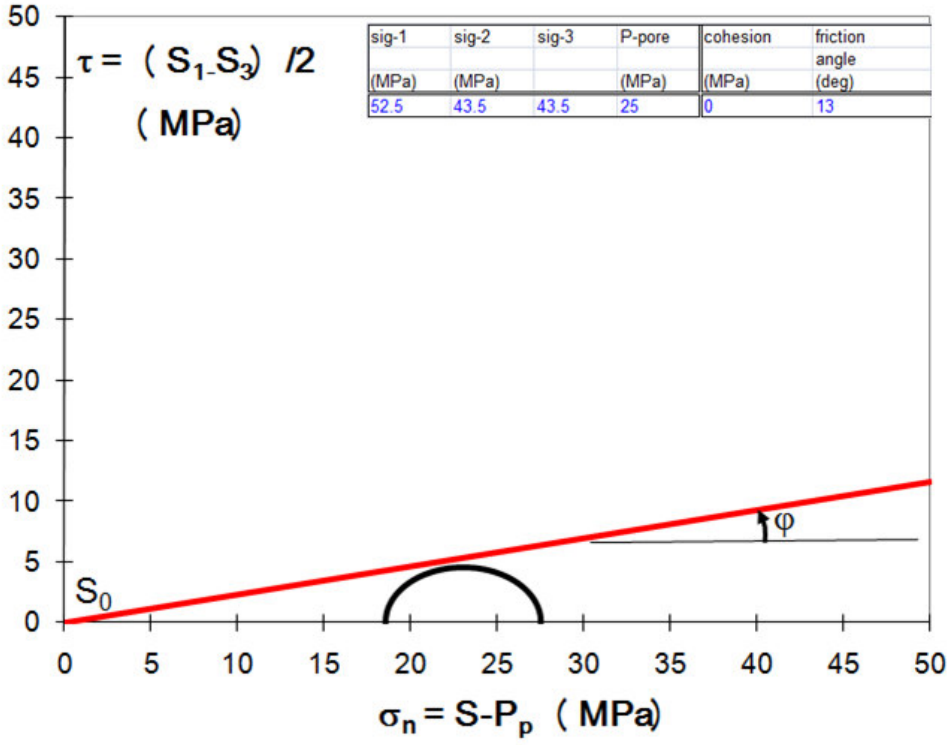

(a)

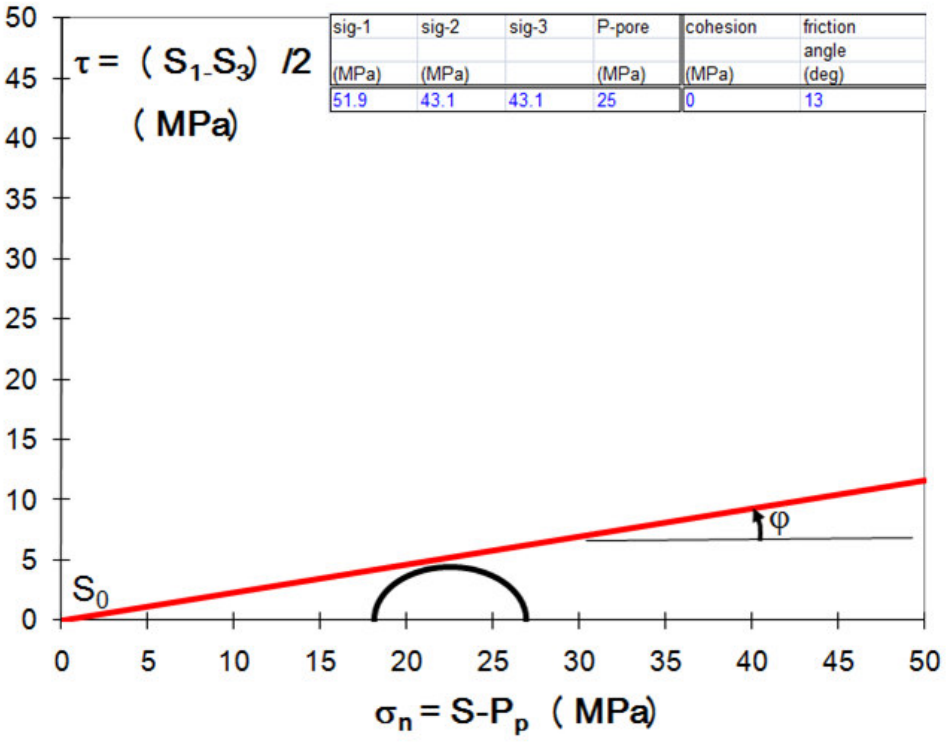

(b)

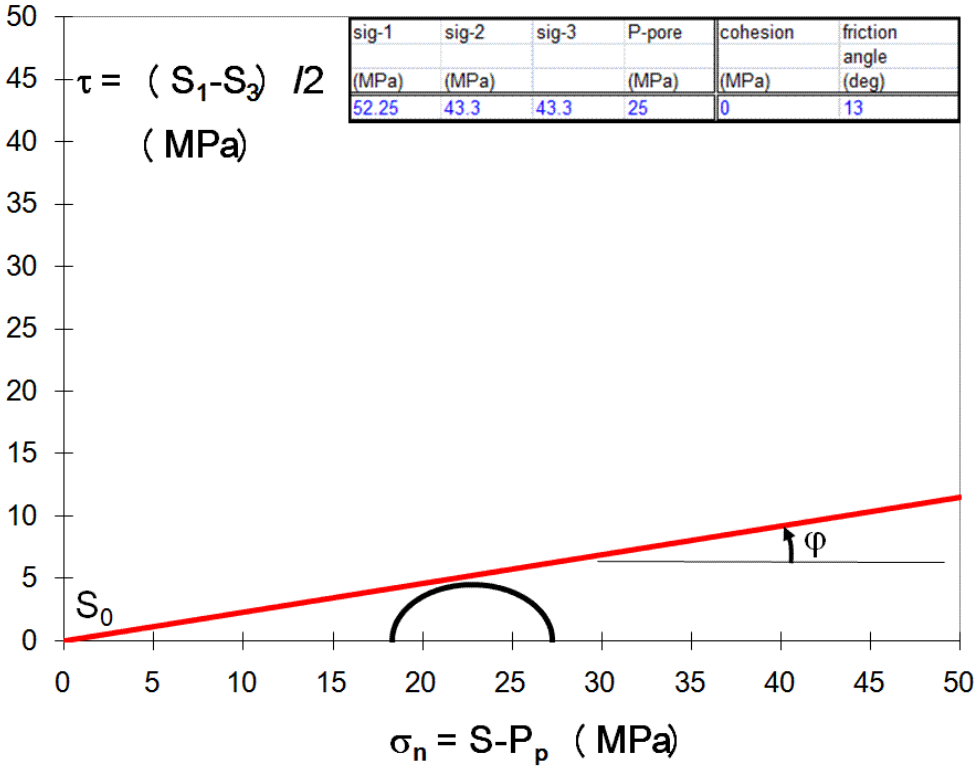

(c)

Figure 10.7 **Mohr circle and failure line for caprock with worst case failure parameters at (a) initial state of stress, (b) state of stress after production, and (c) state of stress after injection.**

Shear capacity results for all locations within and around the area of interest are displayed in Figure 10.8 for the caprock formation with worst case failure rock properties (C=0, FA = 13°). No shear failure is predicted as shear capacity is everywhere less than 1 (the maximum number found within the area of interest is approximately 0.92).

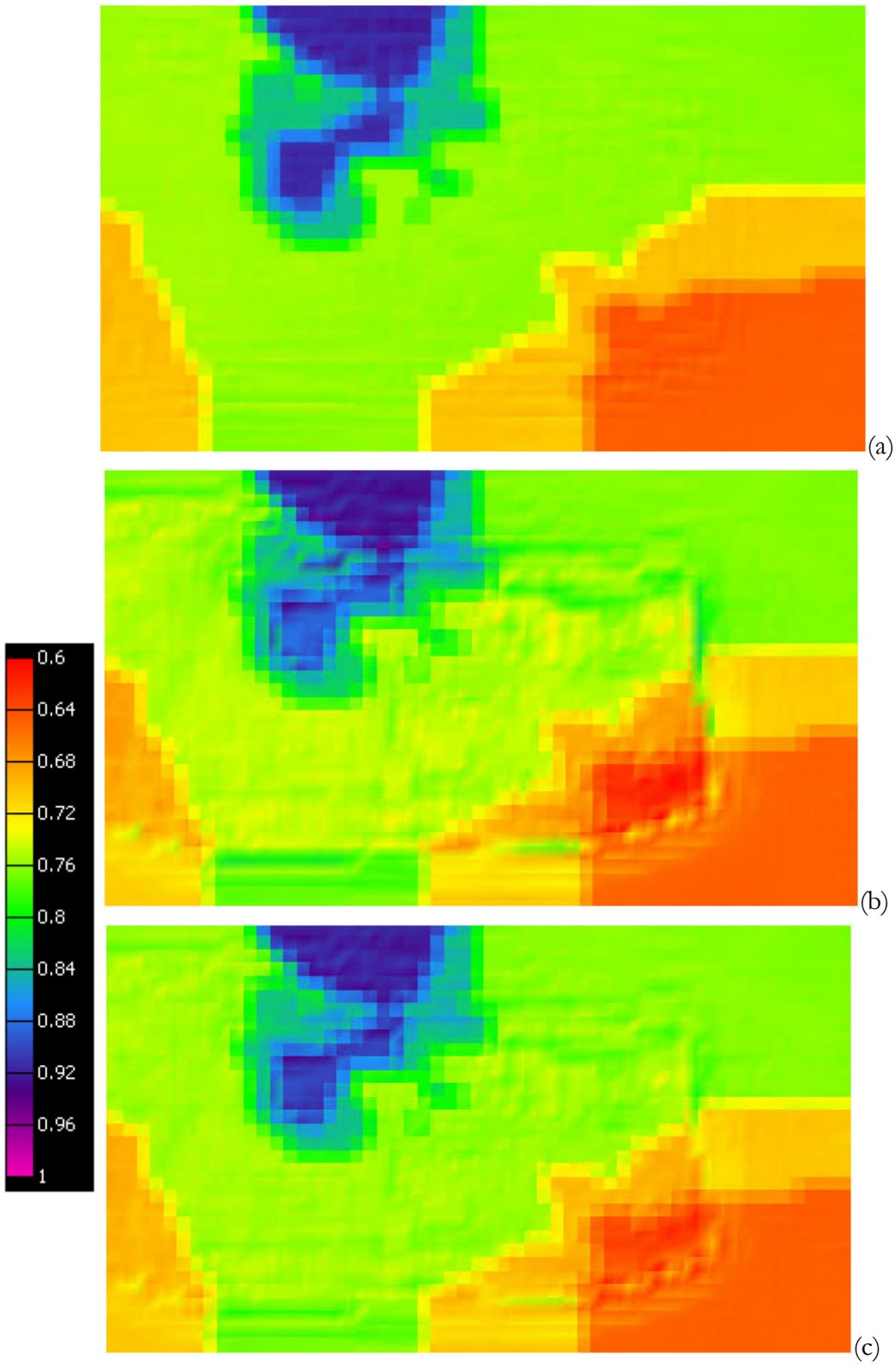

Figure 10.8 **Map of shear capacity results within and around the area of interest for caprock with worst case failure parameters at (a) initial state, (b) after production, and (c) after injection. Range of dimensionless colour scale is here, contrary to other SCU plots, 0.6 – 1.0.**

10.5. Uncertainty analysis, Case F: Poisson's Ratio 0.45 and worst case rock failure parameters of reservoir and caprock

In this section the Poisson's Ratio for all the three Captain reservoir units during the injection phase is assumed to be 0.45. This represents a state where the reservoir sandstone almost behaves as a fluid thereby reducing the gamma horizontal and thereby mimicking the effect of hysteresis as discussed in §3.1.2.3. Results (stress changes and SCU) of this scenario are presented in Table 10-7 for both Captain E&D and the caprock.

For an increase in pore pressure of 8.6 MPa during the injection phase the minimum total principal stress is increased by 2.25 MPa. So, gamma horizontal becomes 0.26 (2.25/8.6). Gamma vertical becomes 0.06 (0.5/8.6) since the maximum total principal stress for this injection case is increased by 0.5 MPa. Comparing this with the values for the gamma of the base case during injection (see §9.2.2) it is seen that gamma horizontal has decreased a lot (from 0.84 to 0.26) and the gamma vertical has a small decrease (from 0.1 to 0.06). Therefore it can be concluded that the geomechanical model of Goldeneye is handling hysteresis as described in §3.1.2.3.

Table 10-7 Key results for Case F (as obtained in the area of interest).

Case F		Change of pore pressure ΔP [MPa]	Change of minimum principal stress $\Delta\sigma_3$ [MPa]	Change of maximum principal stress $\Delta\sigma_1$ [MPa]	Maximum SCU (approx)
Reservoir Captain E&D	Initial to production	-10.1	-8.5	-1.0	0.80
	Production to injection	+8.6	+2.25	+0.5	0.95
Rødby Caprock	Initial to production	0	-0.4	-0.6	0.90
	Production to injection	0	+0.2	+0.35	0.92

The failure parameters of the reservoir are taken as the worst case situation, *i.e.*, cohesion=0 and the friction angle=20°. As the initial state of stress and the stress state after production has not changed the Mohr-Coulomb failure analysis plot (Mohr circle and failure line) is equal to the plot in Figure 10.5(a) and (b). The stress changes during injection are represented by the Mohr circle in Figure 10.9. As the Mohr circle lies below the failure line no shear failure is observed for this scenario.

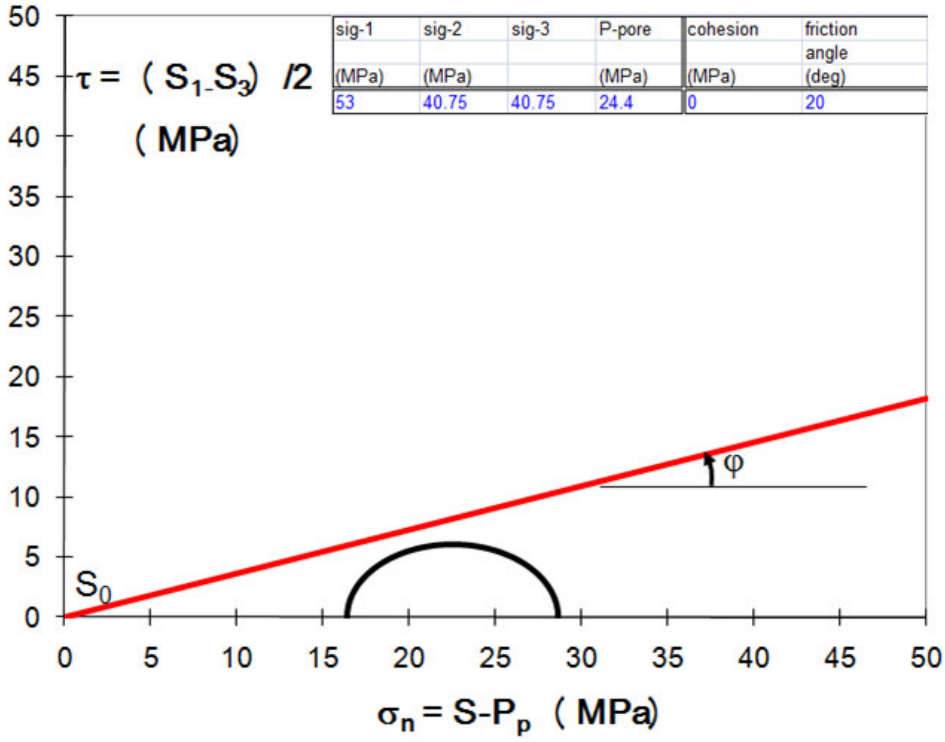

Figure 10.9 **Mohr's circle for Captain E&D reservoir with worst case of failure rock properties at Poisson's ratio of 0.45 during injection phase.**

Shear capacity results at initial and production phase are equal to Case E and displayed as a map view of all locations of the Captain E&D reservoir in Figure 10.6(a) and (b). Shear capacity results after the injection phase for the worst case failure properties are displayed in Figure 10.10. A maximum shear capacity of 0.95 is predicted after the injection phase. These results also show that the effect of hysteresis is not leading to a shear failure problem.

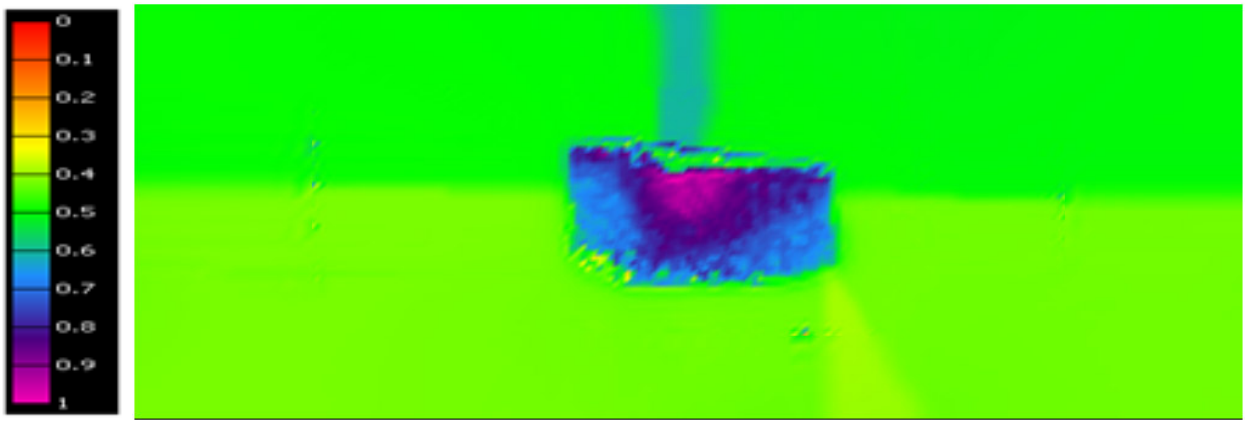

Figure 10.10 **Map of shear capacity results for Captain E&D formation during the injection phase where a Poisson's Ratio of 0.45 and worst case failure parameters were used. Colour scale is dimensionless and ranges between 0 and 1.**

Using a Poisson's Ratio of 0.45 during the injection phase in the Captain E&D reservoir did not lead to stress changes in the caprock. Therefore, results for the caprock are equal to the scenario that was discussed in case E (§10.4.2) and was displayed in Figure 10.8.

10.6. Uncertainty analysis, Case G: Pressure support from aquifer and worst case rock failure parameters of reservoir and caprock

Reservoir pressures provided to "Geomechanical Simulation Software" as described in the previous cases come from the FFM. There the pressure support from the aquifer was modelled analytically as a boundary pressure source at the edge of the FFM. This section investigates the effect of using an explicit and more accurate aquifer support that was available in the Fairway Aquifer Model[11] (FAM). The FAM has more detail in the modelling of neighbouring field effects (varying levels of pressure support caused by the interaction of extraction in those fields and the aquifer). The pressure data from the FAM model extends far to the east and west of the Goldeneye reservoir, it extends even further than the "Geomechanical Simulation Software" model that has a width of 50 km. So, a subset of the available data was mapped into "Geomechanical Simulation Software" and by "Geomechanical Simulation Software" extrapolated from the edges of a convex hull in order to get pressures for all Captain reservoir elements.

Figure 10.11 illustrates the pressure changes in the Captain E&D reservoir (inside the box) and the aquifer due to gas production. The maximum drawdown pressure of 10.9MPa [1580psi] is slightly higher than without explicit aquifer support (10.1MPa, see Figure 9.9).

Figure 10.12 illustrates the pressure changes in the Captain E&D reservoir (inside the box) and the aquifer due to CO_2 injection. The maximum injection pressure increase of 9.6MPa [1400psi] is a bit higher than without explicit aquifer support (8.6MPa, see Figure 9.13).

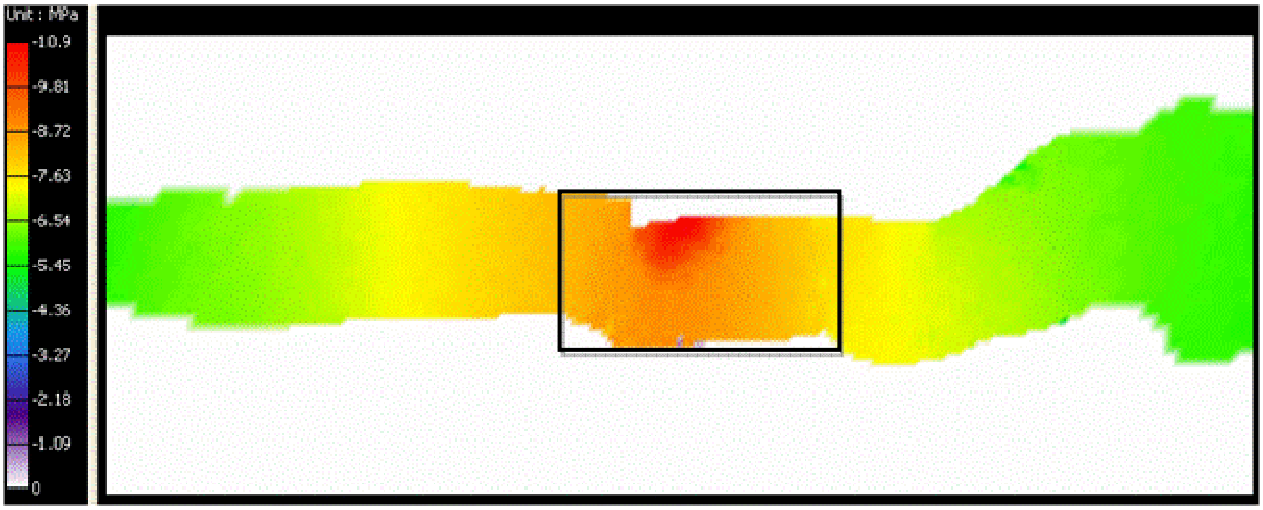

Figure 10.11 Top view map of pressure changes in the Captain E&D reservoir (inside the box) and aquifer due to gas production. Scale is between -10.9 and 0 MPa.

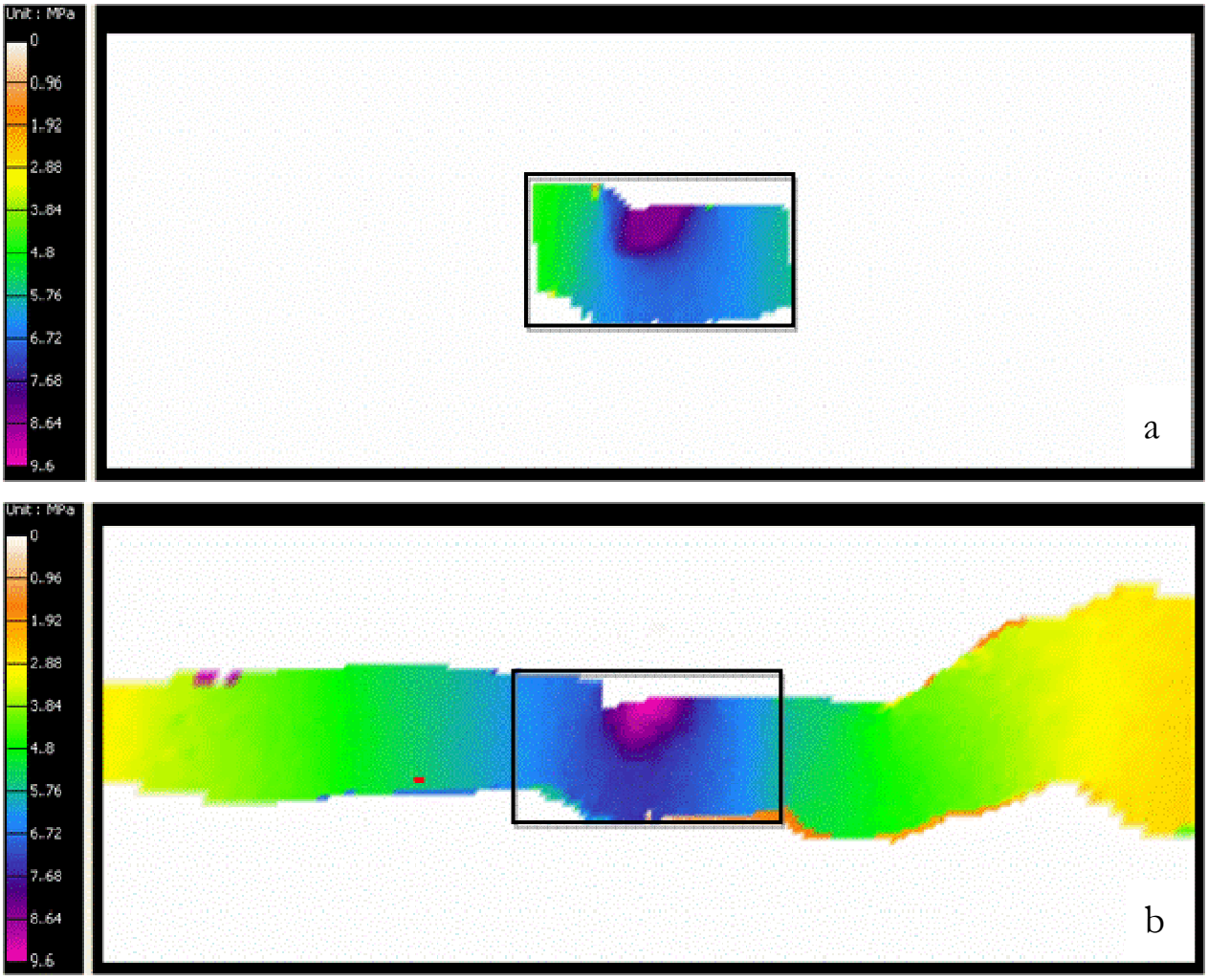

Figure 10.12 **Top view map of pressure changes in the Captain E&D reservoir (inside the box) and aquifer due to CO_2 injection (b). Scale is between 0 and 9.6MPa. For reference figure (a) is shown that displays the pressure change without having pressure data from the aquifer in the model (Case A). There the maximum injection pressure is 8.7MPa.**

Results (stress changes and SCU) of this scenario are presented in Table 10-8 for both Captain E&D and the caprock.

Shear capacity plots for the Captain E&D reservoir are shown in Figure 10.13. The high values at the border and outside (to the north) the defined "Area of interest" are due to unrealistic jumps in the material properties due to missing data and the "Geomechanical Simulation Software" extrapolation algorithm. These high numbers should therefore be ignored. This was also observed at Figure 10.6.

Comparing these results (Figure 10.13) to case E (Figure 10.6) leads to the conclusion there are hardly any differences for the SCU of the Captain E&D reservoir between models where the aquifer pressure support was modelled analytically and numerically. Therefore, it can be concluded that shear failure results based on pressure data from the Fairway Aquifer Model are consistent with those based on pressure data of the Full Field Model.

Shear capacity plots for the caprock are shown in Figure 10.14. The high values at the border and outside (to the north) the defined "area of interest" are due to unrealistic jumps in the material

properties due to missing data and the "Geomechanical Simulation Software" extrapolation algorithm. These high numbers should therefore be ignored. This was also observed at Figure 10.8 but is here a bit more visible.

Comparing these results (Figure 10.14) to case E (Figure 10.8) leads to the conclusion there are hardly any differences for the SCU of the caprock between a model with aquifer pressure support and a model without.

Table 10-8 Key results for Case G (as obtained in the area of interest).

Case G		Change of pore pressure ΔP [MPa]	Change of minimum principal stress $\Delta\sigma_3$ [MPa]	Change of maximum principal stress $\Delta\sigma_1$ [MPa]	Maximum SCU (approx)
Reservoir Captain E&D	Initial to production	15.9-26.3 = -10.4	38.5-47.5 = - 9.0	56.2-56.5 = - 0.3	0.82
	Production to injection	24.9-15.9 = +9.0	44.0-38.5 = + 5.5	56.2-56.2 = 0	0.71
Rødby Caprock	Initial to production	24.5-24.5 = 0	43.7-43.8 = - 0.1	53.6-53.7 = - 0.1	0.92
	Production to injection	24.5-24.5 = 0	43.7-43.7 = 0	53.7-53.6 = + 0.1	0.92

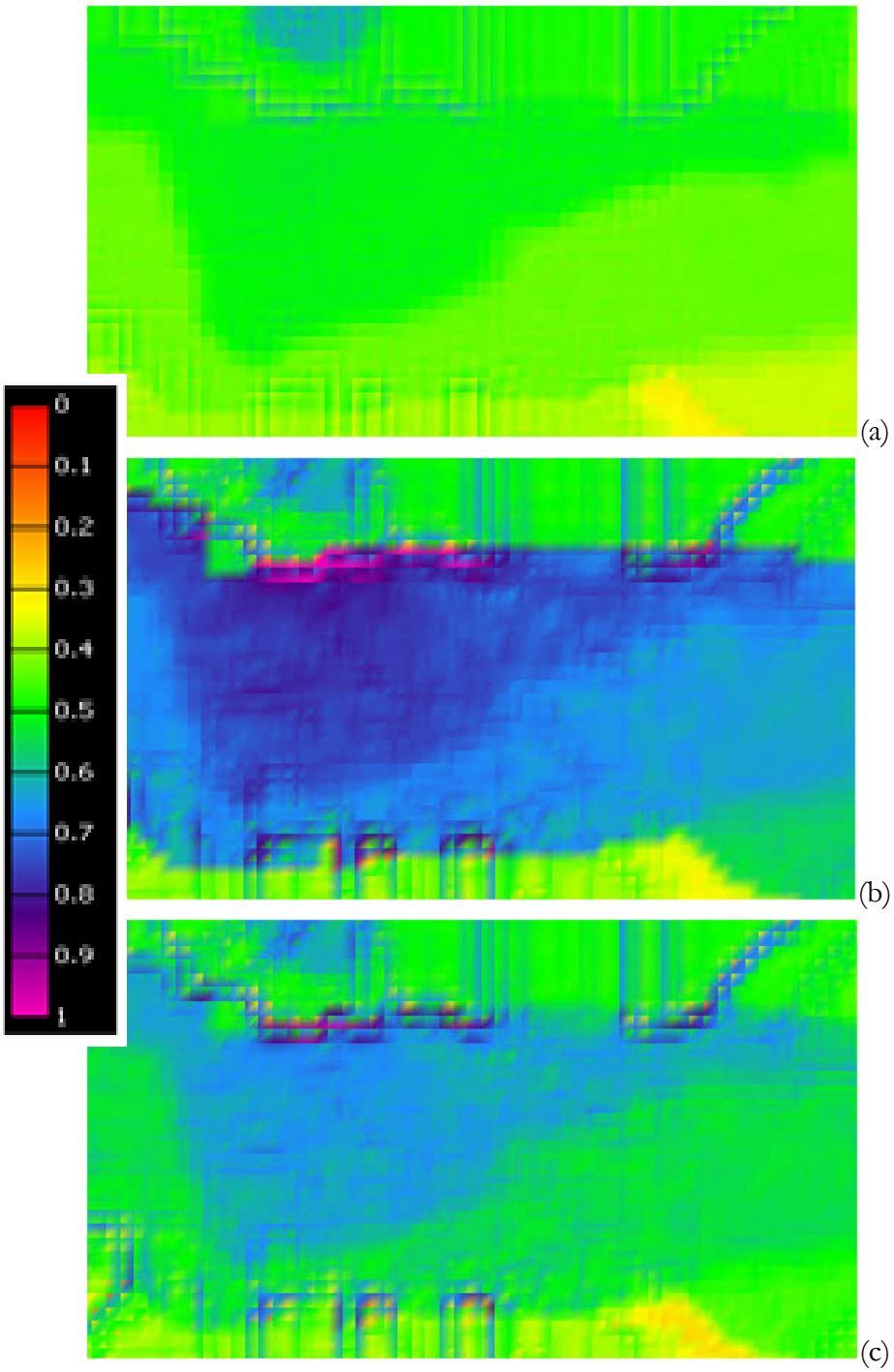

Figure 10.13 **Map of shear capacity results for Captain E&D formation (a) during the initial phase, (b) after the production, and (c) after injection. Pictures show the domain around the "Area of interest". Support from aquifer pressure and worst case failure parameters were used. Colour scale is dimensionless and ranges between 0 and 1.**

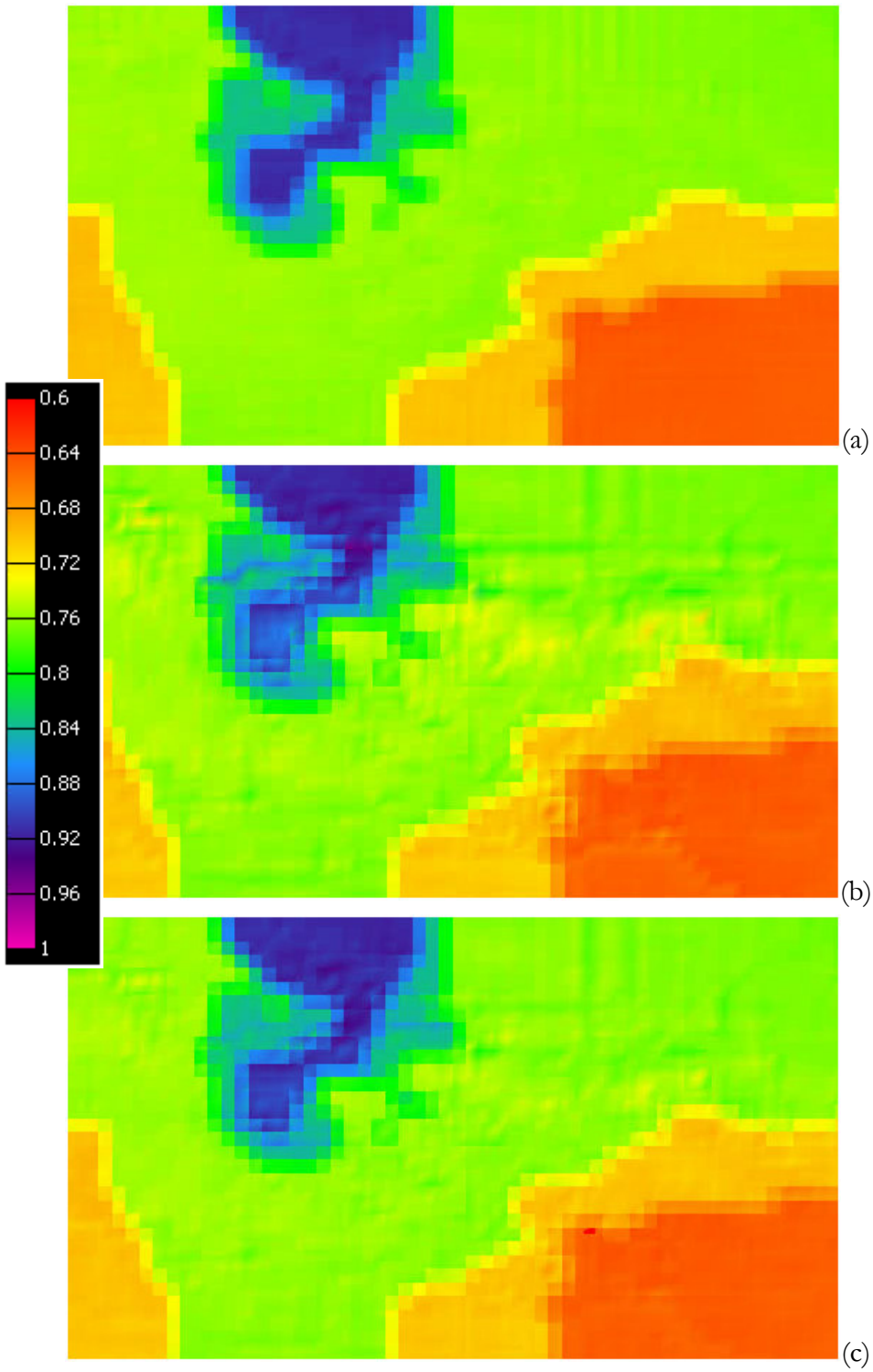

Figure 10.14 **Map of shear capacity results for the caprock formation (a) during the initial phase, (b) after the production, and (c) after injection. Pictures show the domain around the "Area of interest". Support from aquifer pressure and worst case failure parameters were used. Colour scale is dimensionless and ranges here between 0.6 and 1.**

10.7. Uncertainty analysis, Case H: Injection pressure is larger than the hydrostatic pressure and worst case rock failure parameters of reservoir and caprock

This section discusses the risk of rock failure in the reservoir and/or caprock given that the proposed maximum injection pressures (in the injection well itself) is above the hydrostatic pressure (see §5.4 and Figure 5.3) by an amount of 1.5MPa [220psi]. Since, after many years, the aquifer re-pressurizes the field, the case described in this section also holds for the long term.
Figure 5.4(c) shows the injection pressures in the Captain E&D reservoir at the end of the injection period in the year 2025. To these pressures 2.2MPa has been added such that the maximum value is 1.5MPa higher than the hydrostatic value. New pressures are displayed in Figure 10.15 (absolute values).

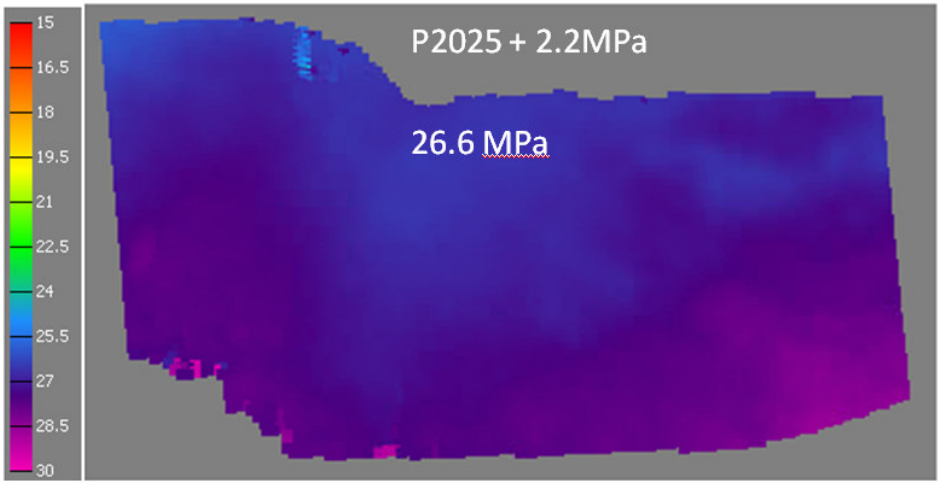

Figure 10.15 **Map of injected pressure in the Captain E&D reservoir in 2025. To the Base case scenario 2.2MPa is added thereby reaching a level above the hydrostatic pressure (25.5MPa at 2549m). Colour scale is in MPa between 15 and 30MPa.**

The highest maximum injector bottom hole pressure is then about 26.6MPa [3857psi]. Figure 10.16 shows the difference between the increased injection pressure and the hydrostatic pressure. The highest difference is about 1.5MPa [218psi] as expected.

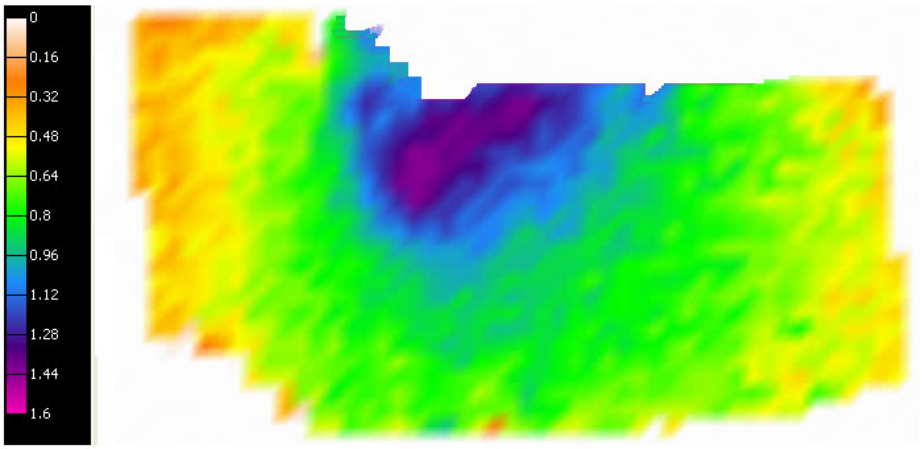

Figure 10.16 Map of difference between injected pressure in the Captain E&D reservoir in 2025 and the hydrostatic pressure. Colour scale is in MPa between 0 and 1.6MPa [232psi].

Results (pressure changes, stress changes, and SCU) of this scenario are presented in Table 10-9 for both Captain E&D reservoir and the Rødby (caprock) formation. Numbers were taken from a slightly different location from the one used for Table 10-6.

Table 10-9 Key results for Case H (as obtained in the area of interest).

Case H		Change of pore pressure ΔP [MPa]	Change of minimum principal stress $\Delta\sigma_3$ [MPa]	Change of maximum principal stress $\Delta\sigma_1$ [MPa]	Maximum SCU (approx)
Reservoir Captain E&D	Initial to production	15.9-26.0 = -10.1	35.9-44.2 = - 8.3	51.4-52.5 = - 1.2	0.81
	Production to injection	26.7-15.9 = +10.8	42.9-35.9 = + 7.0	51.5-51.4 = 0.1	0.61
Rødby Caprock	Initial to production	24.5-24.5 = 0	43.6-43.8 = - 0.2	53.5-53.7 = - 0.2	0.92
	Production to injection	24.5-24.5 = 0	43.6-43.6 = 0	53.6-53.5 = + 0.1	0.93

Shear capacity results for all locations within and around the area of interest are displayed in Figure 10.17 for the Captain E&D reservoir with worst case failure rock properties (C=0, FA = 20°). The high values at the border and outside the defined "Area of interest" are due to unrealistic jumps in the material properties due to missing data and the "Geomechanical Simulation Software" extrapolation algorithm. These high numbers should, therefore, be ignored. The SCU results are close to the SCU results of case E as displayed in Figure 10.6 (c). SCU numbers for a typical location in the area of interest are presented in Table 10-9. No shear failure is predicted in any of the phases as shear capacity is below 1.

Shear capacity results for all locations within and around the area of interest are displayed in Figure 10.18 for the caprock formation with worst case failure rock properties (C=0, FA = 13°). Results are

equal to the results presented in Figure 10.8(c). The extra injection pressure does not lead to a shear failure of the caprock as the shear capacity is everywhere below 1.

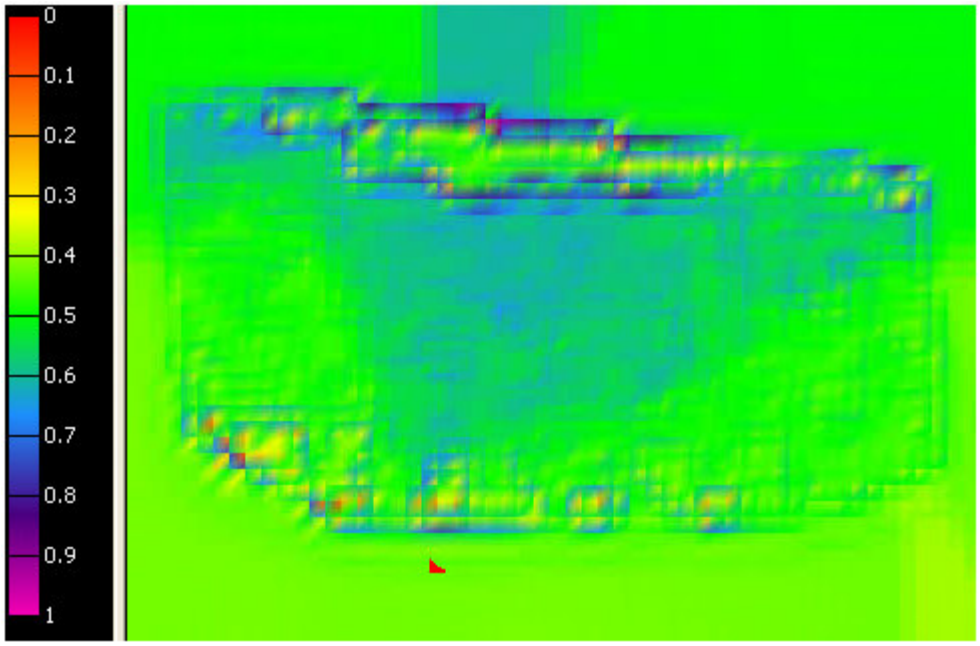

Figure 10.17 **Map of shear capacity results for Captain E&D with worst case failure parameters after injection was increased by 2.2MPa. Colour scale is dimensionless and ranges between 0 and 1.**

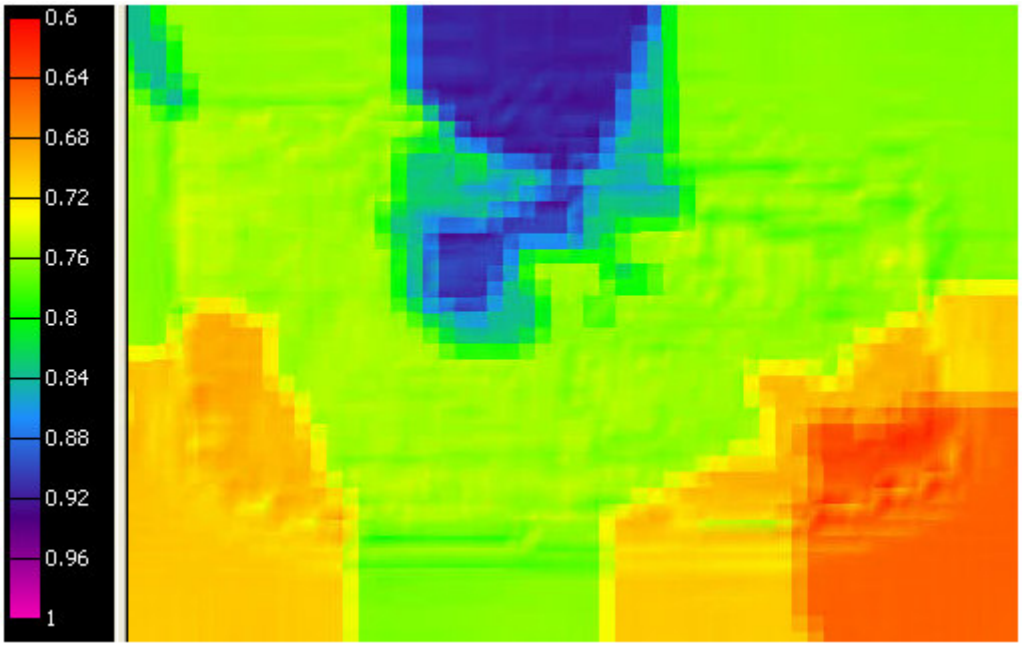

Figure 10.18 **Map of shear capacity results for the caprock formation after having injected the reservoir with a pressure that is everywhere 1.5MPa (218psi) above the hydrostatic pressure. Also worst case failure parameters were used. Colour scale is dimensionless and ranges between 0.6 and 1.**

10.8. Uncertainty case I: Pressure after depletion is lowered to 13.8 MPa [2000 psi] and worst case rock failure parameters of reservoir and caprock

The pressure after depletion in the Base case is about 15.8MPa [~2300psi]. After gas production had stopped, the pressure was approximately 13.8MPa [2000psi]. As the SCU is highest after depletion an extra modelling run was made with these lower pressures to investigate the consequences. The pressures in the reservoir as used in the base case (see §5.4) were therefore lowered by 2MPa [290psi] to a level where the absolute minimum pressure is 13.8MPa [2000psi]. For the SCU investigation the worst case rock failure parameters of reservoir and caprock are taken.

Results (pressure changes, stress changes, and SCU) of this scenario are presented in Table 10-10 for both Captain E&D reservoir and the Rødby (caprock) formation. Note that the location where the SCU is maximal is not necessarily the point where the absolute pressure is minimal.

Table 10-10 Key results for Case I (as obtained in the area of interest).

Case I		Change of pore pressure ΔP [MPa]	Change of minimum principal stress $\Delta\sigma_3$ [MPa]	Change of maximum principal stress $\Delta\sigma_1$ [MPa]	Maximum SCU (approx)
Reservoir Captain E&D	Initial to production	14.6-26.0 = -11.4	37.8-47.8 = - 10.0	57.1-56.8 = 0.3	0.85
Rødby Caprock	Initial to production	24.6-24.6 = 0	44.2-43.9 = 0.2	54.2-54.1 = 0.1	0.94

Shear capacity results for all locations within and around the area of interest are displayed in Figure 10. for the Captain E&D reservoir with worst case failure rock properties (C=0, FA = 20°). The high values at the border and outside the defined "area of interest" are due to unrealistic jumps in the material properties due to missing data and the "Geomechanical Simulation Software" extrapolation algorithm. These high numbers should therefore be ignored. SCU results as shown in Figure 10.19(a) is equal to case E as is shown (with a different colour scale) in Figure 10.6(b). It is observed that a lower pressure after depletion leads to higher SCU values but, no shear failure is predicted as shear capacity is below 1.

Shear capacity results for all locations within and around the area of interest are displayed in Figure 10.20 for the caprock formation with worst case failure rock properties (C=0, FA = 13°). SCU results as shown in Figure 10.20(a) are equal to case E as is shown in Figure 10.8(b). It is observed that a lower pressure after depletion does not lead to higher SCU values in the caprock. No shear failure is predicted as shear capacity is below 1.

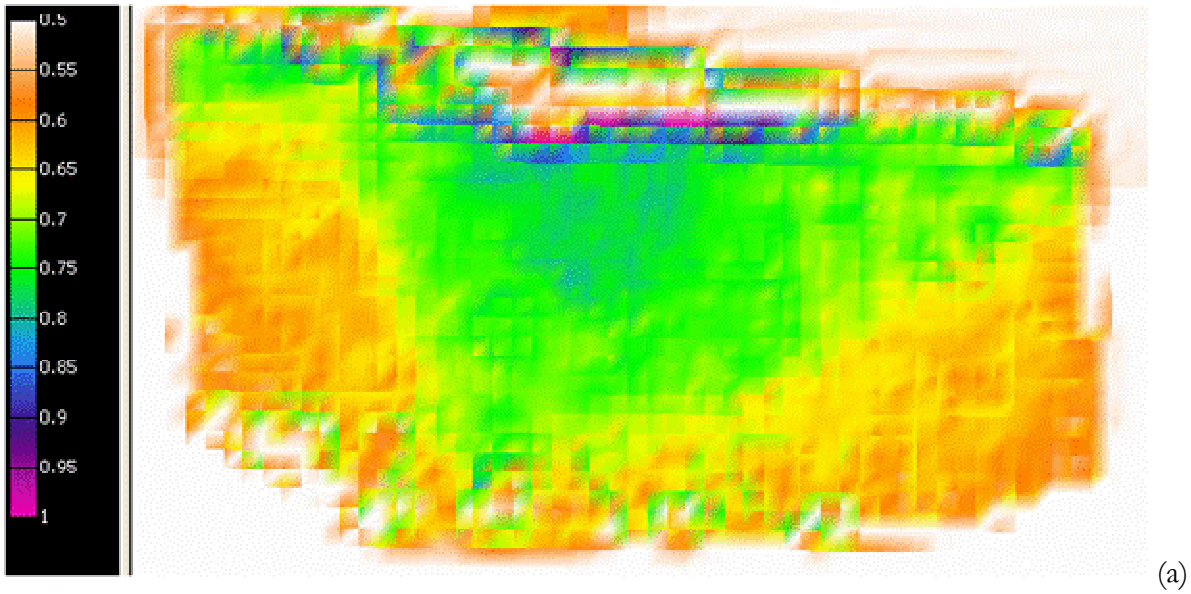

(a)

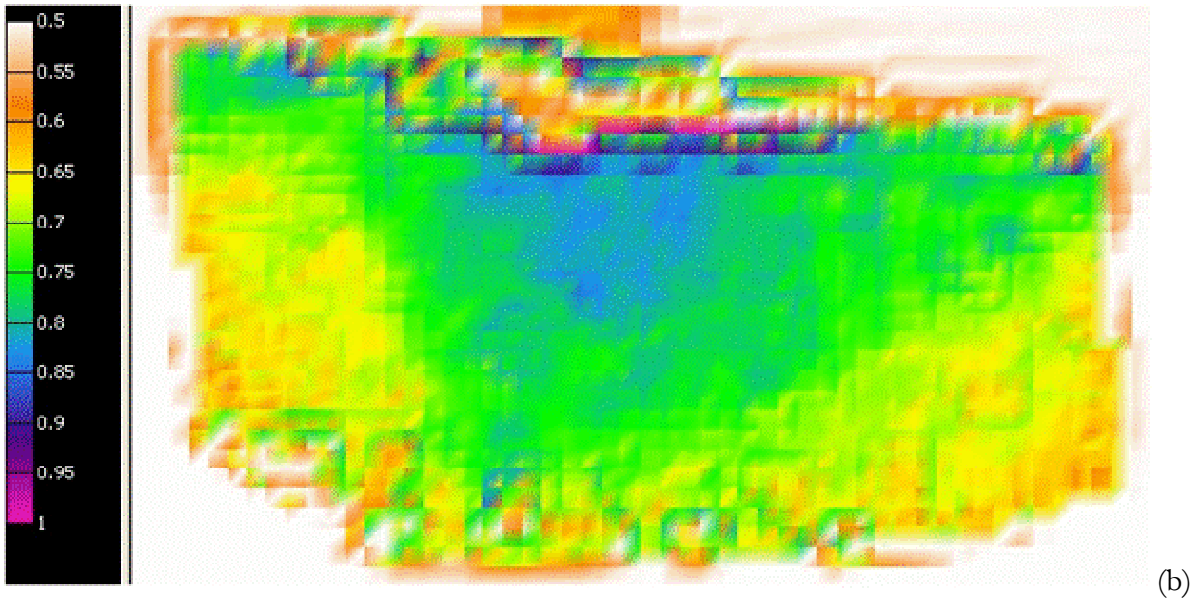

(b)

Figure 10.19 **Map of shear capacity results for Captain E&D with worst case failure parameters after depletion where minimum pressure was 15.8MPa (a), and 13.8MPa (b). Colour scale is dimensionless and ranges between 0.5 and 1.**

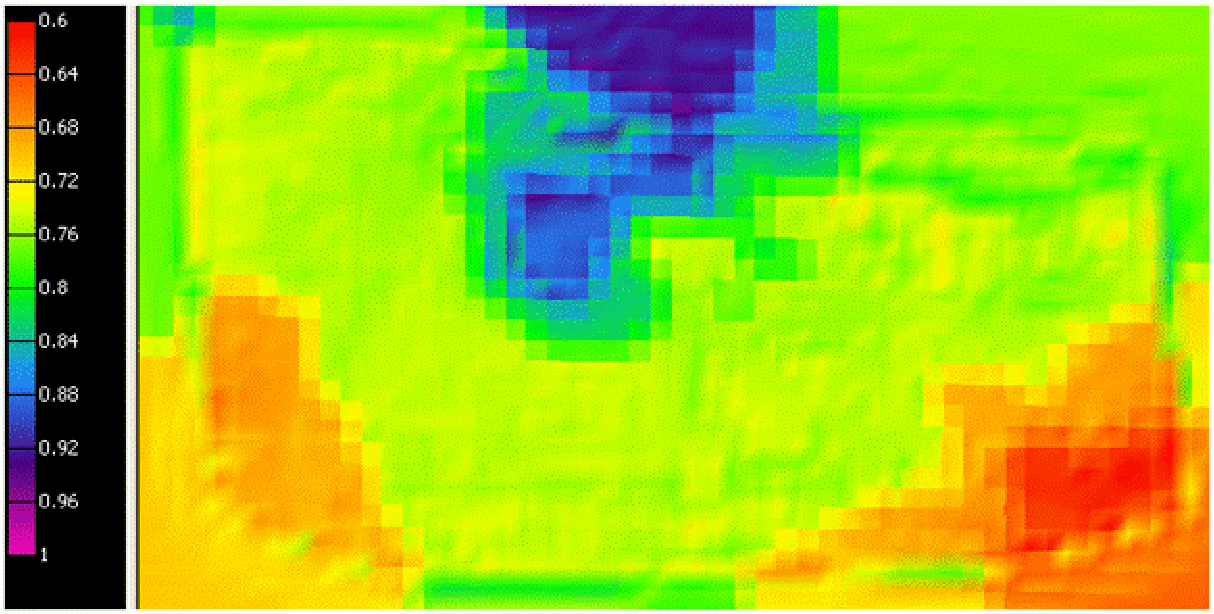

(a)

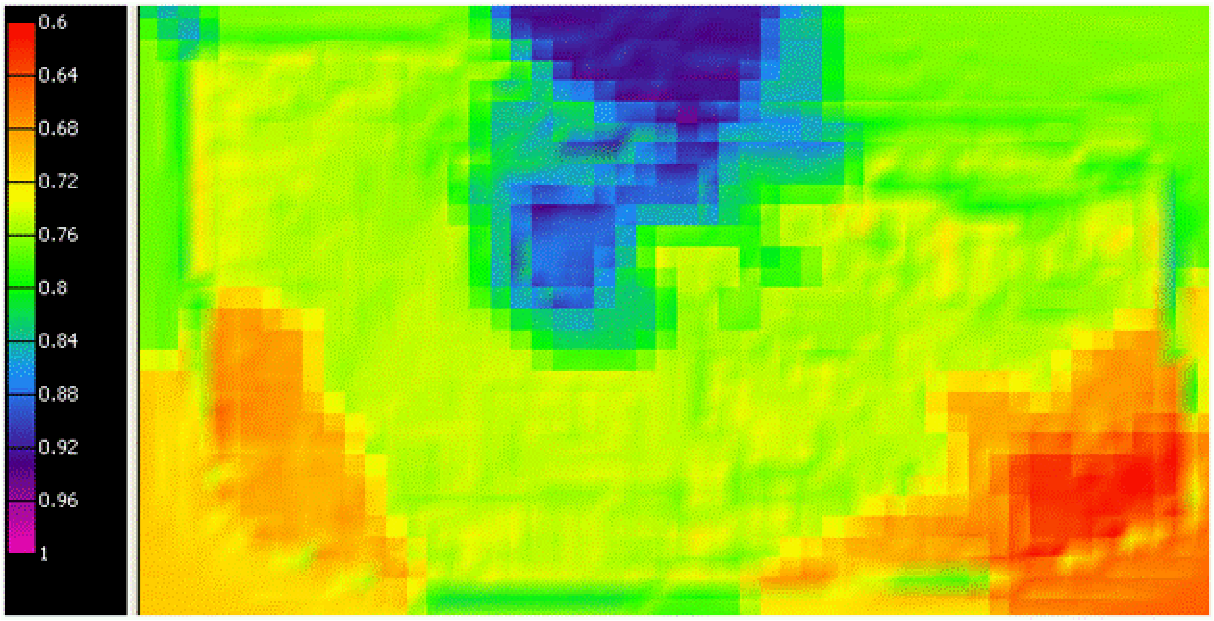

(b)

Figure 10.20 **Map of shear capacity results for caprock with worst case failure parameters after depletion where minimum pressure was 15.8MPa (a), and 13.8MPa (b). Colour scale is dimensionless and ranges between 0.6 and 1.**

11. Fault reactivation

Pressures that change in the reservoir due to gas depletion or CO_2 injection can potentially open fractures and cause slip on faults that exist in the reservoir and overburden formations. In §3.1.3 fault reactivation was discussed in general terms. In this chapter an attempt is made to quantify fault slip. The idea is to focus on the stress injection response within the reservoir and to map these computed stresses on the faults. A methodology to quantify and investigate fault slip is by using the Mohr-Coulomb failure criterion (that uses these mapped stresses). It's a frequently employed, commonly accepted, and simple and robust way to take into account the resistance to the fault slip. When applying this criterion the following assumptions need to be made:

- The initial stress state of the faults, before depletion or injection, is the same as the initial stress sate of the surrounding rock.
- The onset of fault instability is caused by the perturbation of the initial stress state.
- Faults are not critically stressed (note that the stress history of faults is unknown).

The faults that are investigated in this chapter have to be interpreted as the outcome of a possible scenario applied to potential faults (see §11.2 for more details on the uncertainty).

11.1. Introduction

Increased formation pressures due to CO_2 injection can potentially open fractures and cause slip on faults that exist in the reservoir and overburden formations. Increasing the pore fluid pressures (P_f) on faults leads to low effective stresses $\sigma' = \sigma - P_f$. Positive effective normal stresses $\sigma_n' = \sigma_n - P$ press opposing fault blocks together and resist the sliding motion along the fault surface which can be induced by shear stresses (τ) acting parallel to the fault as shown in Figure 12-1. Thus, an increasing pore fluid pressure decreases the normal effective stress and therefore increases the risk of sliding.

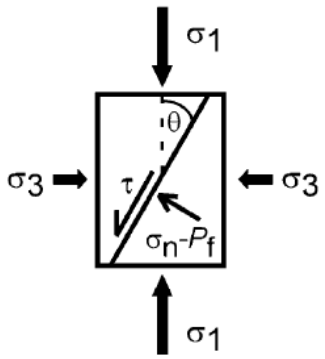

Figure 11.1 Stresses acting on a fault

The shear and effective normal stresses that act on a fault segment are a function of the fault orientation and are in 2D given by (see Chapter 2 of Fjaer[3])

$$\tau = \frac{1}{2}(\sigma_1' - \sigma_3')\sin 2\theta, \tag{13}$$

$$\sigma_n' = \frac{1}{2}(\sigma_1' + \sigma_3') + \frac{1}{2}(\sigma_1' - \sigma_3')\cos 2\theta, \tag{14}$$

where,

τ is the shear stress that might cause sliding,

σ_n' is the effective normal stress that resists sliding,

σ_1 is the total maximum principal stress,

σ_3 is the total minimum principal stress,

$\sigma_1' = \sigma_1 - P_f$ is the effective maximum principal stress,

$\sigma_3' = \sigma_3 - P_f$ is the effective minimum principal stress, and

θ is the angle between the fault and σ_1 as shown in Figure 12-1.

As θ is of direct importance for fault slip analysis, knowledge of the orientation of the stresses with respect to the orientation of the pre-existing faults is needed for analysing the slip tendency of these faults. From a straight forward Mohr-Coulomb analysis the shear capacity parameter can be defined that is a direct indicator for slip tendency (see §9.2):

$$\text{shear capacity} = \frac{\tau}{C + \sigma_n' \tan \varphi} \quad (15)$$

where, C is the cohesion, and

φ is the friction angle of a fault.

A fault does not slip if the shear capacity is less than 1 (see also §9.2).

11.2. Fault interpretation

Seismic was revisited to find any potential structural discontinuities. Few "Fault like" discontinuities were identified in the reservoir and overburden. It is to be noted that these faults are not included in any of the reservoir models simply because they are not manifested in the production data. Moreover, these discontinuities are with very little throw. These discontinuities can be best defined as seismic lineaments which can lead to potential faulting. Figure 11.2 – Figure 11.5 show the faults from different views, and viewpoints in 2D and 3D. The locations are displayed in Figure 11.3. These potential faults, of which the size and vertical positioning might be questionable, are near vertical, have a dominant NW-SE trend, and are consistently developed in the eastern flank.

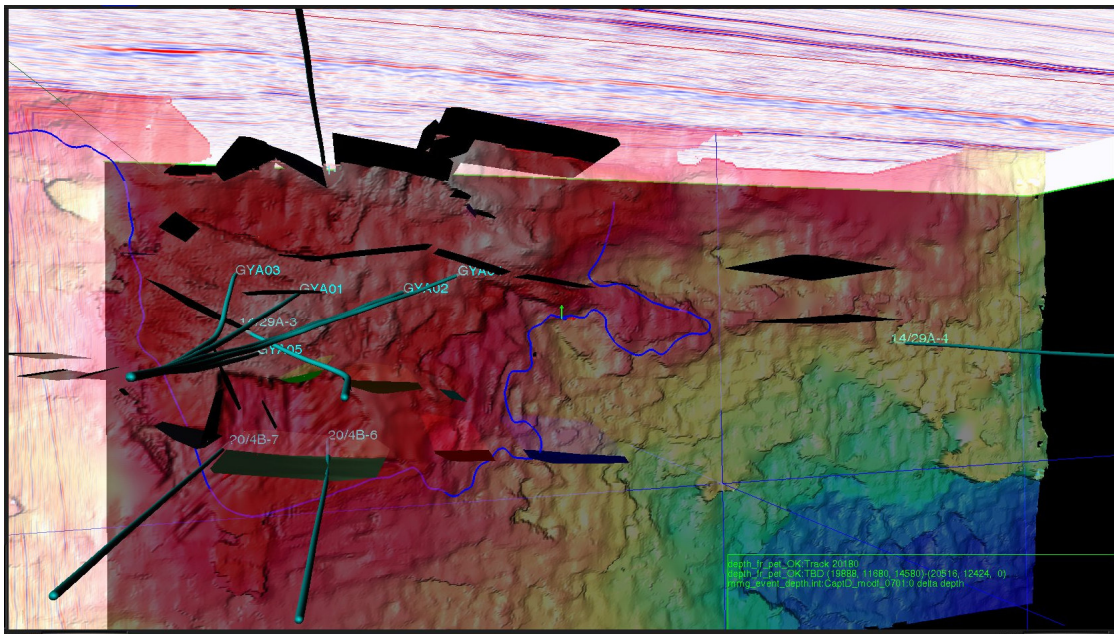

Figure 11.2 **3D top view of the Captain D with faults, gas water contact (blue line), wells, and seismic sections.**

These faults have been interpreted (as sticks) in Shell's proprietary seismic interpretation system, , exported to gOcad – where surfaces were generated – and subsequently imported in "Simplified Visualization Software", Shell proprietary, a structural geology and geomechanics tool. There the stresses (as modelled in "Geomechanical Simulation Software") are projected on each and every fault plane and slip tendency is evaluated. In the following sections this workflow, data input, and results are discussed.

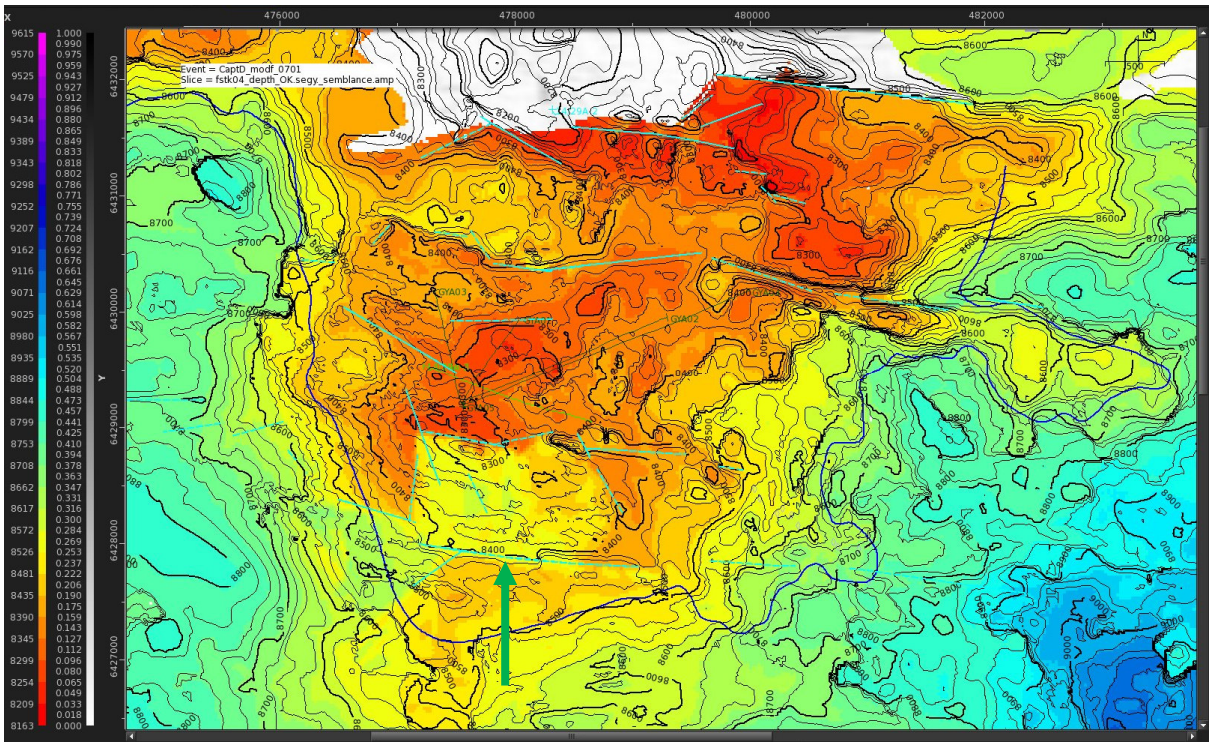

Figure 11.3 **Top view of many faults (indicated by green lines) crossing the Captain D reservoir. Axes show northing (vertical) and easting (horizontal) coordinates. The blue curve is the gas water contact. Green arrow points to a fault for reference.**

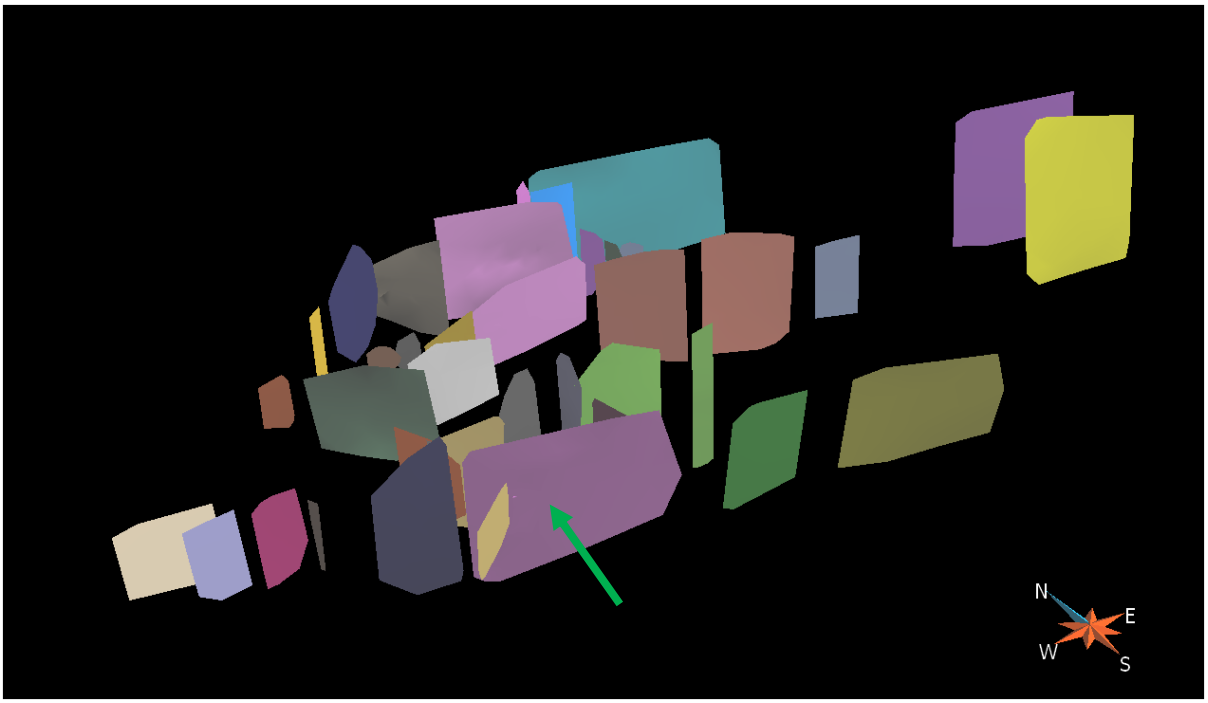

Figure 11.4 **3D bird's-eye view (SW-NE direction) of many faults through the reservoir formations. The green arrow points to a fault that is indicated in Figure 11.3 also by a green arrow.**

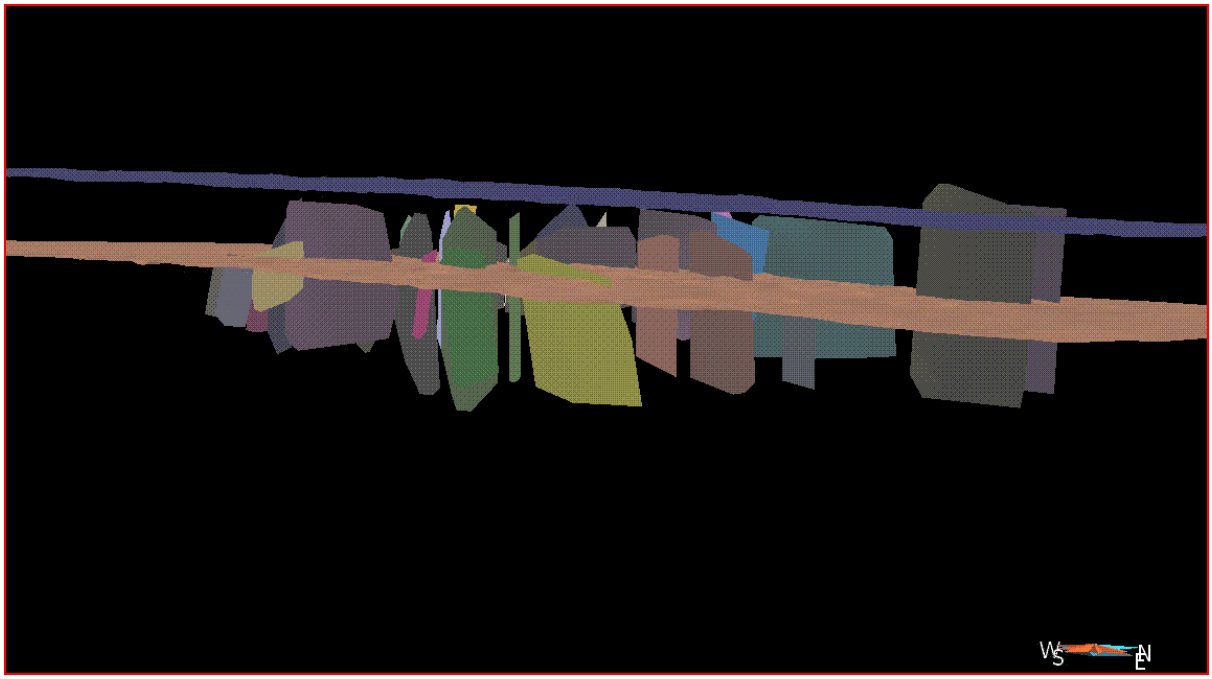

Figure 11.5 **3D bird's-eye view (SE-NW direction) of many faults through the reservoir formations. Most faults are crossing the Top Rødby (light brown surface) and a few cross the Top Ekofisk (dark blue surface).**

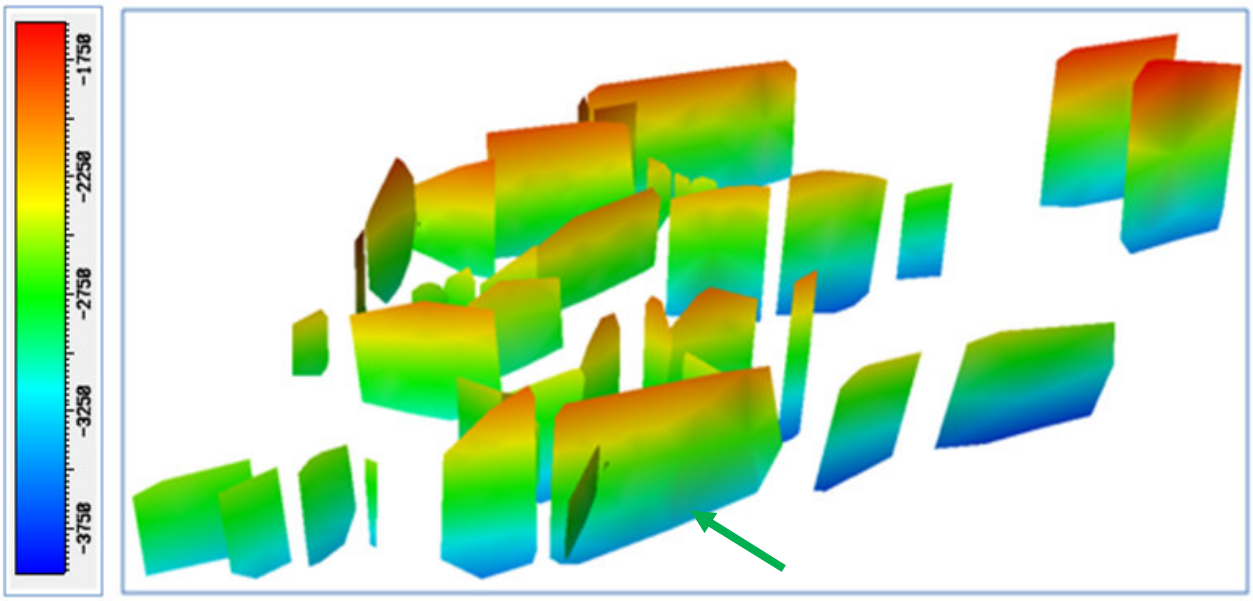

Figure 11.6 **3D bird's-eye view (SW-NE direction) of many faults. Colours indicate depth in m and range from 1600 – 3900m. The green arrow points to a fault that is also pointed to in Figure 11.3.**

11.3. Workflow

Stress states predicted at initial, production, and injection phases (see Chapter 9) for different scenarios (see Chapter 10) are imported into "Simplified Visualization Software" in addition to the faults. "Simplified Visualization Software" then calculates effective normal stress and maximum shear stress in 3D on each and every fault plane. Next, the slip tendency as defined in Eq. (15) is calculated by "Simplified Visualization Software" for the three stress stages: before production (initial), after production of the gas, and after having injected the CO_2. The above workflow is visualised in Figure 11.7. Results are discussed in the next section.

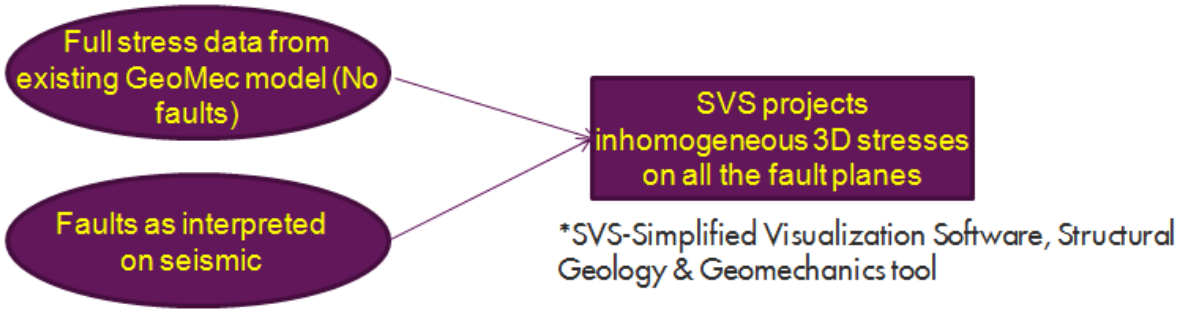

Figure 11.7 Risk on fault reactivation workflow.

11.4. Fault reactivation modelling results and uncertainty

This fault reactivation study is restricted to three scenarios that have been selected from all the different cases as discussed in Chapter 10. First the results from the Base case as discussed in Chapter 9 and summarised in Table 10-2 will be used together with fault slip properties that are equal to the failure parameters (cohesion and friction angle) of the caprock (Rødby formation). The second case is again using the Base case data but now the fault slip properties are chosen to be equal to the failure parameters of the Captain E&D reservoir. The third case is investigating the consequences for the worst case parameters, *i.e.*, case F of Chapter 10 (Poisson's ratio for all the three Captain reservoirs during the injection phase is taken to be 0.45), and fault slip properties are chosen to be equal to the worst case failure parameters. In all three cases the assumption is made that the fault slip properties are close to the failure properties of the formations around the faults. Table 11-1 summarises these three cases.

Table 11-1 Parameter sensitivity study.

SVS Case	Parameter variations as defined in Table 10-1 for stress modelling	Fault rock properties
I	Case A (Base case)	C=6 MPa, φ=13° (equal to Rødby caprock)
II	Case A (Base case)	C=3 MPa, φ=34.4° (equal to Captain reservoir)
III	Case F (Worst case)	C=0, $\varphi=13^0$ (equal to worst case for Rødby reservoir)

For these cases "Simplified Visualization Software" is used to calculate shear stress and effective normal stress in 3D for each and every fault plane. Then, shear capacity numbers are plotted on the faults such that fault reactivation can easily be visually inspected. The next three sections discuss the results of the aforementioned three cases.

11.4.1. Case I

This section discusses the results for the parameters as defined in Table 11-1 for the case I scenario. Effective normal stress and maximum shear stress after the injection phase are displayed in Figure 11.8. It is observed that the effective normal stress increases with depth from 8 to 41MPa. As most of the faults are near vertical and this is also the dominant orientation of the maximum principal stress, the magnitude of the maximum shear stress is expected to be low. A variation between 0 and 2.8MPa is observed.

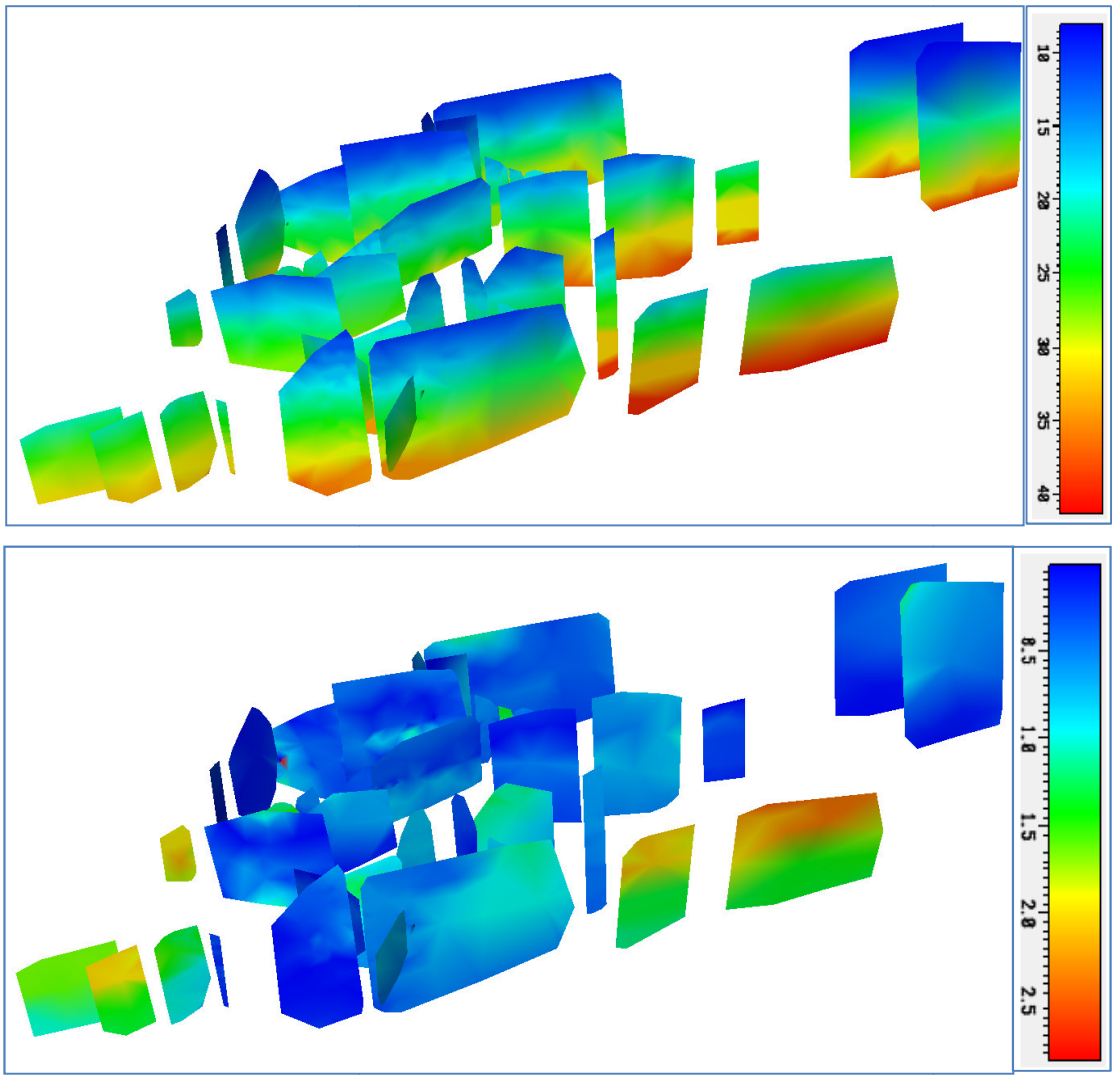

Figure 11.8 **3D bird's-eye view (SW-NE direction; location and viewing direction are equal to Figure 11.6) showing, for the "Simplified Visualization Software" Case I scenario, the effective normal stress (a), and the maximum shear stress (b) on all the faults after injection. Colours indicate stress in MPa.**

Fault failure properties are taken to be equal to the failure properties of the caprock (Rødby Formation that has a cohesion of 6MPa. and a friction angle of 13°). Figure 11.9 shows the shear capacity results as defined in Eq. (15) after injection. As the maximum values are around 0.3, no fault-slip is expected to occur. For the stress states before and after production results are approximately equal to those found after injection and thus the same conclusion holds: no fault-slip is expected to occur.

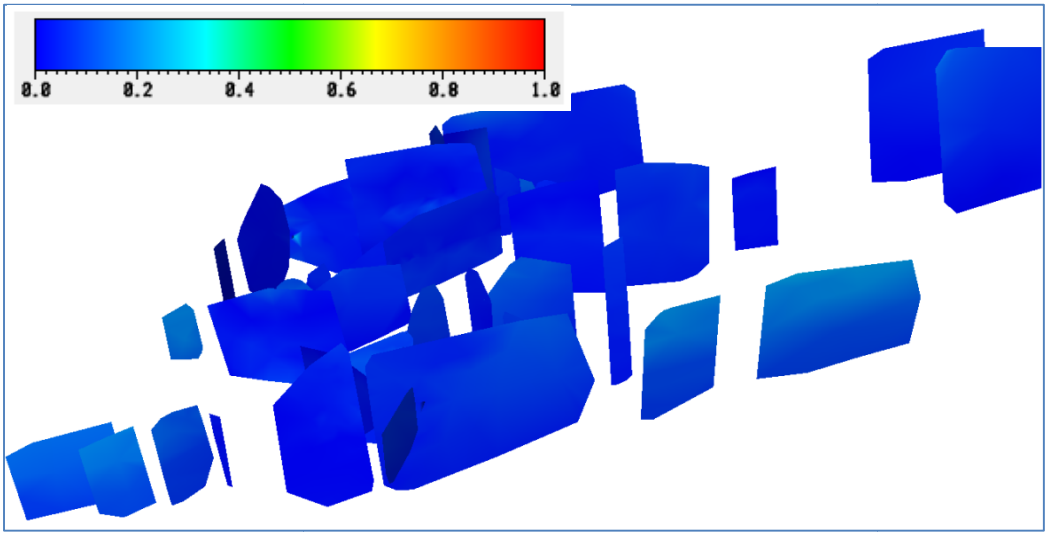

Figure 11.9 **3D bird-eye view (SW-NE direction; location and viewing direction are equal to Figure 11.6) showing, for the "Simplified Visualization Software" Case I scenario shear capacity results of all the faults after injection. Colours indicate shear capacity (fault slip tendency) in dimensionless units.**

11.4.2. Case II

This section discusses the results for the parameters as defined in Table 11-1 for the case II scenario. Fault failure properties are taken to be equal to the failure properties of the Captain E&D reservoir (a cohesion of 3MPa. and a friction angle of 34.4°). Figure 11.10 shows the shear capacity results as defined in Eq. (15) after injection. As the maximum values are around 0.18 no fault-slip is expected to occur. For the stress states before and after production results are approximately equal to those found after injection and thus the same conclusion holds: no fault-slip is expected to occur.

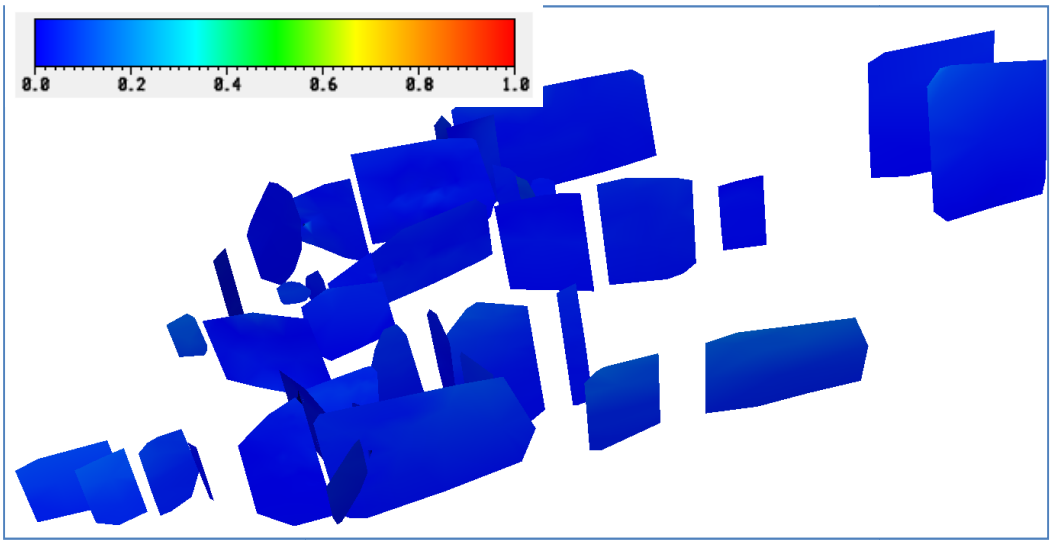

Figure 11.10 **3D bird's-eye view (SW-NE direction; location and viewing direction are equal to Figure 11.6) showing, for the "Simplified Visualization Software" Case II scenario shear capacity results of all the faults after injection. Colours indicate shear capacity (fault slip tendency) in dimensionless units.**

11.4.3. Case III

This section discusses the results for the parameters as defined in Table 11-1 for the case III scenario. Fault failure properties are taken to be the worst case failure properties, a cohesion of 0 and a friction angle of 13°. Figure 11.11 shows the shear capacity results as defined in Eq. (15) after injection. As the values are at most 0.6 no fault-slip is expected to occur. For the stress states before and after production results are approximately equal to those found after injection and thus the same conclusion holds: no fault-slip is expected to occur.

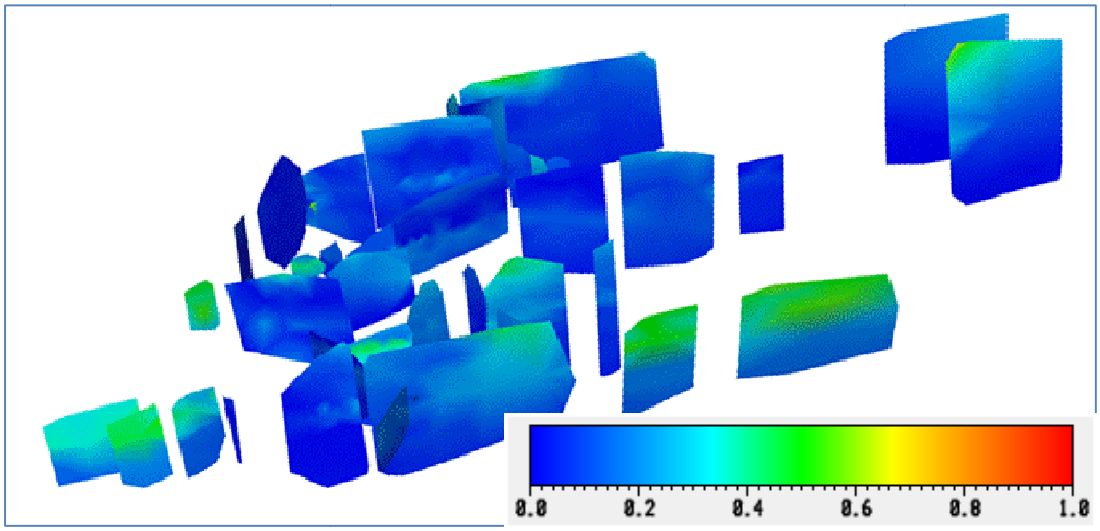

Figure 11.11 **3D bird's-eye view (SW-NE direction; location and viewing direction are equal to Figure 11.6) showing, for the "Simplified Visualization Software" Case III scenario shear capacity results of all the faults after injection. Colours indicate shear capacity (fault slip tendency) in dimensionless units.**

11.5. Conclusions

For every fault, the slip-tendency was investigated by calculating the shear capacity for all the three stress stages (before and after production of the gas, and after injection of the CO_2). No fault-slip is expected to occur. Even the worst case scenario was not significantly close to slip. This conclusion is based on the assumption that the initial stress state of the faults, before depletion or injection, is the same as the initial stress sate of the surrounding rock. Furthermore, it was assumed that the faults are not critically stressed.

This result implies, as discussed in §3.1.3.2, that if faults are currently not leaking (which they are unlikely to be given that a gas field is present) then they are extremely unlikely to start leaking as a result of CO_2 injection.

12. Temperature effects close to the wellbore

During production, the near wellbore temperature in the reservoir and overburden will be little affected as the fluid temperature is equal to or very close to the formation temperature. This will not be true during the injection phase. The background caprock formation temperature is expected to be about 83° C and the temperature of the injected fluid will be about 20° C[20]. This cooling will induce significant stress and strain changes in the reservoir and the overburden. The impact of the cooling on fracture propagation has been considered elsewhere[21]. Here the restriction is made to analyse the near wellbore geomechanical effects of cooling due to thermal diffusion in the overburden.

All wells proposed to be used as injectors have a casing shoe in the caprock (Rødby Formation) and an open annulus in communication with the reservoir below the shoe. Above the shoe, a separate analysis[22] asserts that the cement provides an adequate seal and the reservoir can be considered isolated from the reservoir. Below this point, this is no longer the case. The shoe is located approximately 10m above the base of the Rødby Formation except for well GYA02S1 as noted below and the thickness of the Rødby is approximately 60m at the injector well locations. The question of possible near wellbore failure above the shoe is addressed first followed by an analysis of the situation below the shoe.

12.1. Temperature and pore pressure profile above the casing shoe

Above the shoe, the temperature in the formation just prior to injection is assumed to be 83° C. Expected temperature profiles as a function of time in the near wellbore region above the casing shoe after injection of 20°C CO_2 are shown in Figure 12.1. The temperature profiles as a function of time have been derived by a numerical solution to the thermal diffusion equation in cylindrical coordinates which is:

$$\frac{\partial T}{\partial t} = \frac{\kappa_T}{r}\frac{\partial}{\partial r}\left(r\frac{\partial T}{\partial r}\right) \tag{16}$$

where T is the temperature,

t is the time, and

r is the radius from the axial origin.

The critical input parameter in this equation is the thermal diffusivity, κ_T, and is given by the relation:

$$\kappa_T = \frac{k_T}{\rho\, c} \tag{17}$$

where k_T is the thermal conductivity,

ρ is the density, and

c is the specific heat.

Typical values have been used for these parameters and are k=1.5W/(m°K), ρ=2100kg/m^3, and c=900J/(kg°K). Comparison of these calculations to an analytical approximation of the diffusive

[20] Shell, 2011. Injectivity Analysis Preparation

[21] Shell, 2011. Injection Fracturing Conditions

[22] Shell, 2010. Cement concept select

temperature profile[23] is favourable (see Figure 12.1). As one can see, the most significant temperature changes happen within 5m of the well even after four years of injection.

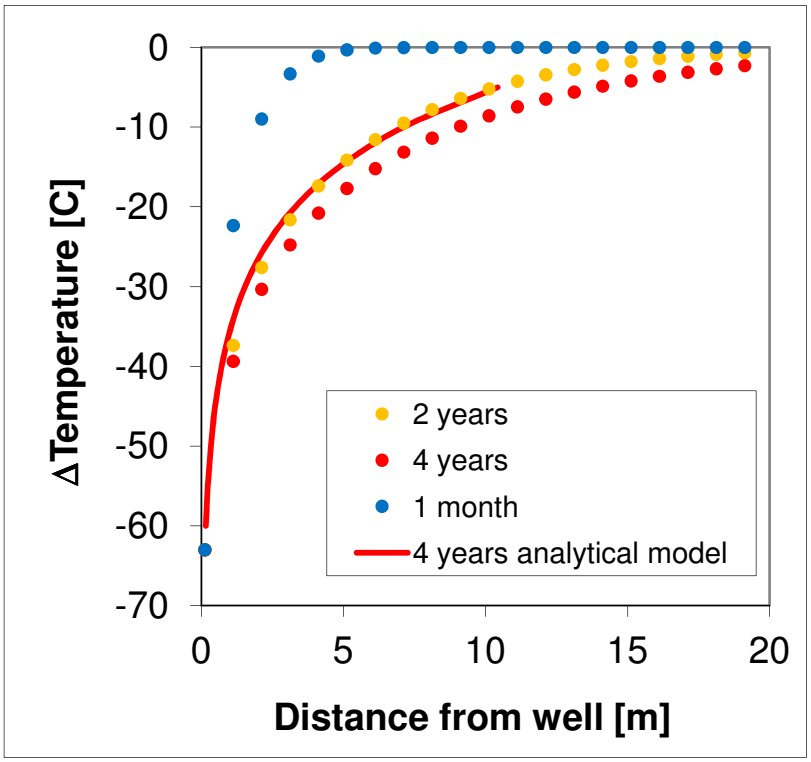

Figure 12.1 **Near wellbore temperature profiles as a function of time. Dotted lines represent numerical solutions to the diffusion equation. Solid line is an approximate analytical solution to the diffusion problem for comparison.**

For materials in the subsurface the temperature distribution is independent of the pore pressure distribution. The pore pressure distribution can be derived assuming diffusive flow and a coupling with the temperature distribution[24], *i.e.*,

$$\frac{\partial p}{\partial t} = \frac{\kappa_p}{r}\frac{\partial}{\partial r}\left(r\frac{\partial p}{\partial r}\right) + c'\frac{\partial T}{\partial t} \tag{18}$$

where κ_p is the hydraulic diffusivity that can be expressed as

$$\kappa_p = \frac{k}{\eta}\left(\frac{\varphi}{K_f} + \frac{b-\varphi}{K_s} + \frac{b^2}{K_{fr} + \frac{4}{3}G_{fr}}\right)^{-1} \tag{19}$$

where k is the permeability,

η is the viscosity,

K_f is the fluid bulk modulus,

K_{fr} is the frame bulk modulus,

K_s is the grain bulk modulus,

[23] Butler, R.M. 1991. *Thermal Recovery of Oil and Bitumen*, Englewood Cliffs, New Jersey: Prentice Hall

[24] Chen, C. and R.T. Ewy (2005), Thermoporoelastic effect on wellbore stability, SPE Journal, pp. 121-129, Paper No. SPE 89039

b is the Biot constant,

G_{fr} is the frame shear modulus, and

φ is the porosity.

Typical values used here are k=1-10 nanoDarcy, η= 1cp, K_f =2.6GPa, K_{fr} =1.6GPa, K_s =37GPa, b=1, G_{fr} =0.96GPa, and φ= 0.12. The parameter c′ is the thermoporoelastic coupling coefficient and can be derived from laboratory experiments. The coupling coefficient can be expanded as:

$$c' = \left.\frac{dp_p}{dT}\right|_{p_c} + \frac{\partial p_p}{\partial p_c}\frac{\partial p_c}{\partial T}$$
$$= \left.\frac{dp_p}{dT}\right|_{p_c} + B\left[\frac{2E_u\alpha_{s,u}}{9(1-\nu_u)}\right] \quad (20)$$

The first term is the change in pore pressure, p_p, with temperature at constant confining pressure, p_c, and can easily be measured in the laboratory, B is the Skempton coefficient, E_u is undrained Young's modulus, $\alpha_{s,u}$ is the undrained solid volumetric thermal expansion coefficient, and ν_u is the undrained Poisson's ratio. Here a representative value of 0.4 MPa/°K for c′ is chosen. Pore pressure profiles using these parameters are shown in Figure 12.2. Here it is assumed that there is a zero fluid flux boundary condition at the wellbore wall and a constant hydrostatic pore pressure in the far field. The zero flux boundary condition is justified as no micro-annulus or radial cracking is expected between the casing, cement, and formation.

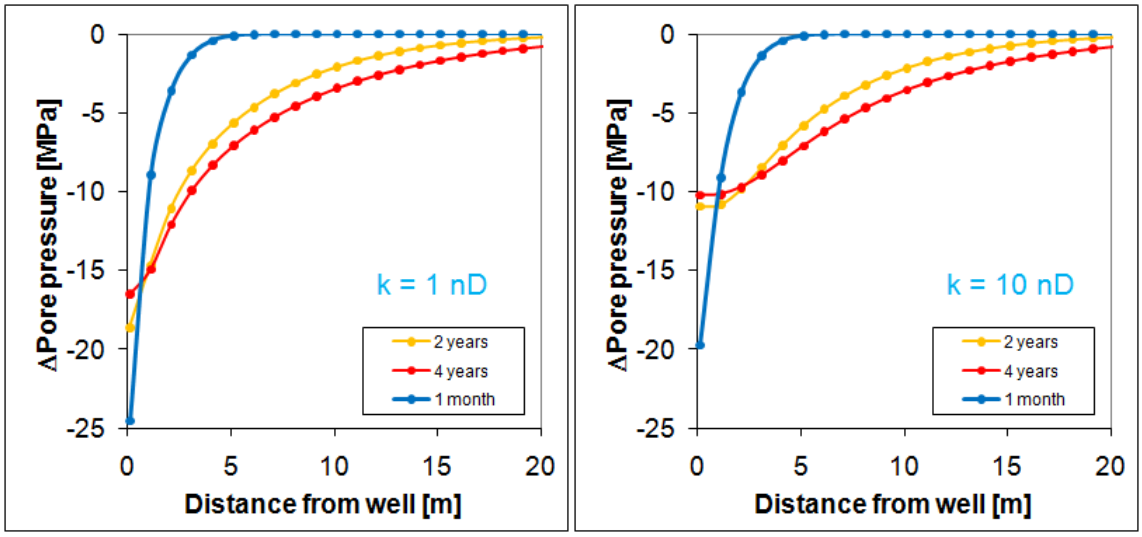

Figure 12.2 Pore pressure profiles as a function of radial distance from the wellbore and time for permeability in the range of 1 (left) to 10 (right) nanoDarcy.

At short time scales, the pore pressure response is undrained and slowly changes to drained behaviour at longer time scales as evidenced by the reduction in the pore pressure gradient from the well bore face as a function of time. As with the temperature the biggest perturbations are in the near wellbore region.

12.2. Near wellbore stress state in cemented region

The impact of the near wellbore pressure and temperature variations in the caprock is assessed using an analytical solution[25] for the stress changes in a heated region around an infinitely extending well. No thermal diffusion or pore pressure diffusion from the far field is present in this model. Instead a step function change is assumed from low to background temperature in the near wellbore region. This model has been shown to produce the same or greater maximum stress perturbations in the near wellbore region compared to more realistic models where the temperature and pore pressure profiles are similar to those shown in Figure 12.1 and Figure 12.2. Using this model, the expansion of the thermoporoelastic coupling coefficient given in Eq. (20) and the input parameters given in Table 12-1, the resulting near wellbore stress state is determined for the undrained (short time scale) state as shown in Figure 12.3. The undrained elastic parameters in Table 12-1 have been determined from sonic logs and the thermal expansion parameters represent the range of values seen in a variety of measurements on shales.

One may note that drained parameters are also listed in Table 12-1. They are present because in some cases the thermal expansivity of the fluid/solid system is so high that the pore pressure would take on negative values for the temperature change considered. As this is unphysical, undrained conditions over a range of temperature change are assumed where the pore pressure is predicted to be greater than or equal to 0 (ΔT_1 in Table 12-1). The remaining amount of temperature change (ΔT_2 in Table 12-1) is applied under drained conditions where the pore pressure is held at a constant value of zero.

Table 12-1 Undrained material parameters for the Rødby Formation used in the near wellbore stress analysis.

Case	$E_{undrained}$	$\nu_{undrained}$	$E_{drained}$	$\nu_{drained}$	$\alpha_{V,drained}$	$\alpha_{V,undrained}$	ΔT	ΔT_1	ΔT_2	$(\Delta p_p/\Delta T)_{p=const}$	B	$p_{p,0}$	$\sigma_{1,0}'$	$\sigma_{3,0}'$
	[Gpa]		[Gpa]		[10^{-6} K^{-1}]	[10^{-6} K^{-1}]	K	K	K	[MPa/K]		[MPa]	[MPa]	[MPa]
low	10	0,38	-	-	-	60	-60	-60	0	0,1	0,8	25	26,9	18,1
base	10	0,38	-	-	-	105	-60	-60	0	0,1	0,8	25	26,9	18,1
high	10	0,38	8,00	0,11	120	150	-60	-47,2	-12,8	0,1	0,8	25	26,9	18,1

[25] Perkins, T.K. and J.A. Gonzalez (2004), Changes in Earth Stresses around a wellbore caused by radially symmetrical pressure and temperature gradients, SPE Journal, pp. 129-140, Paper No. SPE 10080.

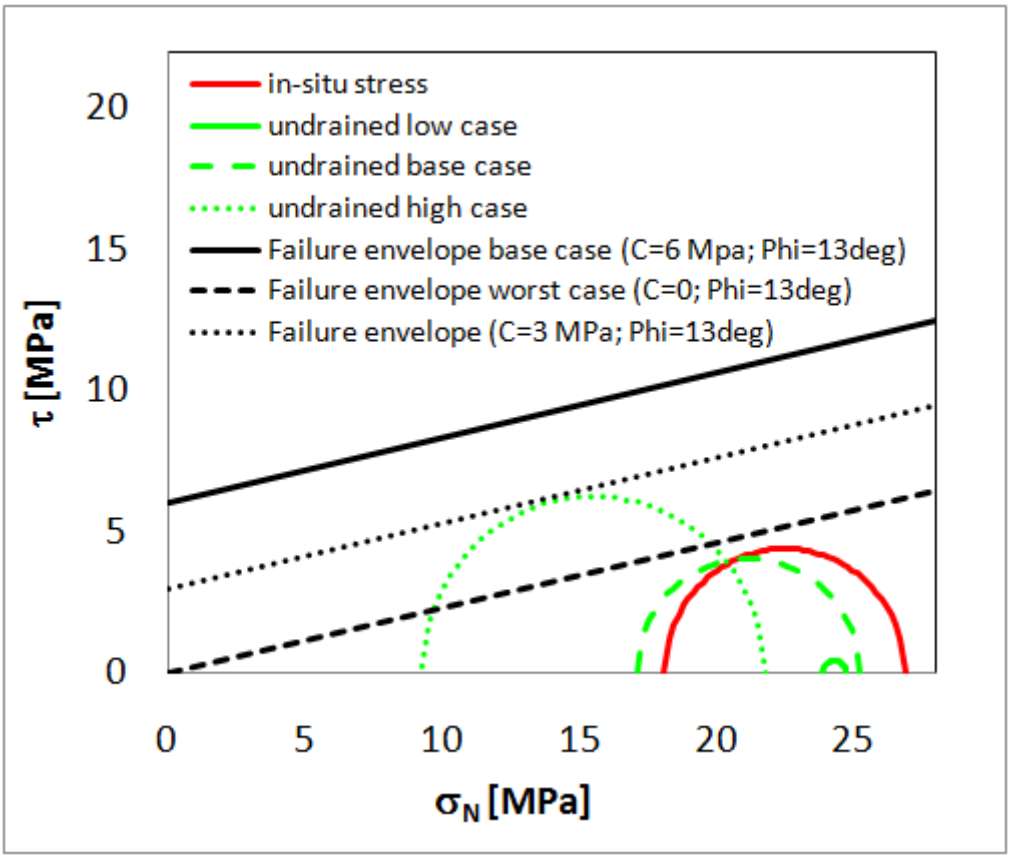

Figure 12.3 **Effective stress state of the near wellbore environment after cooling under undrained conditions. The stress state is displayed in Mohr's space relative to the base case (solid), intermediate (dotted), and worst case (dashed), Mohr-Coloumb failure line for the Rødby shale before (red circle) and after cooling (green circles) for three different scenarios (see Table 12-1).**

One can see from these results that shear failure assuming a Mohr-Coulomb criterion is not expected over the range of uncertainty considered except in the undrained high case with the worst case failure envelope for the Rødby Formation. This combination is considered to be extremely unlikely especially as the high undrained thermal expansion values come from experiments on shallowly-buried, relatively unconsolidated shales which are not an appropriate analogue for the Rødby mudstone. However, the desire was to include this value for completeness in the analysis. Note that tensile failure is not expected in any of the cases considered as evidenced by the fact that the predicted minimum principal stress remains well above zero.

A similar exercise has been carried out assuming drained conditions which would be realized in the long time scale limit. The model parameters are given in Table 12-2 and the results shown in Figure 12.4

Table 12-2 **Drained material parameters for the Rødby Shale used in the near wellbore stress analysis.**

Case	$E_{drained}$	$\nu_{drained}$	α_V [K-1]	ΔT	$p_{p,0}$	$\sigma_{1,0}'$	$\sigma_{3,0}'$
	[Gpa]		[10^{-6} K^{-1}]	K	[MPa]	[MPa]	[MPa]
low	1,62	0,37	60	-60	25	26,9	18,1
base	2,4	0,25	60	-60	25	26,9	18,1
high	8,00	0,11	60	-60	25	26,9	18,1

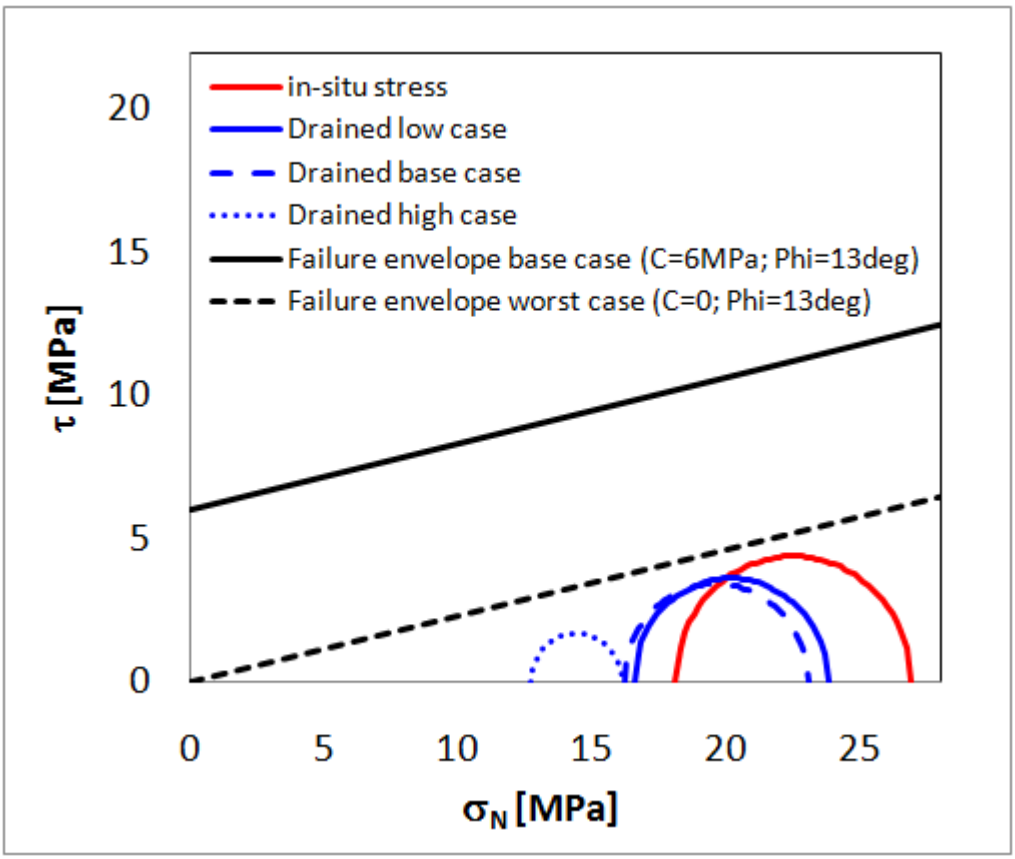

Figure 12.4 **Effective stress state of the near wellbore environment after cooling under drained conditions. The stress state is displayed in Mohr's space relative to the base case (solid) and worst case (dashed) Mohr-Columb failure line for the Rødby shale before (red circle) and after cooling (blue circles) for three different scenarios (see Table 12-2).**

Here, the major source of uncertainty is in the drained elastic parameters and thus the drained thermal expansion values are kept fixed at the base case values for simplicity. The elastic parameters were derived by Gassmann fluid substitution with a range of grain moduli expected for a shale. As Figure 12.4 clearly displays, shear failure assuming a Mohr-Coulomb criterion or tensile failure of the Rødby is not expected within this uncertainty range. Thus, thermal cooling of the formation does not appear to be an issue for the section of the caprock sealed from pressure variations.

12.3. Near wellbore stress state for the caprock exposed to reservoir pressure variations

In the wellbore below the casing shoe, a zero flux boundary condition no longer holds. In this case, pore pressure diffusion from the wellbore face into the formation will occur. This will alter the effective stress state in the near wellbore region significantly from that shown above. In order to evaluate this, the wellbore simulator PBore[26] was employed, which makes it possible to investigate the coupled effects of pore pressure and temperature variations at the wellbore face.

[26] Abousleiman, Y.N., Ekbote, S., Cui, L., Mody, F., Roegiers, J.C. and Zaman, M. 1999. Time-dependent coupled processes in wellbore design and stability: PBORE-3D, Paper SPE 56759 presented at 74th SPE Annual Technical Conference and Exhibition, Houston, Texas, 3-6 October

In the PBore analysis, two cases will be considered; a base case and low case. The low case uses the highest values of κ_T, $E_{drained,}$ and $\alpha_{s,drained}$ to explore the largest expected variations in temperature and pore pressure. The parameters that are input into the PBore model are given in Table 12-3 and the initial stress state, viscosity, permeability, etc. are as above. In Table 12-3 the failure parameters are cohesion (C) and friction angle (θ). For both cases, the pore pressure at the wellbore face and in the far field is set to hydrostatic. This is appropriate for the situation during the initial drilling of the wells (near hydrostatic mud weight used) and at the end of the injection period.

Table 12-3 Base and low case parameters used in the PBore model.

Scenario	$E_{drained}$	$\nu_{drained}$	ν_u	$\alpha_{s,drained}$	α_f	κ_T	C	θ
	[GPa]			[10^{-6} K^{-1}]	[10^{-6} K^{-1}]	[$10^{-7}m^2s^{-1}$]	[MPa]	[deg]
Base	2.4	0.25	0.38	10	500	3	6	13
Low	8	0.11	0.38	60	500	6	0	13

Temperature and pressure perturbations for the base case model assuming 100 nanoDarcy permeability, as is shown in Figure 12.5. The permeability value of 100 nanoDarcy was chosen to ensure the calculations would be conservative. The temperature distribution is very similar to that given in Figure 12.1 as expected. However, the pore pressure distribution now shows a peak near the wellbore due to pore pressure diffusion from the wellbore face in contrast to the distribution shown in Figure 12.2.

In Figure 12.6, the failed zone predicted around the well is compared in two scenarios assuming a permeability of 100 nanoDarcy and the base case rock properties. In the first scenario, the temperature change is accounted for and in the second one it is not. No difference between the two scenarios is found. With this important observation the statement can be made that the failure zone is due to the initial drilling of the well and subsequently exposing the wellbore face to the hydrostatic reservoir pressure. At this time, the total radial stress has to equal the pore pressure in the open annulus due to force balance. This greatly increases the shear stress and causes some failure. As the failure is fairly limited, it should pose no problem in completing the well. Indeed the well summary reports mention some hole instability in the caprock near the top of the reservoir section, but nothing that stopped the running of the completion. The same behaviour is seen when the permeability is reduced to 1 nanoDarcy.

Because the failure zone does not grow when cooling takes place, it means that the temperature has no effect on the size of the failure. This has important implications for the GYA02S1 well as it was completed near the top of the Rødby. These results show that a failed zone is not expected to propagate from the open hole section below the shoe to the top of the Rødby as the shoe is approximately 10m below the top of the Rødby Formation and the failed zone is on the order of centimeters.

Under low case conditions, the hole is completely unstable. Thus, this case is unrealistic as no such problems are experienced during drilling and completing the well. Still, something very useful can be learned from this example. In the no temperature change scenario, the hole is immediately unstable. However, with a temperature reduction, the hole is not immediately unstable. In Figure 12.7, a progression of increasing instability as a function of time is seen. This is not surprising as the effect of temperature is to decrease the pore pressure more than the total stress, leading to an increase in effective stress and driving us away from shear failure as long as the shear stress does not increase significantly in the process. Pore pressure diffusion then leads to a pore pressure increase that the

total stresses cannot match in the near wellbore invironment as the radial stress must equal the pore pressure at the wellbore face. Thus the effective stress goes down, driving the system towards failure.

The important aspect to note here is that temperature should lead to a stabilization and not a destabilization. Thus, if the cohesion of the Rødby is raised, which is the most uncertain failure parameter, such that the hole becomes stable under isothermal conditions, then the addition of cooling will not make the hole unstable and the conclusion about restricted failure around the wellbore under the base case remains valid under low case conditions.

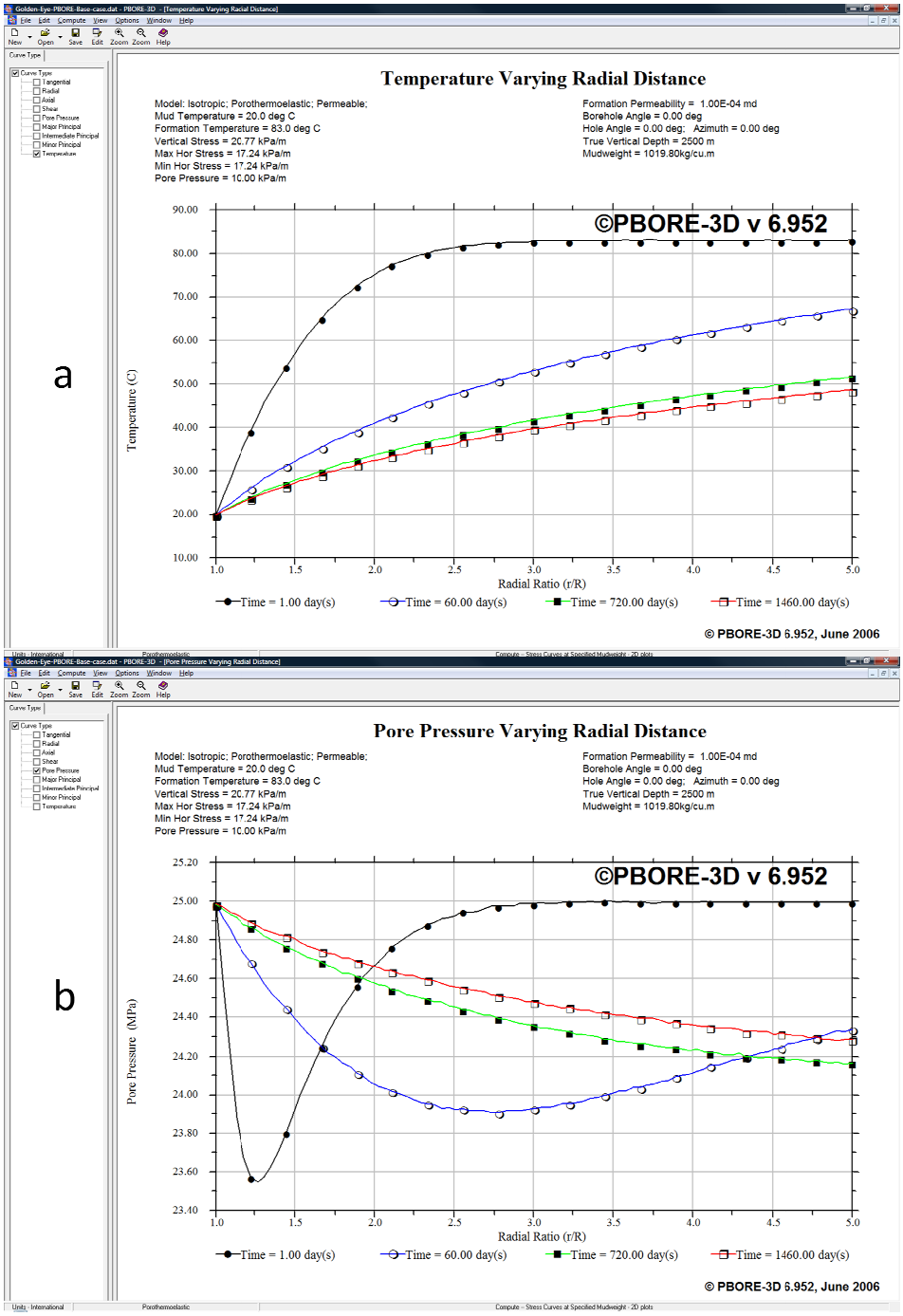

Figure 12.5 **Temperature (a) and pore pressure (b) distributions as a function of time for the base case PBore model assuming a 100 nD permeability. Pore pressure or temperature after 1 day is shown in black, 60 days in blue, 2 years in green and 4 years in red.**

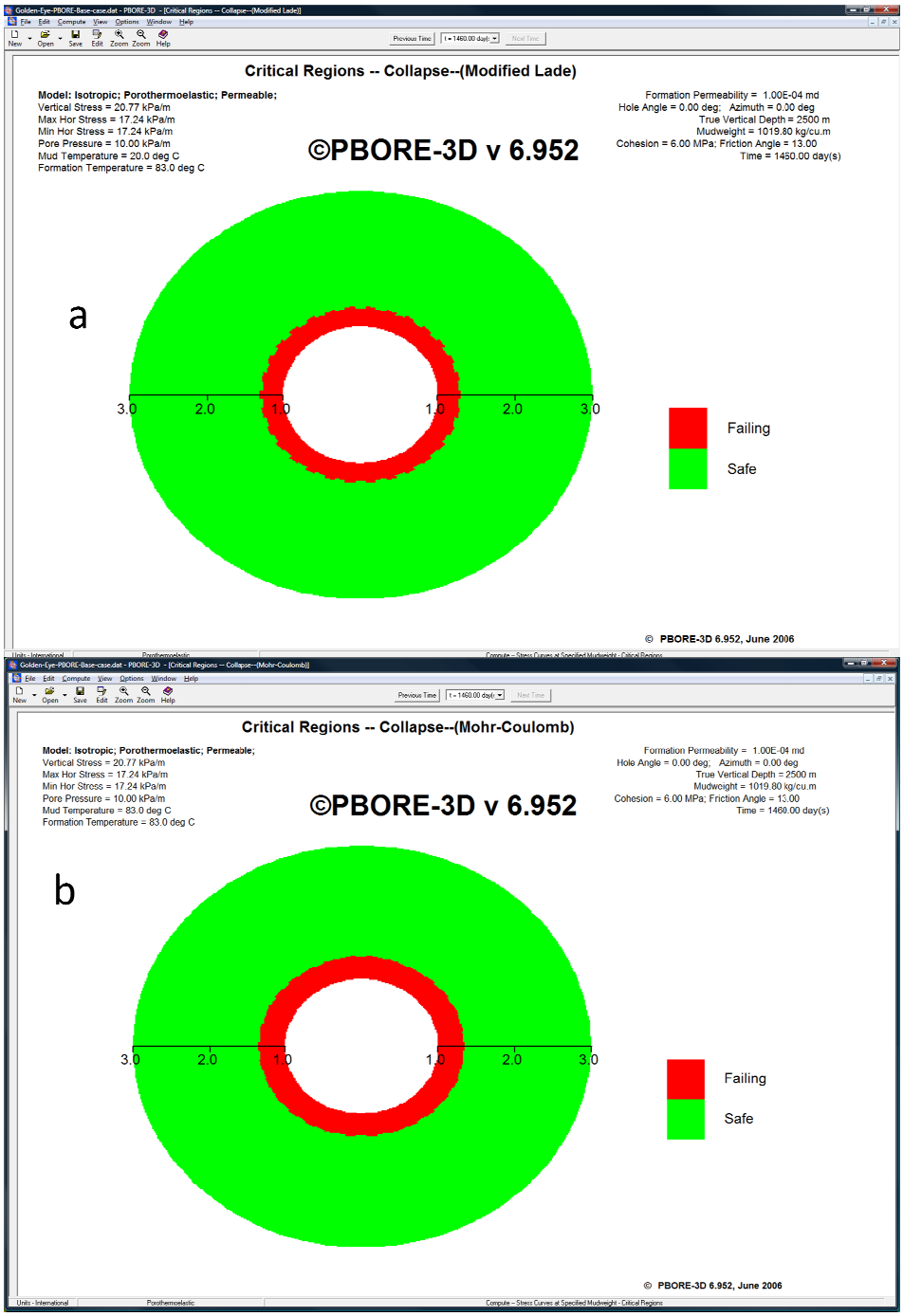

Figure 12.6 **Comparison of the failed zone (red area) around well from the base case PBore simulation with cooling of the formation for 4 years (a), and no temperature change in the formation (b).**

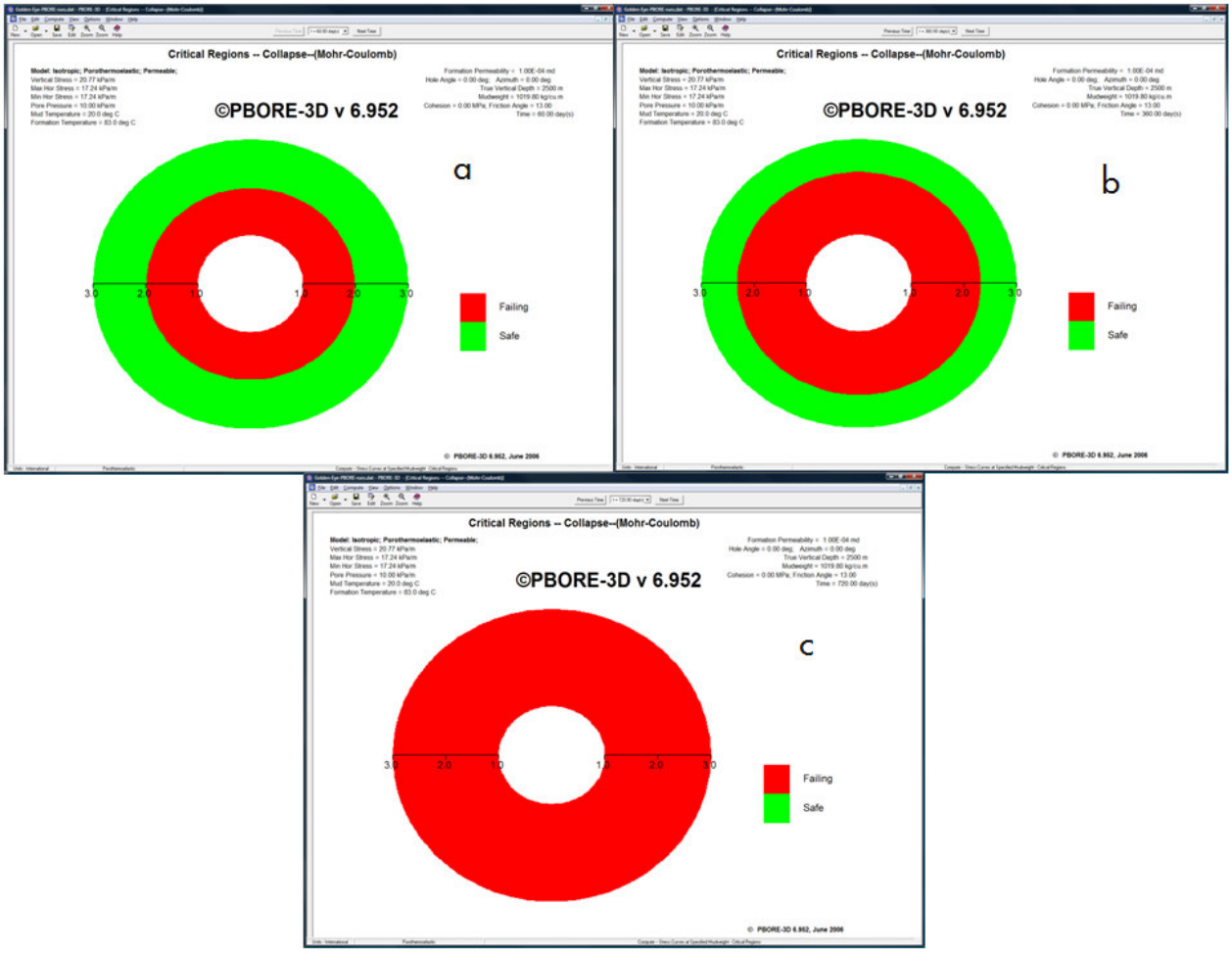

Figure 12.7 **Evolution of wellbore failure (red areas) from the low case PBore simulation as a function of time under cooling conditions. The amount of failure is shown after 60 days (a), 1 year (b), and 2 years (c).**

12.4. Possible changes in permeability if shear failure occurs

In the above analysis, the focus has been on whether failure of the Rødby shale is expected. Implicit in this is the assumption that shear failure will lead to a significant leakage of CO_2 through the Rødby shale. It is not entirely clear that this will be the case. Brittle behaviour generally leads to dilation and permeability increase while ductile behaviour leads to compaction and permeability reduction.

Whether a shale shows brittle or ductile behaviour depends on the stress history, clay content, degree of cementation, and other parameters[27]. A normally consolidated shale tends to deform in a ductile way, while overconsolidated shales (shales that were exposed in the past to higher stresses than present day stresses) exhibit brittle behaviour. The reduction of total mean stress by cooling of the shale would bring it into an overconsolidated state, more prone to brittle failure.

It is also known from x-ray diffraction data and dielectric constant measurements, that the Rødby shale should have a high smectite constant. Smectite-rich rocks generally have a low friction angle

[27] Ingram, G.M. and Urai, J.L. 1999. Top-seal leakage through faults and fractures: the role of mudrock properties. In *Muds and Mudstones: Physical and Fluid Flow Properties*, *Geol. Soc., London, Sp. Publ.*, **158**, ed. A.C. Aplin, A.C., Fleet, A.J. and MacQuaker, J.H., 125-135.

like the Rødby, have a low pre-consolidation pressure and have a low to zero dilation angle[28]. This means that they will behave in a ductile rather than in a brittle fashion most generally. Smectite rich rocks also hydrate easily and disperse in water, thus a water pill applied prior to injection is a highly recommended mitigation measure. In any case, at this point, brittle deformation of the Rødby shale cannot be excluded in the unlikely event of cooling induced rock failure.

Another question of interest is whether shear fractures in Rødby shale would close again after CO_2 injection is stopped and pre-injection stress and temperature conditions are recovered. Previous lab studies with artificially fractured shales have shown that apertures and permeabilities of fractures exposed to normal stresses diminish over time due to creep. However, for the shales studied, the amount of creep may not be sufficient to close the fractures even on geological time scale[29]. From that, it is concluded that a leak due to cooling-induced shear failure of the Rødby caprock would most likely not disappear after CO_2 injection is stopped and pre-injection temperature and stresses are re-established.

12.5. Conclusions

This chapter has concentrated on the possibility of failure of the caprock in the near wellbore region due to temperature changes and the possibility of leakage resulting from failure. In the cemented section above the casing shoe, the results of the analysis presented here show a very low probability of failure of the caprock. Analysis of the caprock below the casing shoe also shows a very low probability of failure due to thermal loading. If failure did occur, it is not clear if it would lead to significant leakage. Failure could lead to a permeability decrease (ductile behaviour) or permeability increase (brittle behaviour). As mentioned in §3.1.5, the CO_2 flux from the permeability increase is likely to be negligible. Regardless, it is recommended to apply a water pill prior to injection to increase the likelihood of ductile behaviour.

[28] Olgaard, D.L., Urai, J., Dell'Angelo, L.N., Nuesch, R. and Ingram, G.M. 1997. The influence of swelling clays on the deformation of mudrocks, *International Journal of Rock Mech & Min. Sci.* 34 (3-4): 235

[29] Cuisiat, F., Grande, L. and Høeg, K. 2002. Laboratory testing of long term fracture permeability in shales, paper SPE 78215, presented at SPE/ISRM Rock Mechanics conference, Irving, Texas, 20-23 October.

13. Conclusions and recommendations

Integrity of the Captain E&D reservoir and the caprock (Rødby formation) is investigated with the aid of a geomechanical simulator. The geomechanical model is composed of

- the structural geometry of the reservoir, overburden and underburden formations,
- in-situ stress and pore pressure profile,
- mechanical rock properties of all the formations, and
- pressure changes in the reservoir due to depletion and injection at different times.

Apart from the structural geometry, for each of these components a range of values were identified with varying likelihood. The values with the highest likelihood were combined into a so called "base case" model. Those values that have a worse effect on the integrity were combined into so called "worse case" models. With these models the effect of different parameters (in itself or combined) were studied. Common accepted criteria for tensile failure and shear failure (Mohr-Coulomb) were used to define norms, and to quantify risks, of failure.

Results from the geomechanical simulations using base case and worst case models show there is no risk of tensile failure and shear failure for both the reservoir and caprock given the injection pressures that are intended to stay below the minimum total principal stress in the reservoir.

Fault slip reactivation was studied in the same rigorous manner as the integrity. The potential faults that were investigated have to be interpreted as the outcome of a possible scenario. For every fault, the slip-tendency was investigated by calculating the shear capacity for all the three stress stages (before and after production of the gas, and after injection of the CO_2). No fault-slip is expected to occur. Even the worst case scenario was not significantly close to slip. This conclusion is based on the assumption that the initial stress state of the faults, before depletion or injection, is the same as the initial stress sate of the surrounding rock. Further, it was assumed that the faults are not critically stressed. This result implies that if faults are currently not leaking (which they are unlikely, to be given that a gas field was present) then they are extremely unlikely to start leaking as a result of CO_2 injection.

During injection of the CO_2 the near wellbore temperature in the top of the reservoir and the bottom of the overburden will be different from the formation temperature. This cooling will induce significant stress and strain changes in the reservoir and the overburden. In this report the near wellbore geomechanical effects of cooling due to thermal diffusion in the overburden is analysed. This section has concentrated on the possibility of failure of the caprock in the near wellbore region due to temperature changes and the possibility of leakage resulting from failure. In the cemented section above the casing shoe, the results of the analysis presented here show a very low probability of failure of the caprock. Analysis of the caprock below the casing shoe also shows a very low probability of failure due to thermal loading. If failure did occur, it is not clear if it would lead to significant leakage. Failure could lead to a permeability decrease (ductile behaviour) or permeability increase (brittle behaviour). As mentioned in §3.1.5, the CO_2 flux from the permeability increase is likely to be negligible. Regardless, it is recommended to apply a water pill prior to injection to increase the likelihood of ductile behaviour.

From a capacity point of view it is important to investigate a possible change of available storage volume due to gas depletion and CO_2 injection. Information on this can be obtained from measurements on core from the reservoir. Compaction experiments carried out in 1998-1999 showed that the compaction of cores from Goldeneye sands is partly elastic (i.e. reversible) and partly plastic (*i.e.*, irreversible). Results from the experiments showed minimal compaction, and the porosity change was about 0.3% (when loaded from 17 - 34MPa (2500 - 5000psi)). As a result this effect can

be considered to have negligible impact on the difference in available pore volume between gas depletion and CO_2 injection.

13.1. Recommendations

It is recommended to quantify the effect different parameters in a probabilistic manner. This can be done by doing more geomechanical simulations.

The worst case failure properties of the shale in the caprock represents an unconsolidated formation. This assumption is good for investigating worst case effects but might be too pessimistic. It is recommended to do a borehole stability analysis where the goal is to simulate the exploration drilling such that modeled and observed plastic wellbore deformation are in agreement. As this deformation is depending on the cohesion of the shale it provides information on the state of consolidation of the caprock shale.

After many, many years the aquifer re-pressurizes the field. It is recommended to investigate this effect more rigorously.

Leaking close to the wellbore due to thermal fracturing was investigated by studying in detail the coupled effects of temperature and pore pressure in the shale close to the wellbore. As the results in this report only holds for vertical wells it is recommended to investigate also the effect of deviated wells. Also it is advisable to use a more sophisticated near well bore modelling above the casing shoe to more rigorously account for the pressure and temperature distribution expected in the near wellbore environment.

14. Glossary of terms

123DI	Shell proprietary software used for seismic interpretation
1D, 2D, 3D	One, two, three Dimensional
ALARP	As Low As Reasonably Practicable, and is a term often used in the environment of safety-critical and high-integrity systems. The ALARP principle is that *the residual risk shall be as low as reasonably practicable*
Barrier	Barriers prevent of mitigate the probability of each threat or prevent, limitthe extent of, or provide immediate recovery from the Consequences
Bg	Formation Volume Factor (Gas)
BHP	Bottom Hole Pressure
Bo	Formation Volume Factor (Oil)
Bow-Tie	The bow-tie is a model that represents how a Hazard can be released, escalate, and how it is controlled. Bow-ties can also be used to support risk management of non-HSSE processes, Hazardous Activities, and HSSE critical processes
CBIL	Circumferential Borehole Imaging Log
CCS	Carbon Capture & Storage
CO_2	Carbon Dioxide
CoP	Cessation of Production
DP	Differential Pressure
EOR	Enhanced Oil Recovery
Escalation Factor	Factors that defeat, or reduce the effectiveness/reliability of a Barrier
ESG	Microseismic monitoring company, Canada. www.esg.ca
FAM	Fairway Aquifer Model
FEED	Front End Engineering Design
FEM	Finite Element Modelling
FFM	Full Field Model
FFSM	Full Field Simulation Model
FMI	Full bore formation Micro-Imager
GBV	Gross Bulk Volume
GIIP	Gas Initially In-Place
gOcad	3rd Party software to build and update 3D subsurface models

GRV	Gross Rock Volume
Hazard	The potential to cause harm, including ill health and injury, damage to property, products or the environment; production losses or increased liabilities. In this report: buoyant CO_2
HCPV	Hydrocarbon Pore Volume
HSSE	Health, Safety, Security, and Environment
IIP	Initially In-Place (volumes)
Injection phase	The injection phase includes the period of site preparation for injection, the injection period itself and the period of well abandonment
InSAR	Interferometric Synthetic Aperture Radar
IPCC	International Panel on Climate Change
KNMI	The Royal Netherlands Meteorological Institute
Leakage	Migrated CO_2 out of the containment that leaks into the biosphere (shallow subsurface and atmosphere). In contrast to seepage, leakage involves medium fluxes and medium concentrations
Leakage scenario	Group of threats that form cause-consequence relations leading to a certain route of migration and eventually leakage into the biosphere
LOP	Leak-off pressure
LOT	Leak-off Test
LT	Limit Test
Mcf	Thousand cubic feet at reservoir conditions
Migration	Escaped CO_2 out of the containment into the subsurface where it moves or trapped in other layers
Mscf	Thousand cubic feet at standard conditions
NAM	Nederlandse Aardolie Maatschappij BV (Joint venture Shell/XOM 50/50)
NPV	Net Pore Volume
NRV	Net Rock Volume
NtG	Net to Gross
PBore	3rd Party software to model bore hole strability
pH	measure of the acidity or basicity of an aqueous solution
PVT	Pressure, Volume, Temperature
PWRI-frac	Shell proprietary software used for modelling the effect of fluid injection on fracture development and growth
Risk	Risk management is the human activity, which integrates recognition of risk, risk

management	assessment, developing strategies to manage it, and mitigation of risk using managerial resources
SCU	Shear Capacity Utilisation
SEC	Securities and Exchange Commission
Seepage	Migrated CO_2 out of the containment that seeps into the biosphere (shallow subsurface and atmosphere). In contrast to leakage, seepage involves low fluxes and low concentrations
SRM	Static Reservoir Model
Threat	Means by which a hazard can be released and thus cause the top event
TNO	Netherlands organization for applied scientific research
Top Event	Incident that occurs when a hazard is realized, or the release of the hazard. The Top Event is typically some type of loss of control or release of energy. If this event can be prevented there can be no effect or consequence from the hazard
UBI	Ultra-sonic Borehole Imager
UCS	Unconfined Compressive Strength
UGS	Underground Gas Storage
XLOT	Extended Leak Off Test

In the text well names have been abbreviated to their operational form. The full well names are given in Table 14-1.

Volumes quoted at 'standard conditions' assume temperature of 60°F and pressure of 14.7psia.

Full well name	Abbreviated well name
DTI 14/29a-A3	GYA01
DTI 14/29a-A4Z	GYA02S1
DTI 14/29a-A4	GYA02
DTI 14/29a-A5	GYA03
DTI 14/29a-A1	GYA04
DTI 14/29a-A2	GYA05

Table 14-1 Well name abbreviations